Target Tracking in Mixed LOS/NLOS Environments

Yi Lili

School of Electrical & Electronic Engineering

Nanyang Technological University

A Thesis submitted to the Nanyang Technological University
in partial fulfillment of the requirements for the degree of

Doctor of Philosophy

2014

Acknowledgements

This thesis would not have been possible without the the guides, support and encouragement of numerous individuals, mentors, family and friends.

First, I would like to express my deepest gratitude to my supervisor, Associate Professor Lin Zhiping and co-supervisors Dr. Sirajudeen Gulam Razul and Dr. Chong-Meng See for their constant encouragement and guidance during the period of my PhD study. I also would like to thank TL @ NTU for the five years financial support of my PhD study. I also would like to thank technicians from the Information System Research lab in School of Electrical and Electronic Engineering, Nanyang Technological University, for their support during my study.

Second, I would like to thank my beloved parents, my husband and my daughters for the endless love and selfless support they have given me throughout the long journey of my study.

Finally, I would like to thank my friends and fellow classmates in Singapore for their support and help.

Abstract

In this thesis, we discuss the problem of tracking the geographic position of a moving target in mixed line-of-sight and non-line-of-sight (LOS/NLOS) environments using measurements including time-of-arrival (TOA), angle-of-arrival (AOA) and time-difference-of-arrival (TDOA).

While many tracking algorithms are available for accurately tracking a moving target in the LOS environment, it is desirable to develop reliable tracking algorithms for accurately tracking a moving target in the mixed LOS/NLOS environments since purely LOS environment seldom exists in practice, particularly in urban areas. When NLOS errors exist, traditional tracking techniques such as least squares (LS), Kalman filter (KF) and extended Kalman filter (EKF) will not work well. Thus, new tracking algorithms are required to mitigate or to remove the NLOS errors to improve the tracking accuracy.

In this thesis, we first propose a new idea called individual measurement detection (IMD), which is one of the central ideas in this thesis. An IMD based EKF tracking strategy in conjunction with the IMD method is then applied to track a moving target with improved tracking performance. This approach is further extended to the case of robust EKF (rEKF) using TOA measurements. This tracking algorithm turns out

to work better than the EKF tracking strategy for exponential NLOS errors. To further improve the tracking accuracy in mixed LOS/NLOS environments especially in severe NLOS conditions, we propose an individual TOA measurement estimation and LOS measurement detection algorithm, which is labeled as IMED. In this approach, each TOA measurement collected at a certain time step is treated individually to estimate a pseudo-measured position of the moving target. Then these pseudo-measured positions are passed to a detector to identify the LOS ones. The average of selected LOS pseudo-measured positions is then used into a KF. The developed tracking algorithms outperform various robust competing estimations found in the literature while no prior knowledge of the NLOS error statistics is required.

The IMD based EKF and the IMD based rEKF tracking approaches are then used into TDOA based tracking problems. With the assistance of the road constraints, which are used as pseudo measurements, the tracking performance is improved with respect to these without road constraints.

To further improve the tracking accuracy of the proposed IMED algorithm, some AOA measurements are incorporated into the IMED algorithm together with TOA measurements. The joint TOA/AOA measurements estimation and LOS measurement detection algorithm is improved with better performance than using TOA measurements only.

Contents

List of Tables

List of Figures

List of Symbols

$\mathbf{x}_k$	State vector of the moving target at time step k
n_x	Dimensionality of the state space
$\mathbb{R}$	Set of real numbers
k	Time steps
$\mathbb{N}$	Set of real numbers
$\mathbf{f}(\cdot)$	State transition function of the moving target
$\mathbf{F}$	State transformation matrix
$\mathbf{v}_{k-1}$	Process noise
$\mathbf{Q}^v$	Covariance matrix of the process noise $\mathbf{v}$
$p(A)$	Probability density function of event A
$p(A \mid B)$	Conditional probability density function of event A given event B
$\mathbf{r}_k$	Measurement vector
n_r	Dimensionality of the measurement vector
$\mathbf{w}_k$	Measurement noise
$\mathbf{h}(\cdot)$	Measurement function
x_k	Position of a moving target on on the x axis at time step k
y_k	Position of a moving target on on the y axis at time step k

$\dot{x}_{k-1}$	Velocity of the target on the x axis at time step k
$\dot{y}_{k-1}$	Velocity of the target on the y axis at time step k
T	Time interval between time steps k and $k-1$
$\mathbf{u}_k$	Random force vector
$\mathbf{Q}^u$	Covariance matrix of the random force vector $\mathbf{u}$
$\mathbf{G}$	Transition matrix
$\left(x_m^S, y_m^S\right)$	Position of the sensor m
M	Number of stationary sensors
$\mathbf{d}$	Noise free distance vector
d_m	Noise free distance between the moving target and sensor m
$\mathbf{r}$	Measured distance vector
r_m	Measured distance between the moving target and sensor m
$\boldsymbol{\eta}$	Mixture LOS and NLOS noise vector
η_m	Mixture LOS and NLOS noise on sensor m
ε_m	The probability of contamination by NLOS errors at sensor m
α	Transition probability from state LOS to NLOS
β	Transition probability from state NLOS to LOS
$\mathcal{N}(\mathbf{x}; \mathbf{m}, \mathbf{P})$	Gaussian distribution with argument $\mathbf{x}$, mean $\mathbf{m}$ and covariance $\mathbf{P}$

$\mathbf{H}$	Measurement transition matrix
$\mathbf{w}$	LOS measurement noise vector
$\mathbf{R}$	Covariance matrix of the LOS measurement noise vector
$\mathbf{x}_k^-$	Prediction state of the moving target
$\mathbf{P}_k$	Error covariance matrix of the state vector
$\mathbf{P}_k^-$	Prediction error covariance matrix of the state vector
$\mathbf{K}_k$	Kalman Gain matrix
$\mathbf{I}$	Identical matrix.
$\hat{\mathbf{F}}_{k-1}$	Jacobian matrix of the nonlinear function $\mathbf{f}(\cdot)$
$\hat{\mathbf{H}}_k$	Jacobian matrix of the nonlinear function $\mathbf{h}(\cdot)$
$\mathbf{x}_k^p$	Position vector of the moving target
$\mathbf{x}_m^p$	Position vector of the moving target determined by sensor m
$\hat{\mathbf{x}}_m^p$	Prediction position vector of the moving target
$\|\cdot\|_{\ell^2}$	ℓ^2 norm
$v_k(\gamma)$	Confidence region
γ	Gate threshold
V_k	The volume of the confidence region
$\|A\|$	Determinant of matrix A
c_{n_x}	Coefficient
$\mathbf{P}_k^{p,-}$	Error covariance matrix of the position vector $\mathbf{x}_k^p$

$\sigma_{x,k}$	Standard deviations of the position estimates on the x axis
$\sigma_{y,k}$	Standard deviations of the position estimates on the y axis
ρ_k	Correlation coefficient
$\mathbf{i}_k$	Innovation vector
$\mathbb{E}(\cdot)$	Expectation operator
$\tilde{\mathbf{x}}^p_{k,m}$	Pseudo-measured position estimated from measurement m
$\bar{\mathbf{x}}^p_k$	Average of LOS pseudo-measured positions
$\boldsymbol{\Delta}\mathbf{r}_k$	Measured distance difference vector
$\boldsymbol{\Delta}\mathbf{d}_k$	Noise-free distance difference vector
μ	Mean of a random vector
σ	Standard deviation of a random vector
θ	Direction of the straight road
$\mathbf{r}_c$	Road constraint vector
$\mathbf{H}_c$	Road constraint transition matrix
$\mathbf{u}_{c,k}$	Road constraint noise
$\boldsymbol{\beta}_k$	Measured angle vector

List of Abbreviations

LOS	Line-of-sight
$NLOS$	Non-line-of-sight
TOA	Time-of-arrival
$TDOA$	Time-difference-of-arrival
AOA	Angle-of-arrival
EKF	Extended Kalman filter
$GNSS$	Global Navigation Satellite System
GPS	Global Positioning System
BDS	Beidou Navigation System
GSM	Global System of Mobile Communication
$UMTS$	Universal Mobile Telecommunications System
pdf	Probability density function
PDA	Probability data association
$MPDA$	Modified PDA
KF	Kalman filter
$TKDE$	Transformation kernel density estimation
$rEKF$	Robust EKF
$IMED$	Individual measurement estimation and detection
CV	Constant velocity

$GLRT$	Generalized likelihood ratio test
IMD	Individual measurement detection
MED	Mean error distance
$RMSE$	Root mean square error
$i.i.d.$	Independent and identically distributed
RF	Radio frequency
$2-D$	Two-dimensional
$FDOA$	Frequency-difference-of-arrival
UKF	Unscented Kalman filter
PF	Particle filter

Chapter 1

Introduction

This thesis deals with the problem of determining the state of a moving target in mixed line-of-sight (LOS) and non-line-of-sight (NLOS) environments by processing received signal parameters such as time-of-arrival (TOA), time-difference-of-arrival (TDOA) and angle-of-arrival (AOA) measurements in conjunction with the geometry of a network of sensors. If direct physical signal propagation paths between the target and each of the sensors exist, meaning all measured signals are in LOS states, accurate state estimates can be derived from classical tracking algorithms such as extended Kalman filter (EKF). However, in practice obstacles reflect the signals and hinder them arriving at the sensors via the direct paths. This phenomenon, named NLOS signal propagation, introduces erroneous signal parameters and consequently high tracking errors into a tracking algorithm. The goal of this thesis is to design statistical algorithms that remove or eliminate NLOS errors to achieve similar tracking accuracy to conventional tracking techniques in LOS environments and do not degrade significantly when the degree of NLOS propagation increases.

1.1 Motivations

Tracking a moving target is an important task in many civilian and military applications and several electronic navigation systems [1–4]. For different applications, electronic navigation systems are categorized into Global Navigation Satellite System (GNSS) [5] and network-based positioning systems [1, 3]. The former ones, including Global Positioning System (GPS), Beidou Navigation Satellite System (BDS), use an electronic device to receive radio signals transmitted from satellites. They provide positioning accuracy up to a few meters given that no obstacles block the signals propagation from satellites [5]. When it comes to worse conditions such as indoor environments, harsh urban environments or hilly terrains, it becomes unreliable because obstacles in the propagation path lead to strong signal degradation and consequently to erroneous position estimates. Network-based positioning systems include Global System for Mobile Communication (GSM), Universal Mobile Telecommunications System (UMTS) as well as sensor networks. Based on any network we can use either geometric or mapping approaches to obtain the position of the moving target [1, 2, 6, 7]. In this thesis, we concentrate on the wireless sensor network constructed by multiple stationary sensors. Based on any kind of sensor network, the classical tracking algorithms such as EKF can achieve high tracking accuracy while the signal propagation paths are all assumed to be LOS.

However, if the assumption of LOS channel for any of the sensors is not fulfilled, the tracking result can completely differ from the expected result under the LOS assumption. This is known as NLOS propagation which is described in Figure 1.1, where MT stands for moving target. The errors introduced by NLOS propagation are very large with respect to the error due to the sensor noise. We model

the measurements contaminated by NLOS errors as outliers here. For simplicity, many standard algorithms do not take into account NLOS propagation. These algorithms lose significantly in tracking accuracy when NLOS propagation occurs. Thus, algorithms that mitigate the affection of NLOS errors are required.

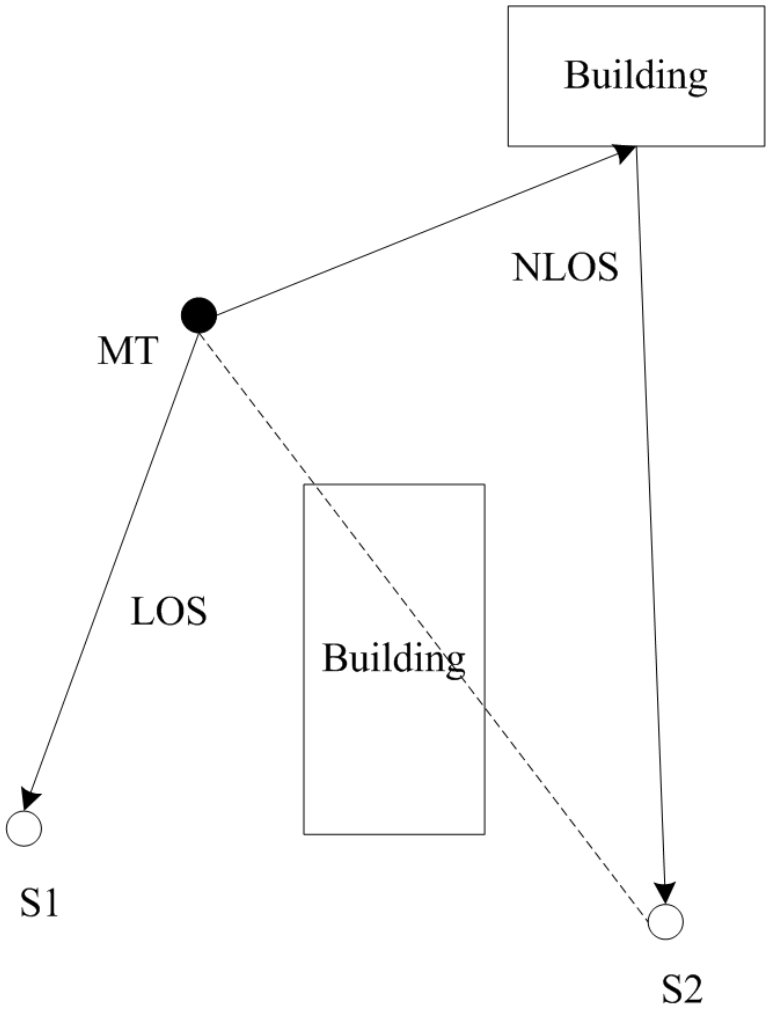

Figure 1.1: LOS and NLOS signal propagation

Target tracking in mixed LOS/NLOS environments has been of considerable interest over the past decades and several algorithms have been proposed to mitigate

the NLOS errors [8–33]. These tracking algorithms proposed for mixed LOS/NLOS measurements may be broadly grouped into two categories: those using the "estimation" approach and those using the "detection" approach.

In the class of "estimation" approach, tracking algorithms make use of the statistical properties of the LOS and NLOS noises and reconstruct the probability density function (pdf) of the mixed LOS/NLOS noise with an estimation procedure [8, 18–21]. They are robust in various NLOS error conditions but are not so efficient as their computational costs are high. A representative of these tracking algorithms is a semi-parametric modified residual algorithm proposed in [8]. In this algorithm, the mixed LOS/NLOS noise statistics are estimated non-parametrically for every set of observations. This algorithm greatly improved the tracking performance of the EKF even in severe NLOS error scenarios. However, additional computational cost has been introduced.

In the class of "detection" approach, tracking algorithms use either the residual or the prior knowledge of the NLOS error in the detection hypotheses according to statistical decision theory [14–16, 22, 23, 32, 34]. With a given threshold, LOS measurements are selected and NLOS contaminated measurements are discarded. One of the tracking algorithms in this category is the recent method based on modified probability data association (MPDA) presented in [22]. This method constructed different subgroups of time-of-arrival (TOA) measurements which were then combined to yield the final estimated position of the moving target. An advantage of this algorithm is that no assumption of any NLOS error model is required. Good performance can be obtained in mild NLOS error conditions. A limitation of the tracking algorithm in [22] is that it needs at least 3 LOS TOA measurements to calculate an LOS position of the moving target in a subgroup.

Hence, in severe NLOS conditions, it is likely that at many time instances, no subgroup is detected as LOS. As a result, no new measurement is available to update the Kalman filter (KF) and the predicted state of the moving target has to be used instead.

Measurement detection is the most popular method to detect and remove the NLOS contaminated measurements from all mixed LOS/NLOS measurements. The simplest detection algorithm is using a theoretical or an experimental bound to detect the measurement [35–40]. If the measurement is within the bound, it is considered as LOS. Otherwise, it is considered as NLOS.

In [35, 37], the measurement detection is done based on the property that the NLOS error is always positive. As the NLOS error is always positive, so the measured range is greater than the true range.

In [36, 38–40], an experimental value is used to detect whether the measurement is LOS or not. The detection criterion is set as follows,

$$r_m - \hat{r}_m < e_{\text{lim}}, \tag{1.1}$$

where $\hat{r}_m$ is the estimated range, and e_{lim} is the threshold set according to the prior knowledge of the tracking environments.

Measurement transformation approach is another popular NLOS mitigation way. It is more robust and reliable than measurement detection approach. Representative algorithms of this class can be summarized as follows.

1. In [41–46], the authors use the prior knowledge of the tracking context, i.e. the pdf and the occurrence probability of NLOS error to mitigate the tracking error deduced by NLOS error. This approach has several limitations, for

example, the prior knowledge of the tracking context is difficult to obtain and it cannot be used in real-time tracking cases. If the tracking context is changed, the tracking algorithms will lose efficiency.

2. Recently, an EKF semi-parametric estimator is proposed in [8, 47]. This estimator relies on transformation kernel density estimation (TKDE) of the noise pdf. As in mixed LOS/NLOS environments, the measurement noise is a mixture LOS/NLOS noise, and the TKDE is used to estimate the pdf of the mixture noise. This approach is able to achieve good performance even in severe NLOS scenarios at the cost of high computational cost.

1.2 Objectives

Although there has been significant progress in NLOS error mitigation, there still exist rooms for further improvements and new development, particularly in performance enhancement for tracking accuracy in NLOS scenarios, when the percentage of NLOS outliers increases. The objective of this thesis lies in achieving accurate position estimations in mixed LOS/NLOS environments while keeping computational complexity at a reasonable level.

To achieve this goal, we concentrate on the following aspects:

1. Detect LOS measurements from mixed LOS/NLOS measurements effectively. To remove the detrimental effects of NLOS errors, the simplest approach is to drop measurement contaminated by NLOS errors. Here we analyze the measurements one by one using a detector based on standard gating or dynamic gating. Measurements within the confidence region determined by

the gating are selected as LOS. Others are treated as NLOS.

2. Make good use of limited LOS measurements. When we remove the NLOS measurements, the number of available measurements is reduced. It means that we lose some of measurements. We have to make full use of the selected limited LOS measurements. Here, we propose to estimate a pseudo-measured position from each of individually selected LOS measurement. The average of the selected pseudo-measured position(s) is then used into a Kalman filter to update the tracking result.

3. To use some additional road information or other measurement information such as joint TOA/AOA to further improve the tracking accuracy.

1.3 Main Contributions

With the above motivations and objectives, we have carried out studies on algorithms to remove NLOS contaminated measurements. The main idea in our study is the proposed individual measurement estimator using one individual TOA or AOA measurement to calculate a pseudo-measured position of the moving target. The main contributions of this thesis are summarized as follows.

1. In Chapter 3, we first propose the idea of individual measurement detection for TOA measurements. The basic idea is that we detect each TOA measurement collected from different sensors separately at each time step using a standard gating or a dynamic gating. Only these selected LOS ones are reserved and then used into an EKF or a robust EKF to estimate the position of the moving target. By removing the NLOS error contaminated measure-

ments, the tracking accuracy of the IMD based EKF and the IMD based rEKF have been improved. The limitation of these tracking scheme is that the number of LOS TOA measurements must be equal to or greater than 3. Hence, in severe NLOS conditions, these tracking schemes do not work well.

2. In Chapter 4, we expand the standard gating based individual detection algorithm into the case of using TDOA measurements. In addition, the road constraint is used into the EKF and the rEKF to further improve the tracking accuracy in mixed LOS/NLOS environments.

3. In Chapter 5, we propose the individual measurement estimation and LOS detection (IMED) algorithm using TOA measurements. An approximated unbiased pseudo-measured position can be calculated by the individual measurement estimation algorithm. The average of the pseudo-measured position(s) can be used into a Kalman filter framework to update the tracking result. This algorithm can achieve good performance especially in severe NLOS conditions since it estimates a position of the moving target even with only one TOA measurement.

4. In Chapter 6, we expand the IMED algorithm into the case of AOA measurements. The joint TOA/AOA measurements and the IMED based KF is proposed to further improve the tracking accuracy. The pseudo-measured position estimated from each individual AOA measurements has been proved to be an approximately unbiased estimation of the true position of the moving target. So these pseudo-measured positions can be used into a KF. With the assistance of the additional AOA measurements, the joint TOA/AOA based tracking algorithm can achieve better performance than the tracking

algorithm proposed in Chapter 5 using TOA only.

Chapter 2

Fundamentals of Target Tracking

In this chapter estimation techniques and tracking algorithms based on different measurements such as TOA, AOA, and TDOA are presented.

First, we deal with the dynamic models, including the state evolution model and the measurement model, for the systems with one moving target and multiple stationary sensors. To specify the state evolution model of the moving target, continuous white noise acceleration model and continuous white process acceleration model [48] are employed. Second, we concentrate on state evolution model for evolution between the LOS state and NLOS state, which is assumed to be a two-state first order Markov chain. Then the classical tracking algorithms including the Kalman filter and the extended Kalman filter are reviewed.

2.1 System Models

In this section, the problem of the target tracking is presented. First, the state models, including the constant velocity and random force moving models of the

moving target, are given. Second, the measurement models for different techniques such as TOA, AOA and TDOA are shown. Then the classical tracking algorithms are reviewed.

2.1.1 State Models

The aim of target tracking is to estimate the state of a moving target sequentially by processing measured data. To specify this dynamic system, two models are needed: the state transition model and the measurement model.

The state transition equation, which defines the evolution of the state vector of the moving target, can be written as,

$$\mathbf{x}_k = \mathbf{f}_k\left(\mathbf{x}_{k-1}, \mathbf{v}_{k-1}\right), \tag{2.1}$$

where $\mathbf{x}_k \in \mathbb{R}^{n_x}$ is the state vector of the dynamic system, n_x is the dimensionality of the state space. $\mathbb{R}$ is the set of real numbers and $k \in \mathbb{N}$ is the time step. $\mathbf{f}\left(\cdot\right)$ is the transition function and $\mathbf{v}_{k-1}$ is the process noise. This is a first order Markov process, and so the probabilistic model of the state evolution $p\left(\mathbf{x}_k \left|\mathbf{x}_{k-1}\right.\right)$ can be induced from the state equation (2.1) when the process noise $\mathbf{v}_{k-1}$ is known.

The measurement model used to estimate $\mathbf{x}_k$ from measured data is defined as,

$$\mathbf{r}_k = \mathbf{h}_k\left(\mathbf{x}_k, \mathbf{w}_k\right), \tag{2.2}$$

where $\mathbf{h}\left(\cdot\right)$ is the measurement function based on the state $\mathbf{x}_k$, and $\mathbf{w}_k$ is the measurement noise. $\mathbf{r}_k \in \mathbb{R}^{n_r}$ is the measurement vector and n_r is the dimensionality of the measurement vector. The likelihood function based on equation (2.2) can

be written as $p(\mathbf{r}_k|\mathbf{x}_k)$. The measurement $\mathbf{r}_k$ is used to update the prior density to obtain the required posterior density of the current state.

2.1.1.1 Bayesian Estimation

From the Bayesian perspective, it is necessary to recursively calculate some degree of belief in the state $\mathbf{x}_k$ with measured data $\mathbf{r}_{1:k} = r_1, \cdots, r_k$ which is the sequence of all measurements up to time k. The aim of the Bayesian filtering problem is to construct the posterior state probability density function based on the previous measurements.

With given initial pdf $p(\mathbf{x}_0|\mathbf{r}_0) \equiv p(\mathbf{x}_0)$, where $\mathbf{r}_0$ is the set of no measurements, the pdf $p(\mathbf{x}_k|\mathbf{r}_{1:k})$ may be obtained recursively in two stages: prediction and update. Using the Chapman-Kolmogorov equation, the prediction step can be written as [49–51],

$$p(\mathbf{x}_k|\mathbf{r}_{1:k-1}) = \int p(\mathbf{x}_k|\mathbf{x}_{k-1}) p(\mathbf{x}_{k-1}|\mathbf{r}_{1:k-1})\, d\mathbf{x}_{k-1}, \tag{2.3}$$

and the update step can be written as

$$p(\mathbf{x}_k|\mathbf{r}_{1:k}) = \frac{p(\mathbf{r}_k|\mathbf{x}_k)\, p(\mathbf{x}_k|\mathbf{r}_{1:k-1})}{p(\mathbf{r}_k|\mathbf{r}_{1:k-1})}. \tag{2.4}$$

2.1.1.2 Continuous White Noise Acceleration Model

The continuous white noise acceleration model is also named as constant velocity (CV) model [48]. The details of this dynamic model are given as follows.

Considering a target moving with constant velocity, the following equations can

be used to describe its evolution over time

$$x_k = x_{k-1} + \dot{x}_{k-1}T, \tag{2.5}$$

$$\dot{x}_k = \dot{x}_{k-1}, \tag{2.6}$$

where x_k is the position of a moving target on direction x, $\dot{x}_{k-1}$ is the velocity of the target and T is the time interval. Considering a target moving in a $2D$ plane, the state vector can be organized as $\mathbf{x}_k = \begin{bmatrix} x_k & y_k & \dot{x}_k & \dot{y}_k \end{bmatrix}^T$, and the state-space evolution can be rewritten as

$$\mathbf{x}_k = \mathbf{F}\mathbf{x_{k-1}}, \tag{2.7}$$

where the transformation matrix $\mathbf{F}$ is,

$$\mathbf{F} = \begin{bmatrix} 1 & 0 & T & 0 \\ 0 & 1 & 0 & T \\ 0 & 0 & 1 & 0 \\ 0 & 0 & 0 & 1 \end{bmatrix} \tag{2.8}$$

When the target is moving in a noisy urban environment, the state-space evolution equation (2.7) is organized as

$$\mathbf{x}_k = \mathbf{F}\mathbf{x_{k-1}} + \mathbf{v_k}, \tag{2.9}$$

where $\mathbf{v}_k$ is assumed to be a zero mean Gaussian distributed process noise with covariance matrix $\mathbf{Q}^v$.

2.1.1.3 Continuous White Process Acceleration Model

The continuous white process acceleration model mentioned in [48] is also named as random force model in [8]. The details of this dynamic model are given as follows.

The state evolution equation of a target moving with random force describes is defined as follows

$$\mathbf{x}_k = \mathbf{F}\mathbf{x}_{k-1} + \mathbf{G}\mathbf{u}_{k-1}, \tag{2.10}$$

where the transition matrices $\mathbf{F}$ and $\mathbf{G}$ are defined as

$$\mathbf{F} = \begin{bmatrix} 1 & 0 & T & 0 \\ 0 & 1 & 0 & T \\ 0 & 0 & 1 & 0 \\ 0 & 0 & 0 & 1 \end{bmatrix}, \tag{2.11}$$

$$\mathbf{G} = \begin{bmatrix} \frac{1}{2}T^2 & 0 \\ 0 & \frac{1}{2}T^2 \\ T & 0 \\ 0 & T \end{bmatrix}, \tag{2.12}$$

and where T is the sampling time interval. The random force vector $\mathbf{u}_k = \begin{bmatrix} u_{1,k} & u_{2,k} \end{bmatrix}^{\mathrm{T}}$ is zero mean Gaussian distributed with covariance matrix $\mathbf{Q}^u$. This model is also mentioned as random force model in [8].

2.1.2 Measurement Models

In this subsection, the common measurement techniques and the corresponding measurement models are discussed.

2.1.2.1 Measurement Techniques

Typical measurements used for localization or tracking estimation include time-of-Arrival, time-difference-of-arrival and angle-of-arrival. TOA and TDOA are the most frequently used techniques because of their simplicity.

TOA measures the signal's arrival time between the moving target and the sensors or base stations in a completely synchronized network. Clock bias is introduced because of the unsynchronized mobile target. TDOA takes the differences of the signal's traveling time to eliminate the clock bias. Absolute distance or range can be calculated based on transmission time and speed of the signal.

AOA involves measurements of the signal arrival angle at a sensor or a base station. Measuring AOA requires the system to be equipped with an antennae array. The AOA measurements can be obtained using algorithms such as the MUSIC and ESPRIT [52, 53].

Figure 2.1 illustrates the geometric positioning of a moving target using AOA and TOA measurements. Here, we assume that a direct signal propagation path between the moving target and each of the sensor exists.

From Figure 2.1, it is easy to see that at least 2 AOA measurements or at least 3 TOA measurements are required to estimate the position of the moving target. To track the moving target using AOA, TOA or TDOA measurements, extended Kalman filter can be used.

However, if the assumption of an LOS signal propagation between the moving target and each of the sensor is not fulfilled, the tracking result can completely differ from the ones expected under the LOS assumption. This phenomenon is known as NLOS propagation. In practice, obstacles such as buildings, trees and hills in

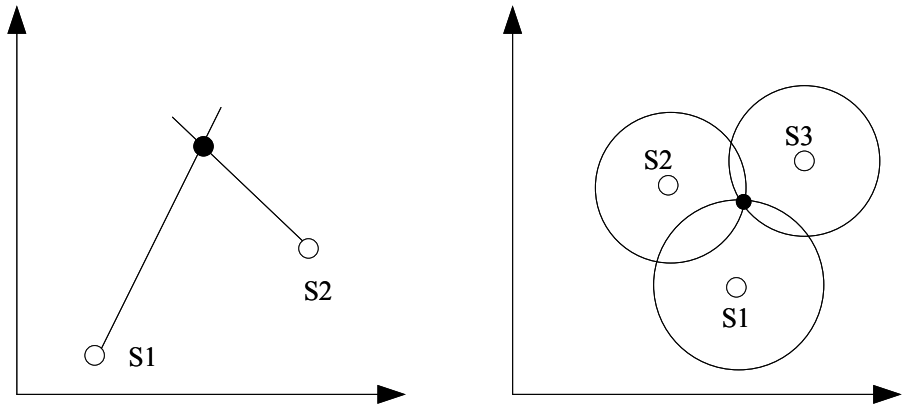

Figure 2.1: Geometric approaches for localization of AOA and TOA techniques

outdoor environments often prevent the signals from propagation along the direct path and reflection or refraction occur at these obstacles. Thus, the assumption of an LOS only environments for every sensor is ideal and not often encountered in practice. As noted earlier, this thesis focus on dealing with the tracking problems in mixed LOS/NLOS environments.

2.1.2.2 Measurement Models

The measurement model relates the state to the measurements as shown in equation (2.2). For different kind of measurements, the function $\mathbf{h}(\cdot)$ is different. Supposed that the positions of sensors are $\left(x_m^S, y_m^S,\right)$ $m = 1, \cdots M$, (x, y) is the position of the target, and $d_m = \sqrt{(x - x_m^S)^2 + (y - y_m^S)^2}$. The measurement functions related to some measurements are shown in Table 2.1.

2.1.2.3 Error Models

In the following discussion we consider processing at time step k. Hence, for simplicity, the subscript k is dropped. In mixed LOS and NLOS environments, we treat the NLOS errors as statistical noise incorporated into the measurement noise

Table 2.1: Measurement functions.

Methods	Measurements	Measurement Function $h_m(\cdot)$
TOA	range	d_m
TDOA	difference of range	$d_m - d_n$
AOA	arrival angle	$\frac{180}{\pi} \arctan \frac{(y-y_m^S)}{(x-x_m^S)} \pm 90^0$

of the measurement model. The measurement equation (2.2) is rewritten as,

$$\mathbf{r} = \mathbf{d} + \boldsymbol{\eta}, \tag{2.13}$$

where the random vector $\mathbf{r}$ is the measurement vector and $\mathbf{d}$ is the noise free distance vector between the target and sensors. The noise vector, $\boldsymbol{\eta} = \begin{bmatrix} \eta_1 & \cdots & \eta_M \end{bmatrix}^{\mathrm{T}}$ is a mixture LOS and NLOS noise.

For each sensor measurement, the measured range can be described as

$$r_m = d_m + \eta_m, \quad m = 1, \cdots, M, \tag{2.14}$$

where η_m is the measurement noise at each sensor m. The probability density function for η_m is

$$p(\eta_m) = (1 - \varepsilon_m) p_{\mathrm{LOS}}(\eta_m) + \varepsilon_m p_{\mathrm{NLOS}}(\eta_m) \tag{2.15}$$

where ε_m is the probability of contamination by NLOS errors at sensor m. The noise is effectively a mixture of LOS and NLOS noise where $p_{\mathrm{LOS}}(\eta_m)$ is zero mean Gaussian distributed and $p_{\mathrm{NLOS}}(\eta_m)$ is mean-shifted Gaussian or Exponentially distributed [3]. To simulate this mixture of LOS and NLOS noise distribution,

we employ a first order Markov process as shown in Figure 2.2. The transition probability matrix of this Markov process is

$$\begin{bmatrix} 1-\alpha & \alpha \\ \beta & 1-\beta \end{bmatrix} \tag{2.16}$$

where α is the transition probability from state LOS to NLOS and β is the transition probability from state NLOS to LOS.

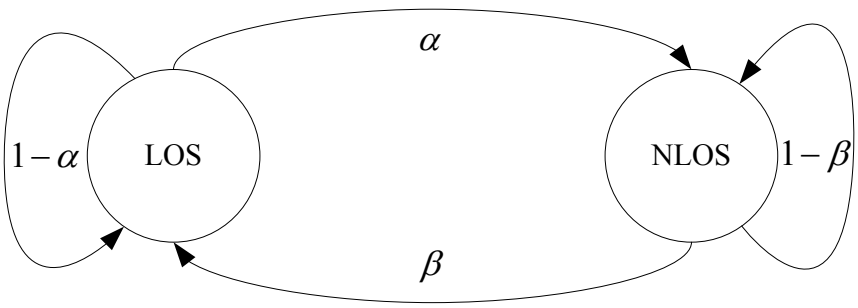

Figure 2.2: First order Markov process

Since the Markov chain is irreducible, recurrent and aperiodic, it admits an invariant distribution which gives our noise mixture of interest. The invariant distribution is related to ε_m in (2.15) by

$$\varepsilon_m = \frac{\alpha}{\alpha + \beta} \tag{2.17}$$

The complete distribution of (2.15) is generated with samples of $p_{\text{LOS}}(\eta_m)$ or $p_{\text{NLOS}}(\eta_m)$ respectively at each state.

2.2 Classical Tracking Algorithms

In this section, the classical tracking algorithms such as the Kalman filter and the extended Kalman filter are reviewed.

2.2.1 Kalman Filter

The Kalman Filter is the optimal Minimum Mean Square Error (MMSE) state estimator for linear Gaussian stochastic systems. Suppose that the posterior density at every time step is a Gaussian distribution parameterized by a mean and a covariance function. Also, the process noise and measurement noise are assumed to be zero mean Gaussian distributed. The initial state $p(x_0)$ is also assumed to be a zero mean Gaussian random vector with certain initial covariance matrix. It is well known that if $p(\mathbf{x}_{k-1}|\mathbf{r}_{1:k-1})$ is Gaussian, then $p(\mathbf{x}_k|\mathbf{r}_{1:k})$ is also Gaussian. The KF algorithm derived from equation (2.3) and (2.4) can be written as the following recursive relationships

$$p(\mathbf{x}_{k-1}|\mathbf{r}_{1:k-1}) = \mathcal{N}\left(\mathbf{x}_{k-1}; \mathbf{m}_{k-1|k-1}, \mathbf{P}_{k-1|k-1}\right), \tag{2.18}$$

$$p(\mathbf{x}_k|\mathbf{r}_{1:k-1}) = \mathcal{N}\left(\mathbf{x}_k; \mathbf{m}_{k|k-1}, \mathbf{P}_{k|k-1}\right), \tag{2.19}$$

$$p(\mathbf{x}_k|\mathbf{r}_{1:k}) = \mathcal{N}\left(\mathbf{x}_k; \mathbf{m}_{k|k}, \mathbf{P}_{k|k}\right), \tag{2.20}$$

where $\mathcal{N}(\mathbf{x}; \mathbf{m}, \mathbf{P})$ is a Gaussian distribution with argument $\mathbf{x}$, mean $\mathbf{m}$ and covariance $\mathbf{P}$ defined as

$$\mathbf{P}_k = \mathbb{E}\left((\mathbf{x}_k - \mathbf{m}_k)(\mathbf{x}_k - \mathbf{m}_k)^T\right). \tag{2.21}$$

The measurement equation of a linear system is

$$\mathbf{r}_k = \mathbf{H}\mathbf{x}_k + \mathbf{w}_k, \tag{2.22}$$

where $\mathbf{H}$ is the transition matrix, $\mathbf{w}$ is the measurement noise with covariance matrix $\mathbf{R}$.

The prediction step of KF is shown as follows

$$\hat{\mathbf{x}}_k^- = \mathbf{F}\hat{\mathbf{x}}_{k-1} + \mathbf{v}_{k-1}, \tag{2.23}$$

$$\mathbf{P}_k^- = \mathbf{F}\mathbf{P}_k\mathbf{F}^T + \mathbf{Q}^v, \tag{2.24}$$

where $\hat{\mathbf{x}}_k^-$ and $\mathbf{P}_k^-$ are the predicted state and the predicted covariance matrices, respectively.

The update step of KF is shown as follows

$$\mathbf{K}_k = \mathbf{P}_k^-\mathbf{H}^T\left(\mathbf{H}\mathbf{P}_k^-\mathbf{H}^T + \mathbf{R}\right)^{-1}, \tag{2.25}$$

$$\hat{\mathbf{x}}_k = \hat{\mathbf{x}}_k^- + \mathbf{K}_k\left(\mathbf{r}_k - \mathbf{H}\hat{\mathbf{x}}_k^-\right), \tag{2.26}$$

$$\mathbf{P}_k = \left(\mathbf{I} - \mathbf{K}_k\mathbf{H}\right)\mathbf{P}_k^-, \tag{2.27}$$

where $\mathbf{P}_k$ is the state covariance matrix. $\mathbf{K}_k$ is the Kalman Gain matrix which corrects the predicted prior state pdf for deriving the posterior. $\mathbf{I}$ stands for an identical matrix.

2.2.2 Extended Kalman Filter

The Extended Kalman Filter (EKF) is a variant of the KF for non-linear systems. It is based on the Taylor expansion. The EKF is the most well-studied and widely used nonlinear tracking algorithm.

The nonlinear state transition and measurement equations are as following

$$\mathbf{x}_k = \mathbf{f}_k\left(\mathbf{x}_{k-1}\right) + \mathbf{v}_{k-1}, \tag{2.28}$$

$$\mathbf{r}_k = \mathbf{h}_k\left(\mathbf{x}_k\right) + \mathbf{w}_k, \tag{2.29}$$

where the functions $\mathbf{f}\left(\cdot\right)$ and $\mathbf{h}\left(\cdot\right)$ are continuously differentiable nonlinear functions of the state. The EKF linearizes the state transition function with a first-order Taylor expansion at the previous estimated state. Similarly, the measurement function is also linearized.

The prediction step of the EKF is shown as follows

$$\hat{\mathbf{F}}_{k-1} = \frac{\partial \mathbf{f_{k-1}}\left(\mathbf{x_k}\right)}{\partial \mathbf{x}_k}\Big|_{\mathbf{x}_k=\hat{\mathbf{x}}_{k-1}}, \tag{2.30}$$

$$\hat{\mathbf{x}}_k^- = \mathbf{f}_{k-1}\left(\hat{\mathbf{x}}_{k-1}\right), \tag{2.31}$$

$$\mathbf{P}_k^- = \hat{\mathbf{F}}_{k-1}\mathbf{P}_{k-1}\hat{\mathbf{F}}_{k-1}^T + \mathbf{Q}^v, \tag{2.32}$$

The update step of the EKF is shown as follows

$$\hat{\mathbf{H}}_k = \frac{\partial \mathbf{h_k}\left(\mathbf{x_k}\right)}{\partial \mathbf{x}_k}\Big|_{\mathbf{x}_k=\hat{\mathbf{x}}_k^-}, \tag{2.33}$$

$$\mathbf{K}_k = \mathbf{P}_k^- \hat{\mathbf{H}}_k^T \left(\hat{\mathbf{H}}_k \mathbf{P}_k^- \hat{\mathbf{H}}_k^T + \mathbf{R}\right)^{-1}, \tag{2.34}$$

$$\hat{\mathbf{x}}_k = \hat{\mathbf{x}}_k^- + \mathbf{K}_k\left(\mathbf{r}_k - \mathbf{h}_k\left(\hat{\mathbf{x}}_k^-\right)\right), \tag{2.35}$$

$$\mathbf{P}_k = \left(\mathbf{I} - \mathbf{K}_k \hat{\mathbf{H}}_k\right)\mathbf{P}_k^-. \tag{2.36}$$

where $\hat{\mathbf{F}}_{k-1}$ and $\hat{\mathbf{H}}_k$ are the Jacobian matrices of the nonlinear functions $\mathbf{f}(\cdot)$ and $\mathbf{h}(\cdot)$ evaluated respectively at $\hat{\mathbf{x}}_{k-1}$ and $\hat{\mathbf{x}}_k$. The EKF is approximated using the Taylor expansion. It is not strictly unbiased estimation algorithm.

2.3 Conclusion

In this chapter, we discuss the fundamental techniques and algorithms related to target tracking. Some measurement techniques and the classical tracking algorithms such as Kalman filter and extended Kalman filter are introduced. The error models are also presented. In the following chapters, we propose new tracking schemes base on these techniques and algorithms.

Chapter 3

Measurement Detection and Dynamic Tracking Schemes using TOA Measurements

In this chapter, the standard gating based TOA detection approach and the individual measurement detection algorithm for determining the LOS measurements are presented. Based on these detection approaches, the EKF and the robust EKF based tracking schemes are proposed.

3.1 Introduction

Time-of-arrival is an important and popular technique in target tracking. Several research work on TOA and target tracking have been proposed in the past decades. The major sources of error in TOA measurements are measurement noise and non-line-of-sight (NLOS) signal propagation. The measurement noise is usually

modeled as a zero mean Gaussian random variable, while the NLOS error usually has an unknown distribution with a positive mean, which is usually assumed to be a mean-shifted Gaussian distribution or an exponential distribution [8] since any indirect propagation path is always longer than the direct one. Compared with the measurement noise, the NLOS error causes severe degradation of the tracking accuracy.

In this chapter, gating based measurement detection approaches are proposed to detect LOS measurements from all mixed LOS/NLOS measurements. The standard gating based detection algorithm is based on the statistical properties of the LOS measurements. It uses the 3σ confidence region to detect measurements separately every time step. Only these fall into the 3σ confidence region are considered as LOS while others are considered as NLOS and dropped.

The dynamic gating based individual measurement detection approach is also presented in this chapter. TOA measurements are employed and the LOS measurements are detected by the proposed IMD approach at each time step. The LOS TOA measurements are selected and stored in a dynamic data array while the NLOS TOA measurements are discarded.

After detection the LOS measurements from all mixed LOS/NLOS measurements, the EKF or the rEKF are then used to track the moving target using the selected LOS measurements. Simulation results have given to demonstrate the performance of the proposed detection algorithm and the corresponding dynamic tracking schemes. In mixed LOS/NLOS environments, they do perform better than the standard tracking algorithms especially in mild NLOS conditions.

The rest of this chapter is organized as follows. The individual measurement detection algorithm based on standard gating for TOA measurements is described

in Section 3.2. The proposed dynamic individual measurement detection algorithm is presented in Section 3.3. Corresponding the EKF and the rEKF are shown in Section 3.4 and Section 3.5, respectively. Simulation results are given in Section 3.6. Conclusions are drawn in Section 3.7.

3.2 Gating Based Detection

We discuss the detection problem of the TOA measurements from the generalized likelihood ratio test which is given as follows.

3.2.1 Generalized Likelihood Ratio Test

Here, we consider a dynamic system consisting of one moving target under random force and M stationary sensors, which are employed to collect TOA measurements. The state of the moving target at time step $k\,(k = 1, \cdots, K)$ is denoted as $\mathbf{x}_k = \begin{bmatrix} x_k & y_k & \dot{x}_k & \dot{y}_k \end{bmatrix}^T$, containing the instantaneous position (x_k, y_k) and the instantaneous speed $(\dot{x}_k, \dot{y}_k)$. Stationary sensors are located at $\left(x_m^S, y_m^S\right), m = 1, \cdots, M$.

To analyze and make inferences about the dynamic system, the state space model, which consists of a state evolution equation and a measurement equation, is required. The state evolution equation describes the evolution of the state over time and the measurement equation represents the relationship between the state and the measured data. The state space model of the dynamic system is defined in Chapter 2, Section 2.1.3. The measurement noise model in mixed LOS/NLOS environments is described in Chapter 2, Section 2.2.3.

Generalized likelihood ratio test (GLRT) is a very useful and powerful math-

ematical method in statistical signal processing. To make use of the GLRT to analyze the tracking problem in mixed LOS/NLOS environments, we assume that the pdf of NLOS error is a mean-shifted Gaussian distribution with known mean μ_N and standard deviation σ_N. The LOS measurement noise is a zero mean Gaussian distribution with standard deviation σ_L. Two hypothesis tests are proposed as follows

$$\begin{aligned} H_0 &: r_m - \hat{r}_m \sim \mathcal{N}(\mu_N, \sigma_N), \\ H_1 &: r_m - \hat{r}_m \sim \mathcal{N}(0, \sigma_L), \end{aligned} \tag{3.1}$$

where r_m denotes the measurement collected by the stationary sensor m and $\hat{r}_m$ stands for the predicted measurement which is calculated using the predicted state of the moving target and the measurement function.

The detector decides H_1 if the likelihood ratio exceeds a threshold

$$L(x) = \frac{p(x, H_1)}{p(x, H_0)} > \gamma, \tag{3.2}$$

where $x = r_m - \hat{r}_m$.

Since

$$p(x, H_0) = \frac{1}{\sqrt{2\pi}\sigma_N} \exp\left(-\frac{1}{2\sigma_N^2}(x - \mu_N)^2\right), \tag{3.3}$$

$$p(x, H_1) = \frac{1}{\sqrt{2\pi}\sigma_L} \exp\left(-\frac{1}{2\sigma_L^2}x^2\right), \tag{3.4}$$

we have

$$L(x) = \frac{\sigma_N}{\sigma_L} \exp\left(-\frac{1}{2\sigma_L^2}(x)^2 + \frac{1}{2\sigma_N^2}(x-\mu_N)^2\right) > \gamma \tag{3.5}$$

The false alarm probability is defined as

$$\begin{aligned} P_{FA} &= P(H_1; H_0) = \Pr(x > \gamma; H_0) \\ &= \int_{-\infty}^{\gamma} \frac{1}{\sqrt{2\pi}\sigma_N} \exp\left(-\frac{1}{2\sigma_N^2}(t-\mu_N)^2\right) dt \\ &= Q\left(\frac{x-\mu_N}{\sigma_N}\right). \end{aligned} \tag{3.6}$$

For example, the LOS noise on each sensor is assumed to be $\mathcal{N}(0, 150)$ and the NLOS on the sensor is $\mathcal{N}(400, 1400)$. The optimal threshold for a GLRT, which is when the false alarm equals to the false reject as shown in Figure 3.1, is about $402m$. The calculated false alarm rate is 0.0025. More results calculated under different pdfs of NLOS error are summarized in Table 3.1.

3.2.2 Standard Gating Detection

Since the pdf of NLOS is unknown in practice. The GLRT algorithm and the calculated optimal threshold cannot be implemented. We propose a standard gating, which is determined by the standard deviation of the LOS noise, to replace GLRT. Usually the standard deviation of LOS noise on each sensor is easy to obtain and it is always used as a known parameter in the tracking algorithm.

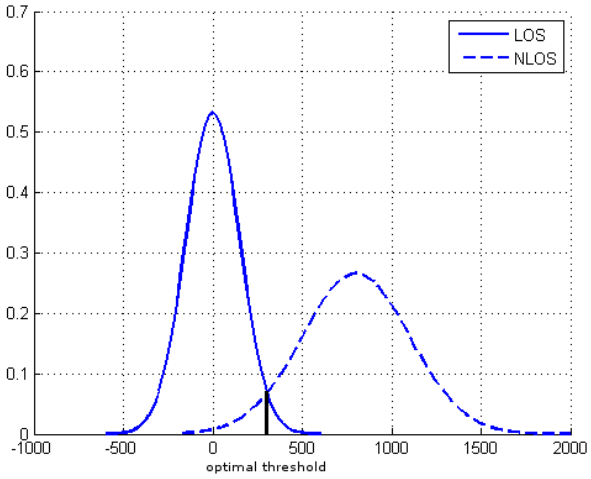

Figure 3.1: Optimal threshold for LOS $\mathcal{N}(0, 150)$ and NLOS $\mathcal{N}(400, 1400)$.

To detect LOS TOA measurements, two hypotheses are proposed

$$H_0 \quad : \quad r_{m,k} \in CR_{m,k}, \tag{3.7}$$

$$H_1 \quad : \quad r_{m,k} \notin CR_{m,k}, \tag{3.8}$$

where $CR_{m,k}$ stands for the $3\sigma_L$ confidence region which is determined by the LOS TOA measurement noise. If hypothesis H_0 is correct, the measurement is considered as LOS, otherwise as NLOS. In real applications, it is impossible to obtain the noise-free range vector. So the prediction range vector, calculated from the measurement equation, is used as an alternative.

To evaluate the performance of the standard gating based hypothesis tests, numerical studies were performed under different pdfs of LOS noise and NLOS errors. Results of these are summarized in Table 3.1.

The difference between the theoretical false alarm probability calculated by

Table 3.1: False Alarm Probability given by GLRT and standard gating detections

Gaussian (μ_N, σ_N)	$(800, 400)$	$(1000, 400)$	$(1200, 400)$	$(1400, 400)$
	Gaussian $(\mu_L, \sigma_L) = (0, 100)$			
Threshold	192m	226m	262m	299m
FA-GLRT	0.066	0.027	0.0096	0.003
FA-SG	0.106	0.040	0.012	0.003
	Gaussian $(\mu_L, \sigma_L) = (0, 150)$			
Threshold	253m	301m	350m	402m
FA-GLRT	0.085	0.040	0.017	0.0062
FA-SG	0.19	0.085	0.031	0.0089

the GLRT and the simulated results calculated by the standard gating is very small. Thus, we can use the standard gating based detection approach into some applications with multiple sensor networks to simplify the detection algorithm.

3.3 Individual Measurement Detection

In this section, we propose a dynamic gating based individual measurement detection (IMD) approach to decide whether an individual TOA measurement is LOS or NLOS. To implement the IMD algorithm, we first use the one-dimension TOA measurement to estimate a two-dimension pseudo position of the moving target. Then, the error covariance of the state vector is used to give a dynamic gating to detect whether the mapped position is LOS or not.

In the IMD algorithm, the dynamic gating is calculated at every time step to select the LOS measurements while the standard gating is a fixed gating. The advantage of using a dynamic gating is that the detection region is adjusted according to the estimated state and the related error covariance matrix. With the converging of the EKF, the detection region will converge. When using the standard gating based method, the detection region remains the same during the whole tracking period.

The details of the proposed IMD algorithm are given in the following sections.

3.3.1 Measurement Estimation

In the absence of noise, an accurate estimation of the position of the moving target can be obtained using geometric equations. For a TOA measurement, which is usually deemed as a range measurement, each measurement gives a certain range which determines a circle centered at the sensor. Three circles fix one intersection which is the estimated position of the moving target.

In the presence of measurement noises, the individual measurement function for each sensor m is

$$r_m = d_m + w_m = h_m(\mathbf{x}) + w_m, \tag{3.9}$$

where w_m is the measurement LOS noise on sensor m. For a TOA measurement, $h_m(\mathbf{x})$ is given by

$$h_m(\mathbf{x}) = \sqrt{(x - x_m^S)^2 + (y - y_m^S)^2}, \tag{3.10}$$

It is observed from the above expression that $h_m(\mathbf{x})$ depends on the position (x, y) only. Hence, to estimate the position of the moving target using a geometric approach, we focus on a sub-vector of the state vector instead of the state vector itself. That is, we let $\mathbf{x}_m^p := [\ x_m \quad y_m\ ]^T$. From (3.9) and (3.10), it can be seen that a given measurement r_m is associated with the set of points $\mathbf{x}_m^p$ that satisfy

$$\left(x_m - x_m^S\right)^2 + \left(y_m - y_m^S\right)^2 = r_m^2. \tag{3.11}$$

In fact, these points form a circle centered at (x_m^S, y_m^S) with radius r_m. To determine which point in this circle is the most likely estimated position, we

next use the state evolution model to obtain the predicted state vector $\hat{\mathbf{x}}_k^- = [\ x_k^- \quad y_k^- \quad \dot{x}_k^- \quad \dot{y}_k^-\ ]^T$. Similar to the definition of $\mathbf{x}_m^p$, we define $\hat{\mathbf{x}}_k^{p,-} := [\ x_k^- \quad y_k^-\ ]^T$ which gives the predicted position from the predicted state vector of the moving target. The key idea of the IMD approach is to determine the point in the circle that is closest to $\mathbf{x}_m^p$ as shown in Figure 3.2. This can be formulated as a constrained optimization in the following

$$\hat{\mathbf{x}}_m^p = \underset{\mathbf{x}_m^p}{\arg\min} \left\| \mathbf{x}_m^p - \hat{\mathbf{x}}_k^{p,-} \right\|_{\ell^2}, \tag{3.12}$$

subject to the constraint given in (3.11). Note that $\|\cdot\|_{\ell^2}$ stands for the ℓ^2 norm.

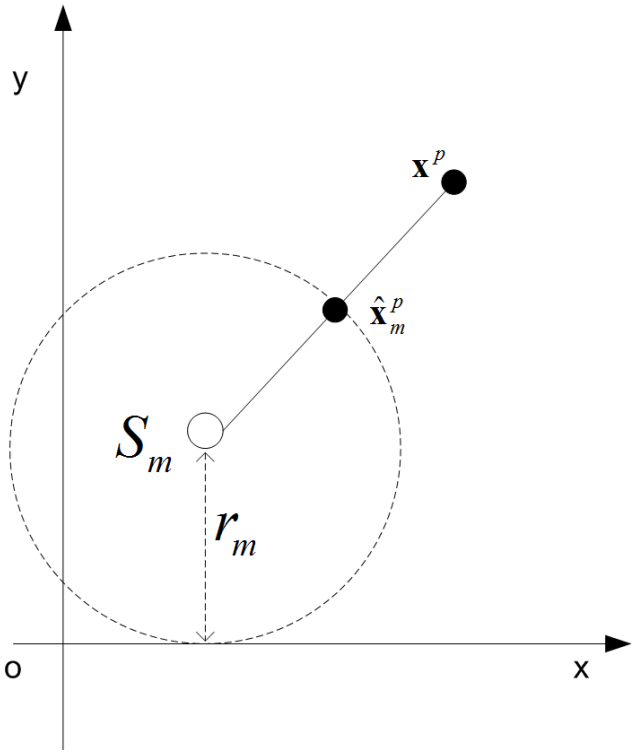

Figure 3.2: Determination of $\hat{\mathbf{x}}_m^p$.

The solution $\hat{\mathbf{x}}_m^p$ can be obtained easily by using a geometrical approach outlined briefly here. $\hat{\mathbf{x}}_m^p$ is just the crossing point of the circle centered at (x_m^S, y_m^S) with radius r_m and the straight line linking the prediction position $\hat{\mathbf{x}}_k^{p,-}$ of the moving target and the sensor.

The measurement error is not taken into account in determining $\mathbf{x}_m^p$, because $\mathbf{x}_m^p$ is determined under the condition that if this TOA sens or measurement were LOS, then other TOA sensor LOS measurements would all geometrically intersect (Range circles) about this point.

Once the derived measurement position from each individual measurement is determined, the next step is to decide whether the derived measurement position is LOS or NLOS. This is presented in the following subsection.

3.3.2 Measurement Detection

In this subsection, we present a new method for detecting a LOS measurement from the position estimated from an individual measurement.

We begin with a general discussion so that it will become clear that the proposed IMD approach is applicable to a wide range of scenarios not just restricted to the specific problem considered here. Consider the general system model and assume that the probability density function of the state vector is Gaussian with the following distribution

$$p\left(\mathbf{x}_k \left| \mathbf{r}_{1:k-1} \right.\right) = \mathcal{N}\left(\mathbf{x}_k; \hat{\mathbf{x}}_{k|k-1}, \mathbf{P}_{k|k-1}\right), \tag{3.13}$$

where $\mathbf{x}_k$ is the state vector of the moving target at time step k, $\mathcal{N}(\mathbf{x}; \mathbf{m}, \mathbf{P})$ denotes a Gaussian distribution with argument $\mathbf{x}$, mean $\mathbf{m}$ and covariance matrix $\mathbf{P}$. The

mean is calculated by the state evolution equation (2.1)

$$\hat{\mathbf{x}}_k^- = \mathbf{f}\left(\hat{\mathbf{x}}_{k-1}\right), \tag{3.14}$$

and the covariance is calculated by

$$\mathbf{P}_k^- = \hat{\mathbf{F}}_k \mathbf{P}_{k-1} \hat{\mathbf{F}}_k^T + \mathbf{Q}^v. \tag{3.15}$$

From equation (3.13), a confidence region $v_k(\gamma)$ can be determined,

$$v_k(\gamma) = \left\{ \mathbf{x} : \left[\mathbf{x} - \hat{\mathbf{x}}_k^-\right]^T \mathbf{P}_k^{-1} \left[\mathbf{x} - \hat{\mathbf{x}}_k^-\right] \leq \gamma \right\}, \tag{3.16}$$

where γ is the gate threshold for determining the size of the confidence region. The volume of the confidence region V_k is

$$V_k = c_{n_x} \left|\gamma \mathbf{P}_k^-\right|^{\frac{1}{2}} = c_{n_x} \gamma^{\frac{n_x}{2}} \left|\mathbf{P}_k^-\right|^{\frac{1}{2}}, \tag{3.17}$$

where $|A|$ denotes the determinant of matrix A. The coefficient c_{n_x} is defined as the volume of the n_x-dimensional unit hypersphere which depends on the dimension of the measurement, for example, $c_1 = 2, c_2 = \pi, c_3 = \frac{4}{3}\pi$, etc. The main purpose of introducing the confidence region is to use it to differentiate whether an updated state vector based on new measurements is close enough to the state vector predicted in the previous step.

In our specific problem of deciding whether the obtained derived measurement positions $\hat{\mathbf{x}}_m^p$ of the moving target are LOS or NLOS, we also use the concept of the confidence region. Since each of the derived measurement positions contains only

two elements describing the x and y position of the moving target, the confidence region becomes

$$v_k(\gamma) = \left\{ \mathbf{x} : \left[\mathbf{x} - \hat{\mathbf{x}}_k^{p,-}\right]^T \left(\mathbf{P}_k^{p,-}\right)^{-1} \left[\mathbf{x} - \hat{\mathbf{x}}_k^{p,-}\right] \leq \gamma \right\}, \tag{3.18}$$

where

$$\mathbf{P}_k^{p,-} = \begin{bmatrix} \sigma_{x,k}^2 & \rho_k \sigma_{x,k} \sigma_{y,k} \\ \rho_k \sigma_{x,k} \sigma_{y,k} & \sigma_{y,k}^2 \end{bmatrix}, \tag{3.19}$$

with $\sigma_{x,k}$ and $\sigma_{y,k}$ being the standard deviations of the position estimates on the x axis and y axis, respectively, and $0 \leq \rho_k < 1$ being the correlation coefficient.

Let $\mathbf{P}_k^- = \mathbf{P}_k^{p,-}$ and $n_x = 2$ in (3.17), the area of the confidence region is calculated as

$$V_k = c_2 \left|\gamma \mathbf{P}_k^{p,-}\right|^{\frac{1}{2}} = \pi\gamma \left|\mathbf{P}_k^{p,-}\right|^{\frac{1}{2}} = \pi\gamma\sigma_{x,k}\sigma_{y,k}\sqrt{1-\rho_k^2}. \tag{3.20}$$

For a given threshold γ, the confidence region determined by equation (3.18) is an ellipse in general as shown in Figure 3.3, here we assume $\rho_k = 0$. In the special case where $\rho_k = 0$, $\sigma_{x,k} = \sigma_{y,k}$, and with $\gamma = 9$, the confidence region becomes a circle with a radius of $3\sigma_{x,k}$. This circular confidence region is just the 3σ confidence region determined by a 2-D Gaussian distribution centered at $\hat{\mathbf{x}}_k^{p,-}$. With the confidence region defined in (3.18), now if a derived measurement position falls into this confidence region, it is considered as LOS and the corresponding TOA measurement is then stored. Otherwise, it is considered as a measurement contaminated by NLOS error and hence dropped. This process is repeated for each of the M measurements at time step k, for $k = 1, 2, \ldots$.

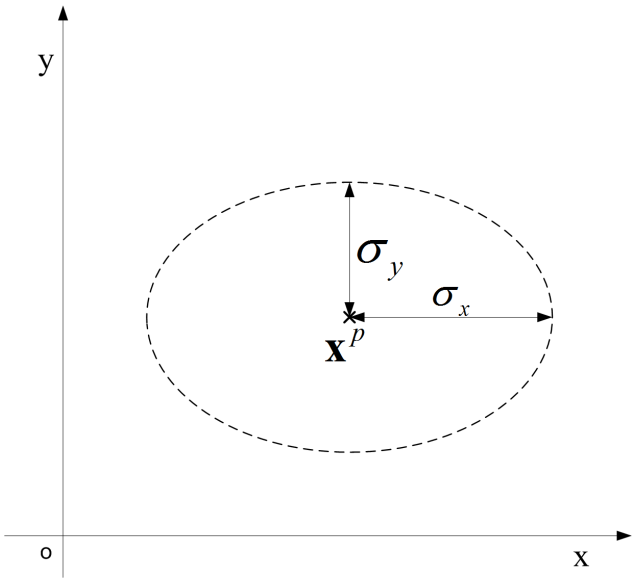

Figure 3.3: Confidence region.

At time step k, if all of the measurements are LOS, the corresponding derived measurement positions are all LOS and they fall in the confidence region. In the mixed LOS/NLOS environments, some of the measurements are LOS while others are NLOS. Hence, only the derived measurement positions associated with LOS fall into the confidence region, while others fall outside the confidence region.

At the end of the individual measurement detection at each time step k, all the LOS measurements are stored and this set is denoted as,

$$\mathbf{r}_{m_k} = \{r_{j,k}\}_{j=1}^{m_k}, \tag{3.21}$$

where $r_{j,k}$ is the LOS measurement j and m_k is the total number of LOS measurements at time step k. Note that in the LOS environment, m_k is a static value determined by the number of sensors M, but in the mixed LOS/NLOS environments, the value of $m_k \leq M$ is dynamic and it is determined by the total number

of LOS measurements detected at each time step k.

After detecting LOS measurements from all mixed LOS/NLOS measurements, the selected LOS measurements are then used into an EKF or a robust EKF. The tracking schemes will be discussed in detail as follows.

3.4 The IMD based Extended Kalman Filter

After detecting each of the measurements, only selected LOS ones are reserved. They are then used into an EKF, described in the following section, to track the moving target.

At each time step k, after measurement detection, an LOS measurement vector is obtained, which has a dynamic dimension. Using these LOS measurements, target tracking can be done with an EKF or a rEKF tracking algorithms. The prediction and update equations of the EKF are summarized as follows

$$\hat{\mathbf{x}}_k^- = \mathbf{F}\hat{\mathbf{x}}_{k-1}, \tag{3.22}$$

$$\mathbf{P}_k^- = \mathbf{F}\mathbf{P}_{k-1}\mathbf{F}^T + \mathbf{G}\mathbf{Q}_{k-1}\mathbf{G}^T, \tag{3.23}$$

$$\mathbf{K}_k = \mathbf{P}_{k^-}\mathbf{H}_{m_k}^T\left(\mathbf{H}_{m_k}\mathbf{P}_k^-\mathbf{H}_{m_k}^T + \mathbf{R}_{m_k}\right)^{-1}, \tag{3.24}$$

$$\hat{\mathbf{x}}_k = \hat{\mathbf{x}}_k^- + \mathbf{K}_k\mathbf{i}_{m_k}, \tag{3.25}$$

$$\mathbf{P}_k = \left(\mathbf{I} - \mathbf{K}_k\mathbf{H}_{m_k}\right)\mathbf{P}_k^-. \tag{3.26}$$

Since we use TOA measurements in this chapter, the measurement function $\mathbf{h}_{m_k}(\mathbf{x_k})$

is expressed as

$$\mathbf{h}_{m_k}(\mathbf{x}_k) = \begin{bmatrix} \sqrt{(x_k - x_1^S)^2 + (y_k - y_1^S)^2} \\ \vdots \\ \sqrt{\left(x_k - x_{m_k}^S\right)^2 + \left(y_k - y_{m_k}^S\right)^2} \end{bmatrix}. \tag{3.27}$$

The EKF linearizes the nonlinear function $\mathbf{h}_{m_k}(\cdot)$ using the first order Taylor expansion. At time step k, $\mathbf{h}_{m_k}(\mathbf{x}_k)$ is approximated around the predicted state $\hat{\mathbf{x}}_k^- = \mathbf{F}\hat{\mathbf{x}}_{k-1}$ as follows

$$\mathbf{h}_{m_k}(\mathbf{x}_k) = \mathbf{h}_{m_k}(\hat{\mathbf{x}}_k^-) + \frac{\partial \mathbf{h}_{m_k}(\mathbf{x_k})}{\partial \mathbf{x_k}}\Big|_{\mathbf{x_k}=\hat{\mathbf{x}}_k^-} \left(\mathbf{x}_k - \hat{\mathbf{x}}_k^-\right). \tag{3.28}$$

In the EKF, the partial derivative of $\mathbf{h}_{m_k}(\mathbf{x})$ with respect to the variable $\mathbf{x} = [\ x \quad y \quad \dot{x} \quad \dot{y}\ ]^T$, denoted by the Jacobian matrix, is given as

$$\begin{aligned} \mathbf{H}_{m_k}(\mathbf{x}) &:= \frac{\partial \mathbf{h}_{m_k}(\mathbf{x})}{\partial \mathbf{x}} \\ &= \begin{bmatrix} \frac{\partial h_{1,k}(\mathbf{x})}{\partial x} & \frac{\partial h_{1,k}(\mathbf{x})}{\partial y} & 0 & 0 \\ \vdots & \vdots & \vdots & \vdots \\ \frac{\partial h_{m_k,k}(\mathbf{x})}{\partial x} & \frac{\partial h_{m_k,k}(\mathbf{x})}{\partial y} & 0 & 0 \end{bmatrix}. \\ &= \begin{bmatrix} \frac{x - x_1^S}{\sqrt{\left(x-x_1^S\right)^2 + \left(y-y_1^S\right)^2}} & \frac{y - y_1^S}{\sqrt{\left(x-x_1^S\right)^2 + \left(y-y_1^S\right)^2}} & 0 & 0 \\ \cdots & \cdots & \cdots & \cdots \\ \frac{x - x_M^S}{\sqrt{\left(x-x_M^S\right)^2 + \left(y-y_M^S\right)^2}} & \frac{y - y_M^S}{\sqrt{\left(x-x_M^S\right)^2 + \left(y-y_M^S\right)^2}} & 0 & 0 \end{bmatrix} \end{aligned} \tag{3.29}$$

Note that the last two columns are zero since $\mathbf{h}_{m_k}(\mathbf{x})$ is independent of $\dot{x}$ and $\dot{y}$.

Hence, the linearized dynamic measurement equation given in Chapter 2 becomes

$$\mathbf{r}_{m_k} = \mathbf{h}_{m_k}\left(\hat{\mathbf{x}}_k^-\right) + \mathbf{H}_{m_k}(\hat{\mathbf{x}}_k^-)\left(\mathbf{x}_k - \hat{\mathbf{x}}_k^-\right) + \mathbf{w}_{m_k}. \tag{3.30}$$

The innovation vector $\mathbf{i}_k$ is defined as

$$\mathbf{i}_{m_k} = \begin{cases} \mathbf{r}_{m_k} - \mathbf{h}_{m_k}\left(\hat{\mathbf{x}}_k^-\right), & m_k \geq 3 \\ 0, & \text{otherwise} \end{cases} \tag{3.31}$$

Note that in the above EKF, the covariance matrix $\mathbf{R}_{m_k}$ of the measurement noise vector $\mathbf{w}_{m_k}$, the matrix $\mathbf{H}_{m_k}$ and the nonlinear measurement function $\mathbf{h}_{m_k}(\cdot)$ are all dynamic in their dimensions. The covariance matrix $\mathbf{R}_{m_k}$ of the measurement noise vector $\mathbf{w}_{m_k}$ is set as $\mathbf{R}_{m_k} = diag\left\{\sigma_{r,1}^2, \cdots, \sigma_{r,m_k}^2\right\}$, where $\sigma_{r,m}$ $(1 \leq m \leq m_k)$ is the standard deviation of the LOS measurement noise on the sensor m. Assuming also $\mathbf{P}_0$, which is the initial error covariance, then the filter gain $\mathbf{K}_k$ can be calculated by equation (3.24), and the state vector of the moving target can be updated by equation (3.25). The proposed algorithm will perform poorly when the number of LOS measurements available is less than 3 for a long continuous durations.

The tracking algorithm based on the proposed individual measurement detection algorithm and the EKF is summarized in as follows.

Proposed Tracking Algorithm

Given:

1. An initial state of the moving target $\mathbf{x}_0$ and the corresponding initial error covariance matrix $\mathbf{P}_0$
2. Standard deviation $\sigma_m, m = 1, \cdots, M$ of the LOS measurement noise

IMD based EKF

- **For** $k = 1 : 1 : K$
  - Do prediction to obtain $\hat{\mathbf{x}}_k^-$ and $\mathbf{P}_k^-$
  - set $n_k = 0$;
  - **For** $m = 1 : 1 : M$
    - Calculate the predicted range $\hat{d_m}$
    - Calculate the corresponding $\mathbf{R}_{m_k}$
    - **If** $|r_m - \hat{d_m}| \leq R_m$ (R_m is the (m, m) element of $\mathbf{R}_{m_k}$)
      - Reserve r_m as LOS measured range
      - $n_k = n_k + 1$
    - **Else**
      - Drop r_m
    - **End If**
  - **End For**
  - **If** $n_k \geq 3$
    - Reorganize the measurement vector with dimension n_k
    - Reorganize the measurement vector covariance with dimension n_k
    - Calculate the Kalman gain $\mathbf{K}_k$
    - Update the predicted state using the reorganized measurement vector
    - Update the error covariance matrix $\mathbf{P}_k$
  - **Else**
    - Use the predicted state as the estimated state for time step k
    - Update the error covariance matrix $\mathbf{P}_k$ using the prediction error covariance matrix
  - **End If**
- **End For**

3.5 The IMD based Robust Extended Kalman Filter

To track a moving target using the LOS TOA measurements detected by the standard gating based approach, dynamic robust EKF is adopted. Other than the extended Kalman filter (EKF), the robust EKF is another classical alternative tracking algorithm. The classical robust EKF [8] is modified as a dynamic robust EKF, which is briefly described here.

Other than the extended Kalman filter (EKF), the robust EKF is another classical alternative employed as a tracking algorithm. The classical robust EKF [8] is modified and the dynamic robust EKF is briefly described here based on the previous subsection.

Rewrite the state evolution equation (2.9) and the linearized measurement equation (3.30) as

$$\begin{bmatrix} \mathbf{I}_4 \\ \mathbf{H}_{m_k} \end{bmatrix} \mathbf{x}_k = \begin{bmatrix} \mathbf{F}\hat{\mathbf{x}}_{k-1} \\ \mathbf{r}_{m_k} - \mathbf{h}_{m_k}\left(\hat{\mathbf{x}}_k^-\right) + \mathbf{H}_{m_k}\hat{\mathbf{x}}_k^- \end{bmatrix} + \boldsymbol{\xi}_k, \tag{3.32}$$

where $\mathbf{I}_4$ is the 4×4 identify matrix. And

$$\boldsymbol{\xi}_k = \begin{bmatrix} \mathbf{F}\left(\mathbf{x}_{k-1} - \hat{\mathbf{x}}_{k-1}\right) + \mathbf{G}\mathbf{u}_{k-1} \\ -\mathbf{w}_{m_k}, \end{bmatrix} \tag{3.33}$$

satisfies that

$$\mathbb{E}\left[\boldsymbol{\xi}_k \boldsymbol{\xi}_k^T\right] = \begin{bmatrix} \mathbf{P}_k^- & 0 \\ 0 & \mathbf{R}_{m_k} \end{bmatrix} = \mathbf{C}_k \mathbf{C}_k^T, \tag{3.34}$$

where $\mathbf{P}_k^-$ and $\mathbf{R}_{m_k}$ are the same as given in the previous section. Matrix $\mathbf{C}_k$ is obtained using Cholesky decomposition [54]. Let

$$\mathbf{S}_k = \mathbf{C}_k^{-1} \begin{bmatrix} \mathbf{I}_4 \\ \mathbf{H}_{m_k} \end{bmatrix}, \tag{3.35}$$

$$\boldsymbol{\rho}_k = -\mathbf{C}_k^{-1} \boldsymbol{\xi}_k, \tag{3.36}$$

$$\tilde{\boldsymbol{r}}_{m_k} = \mathbf{C}_k^{-1} \begin{bmatrix} \hat{\mathbf{x}}_k^- \\ \mathbf{r}_{m_k} - \mathbf{h}_{m_k}\left(\hat{\mathbf{x}}_k^-\right) + \mathbf{H}_{m_k}\hat{\mathbf{x}}_k^- \end{bmatrix}. \tag{3.37}$$

Then the linear regression model (3.32) can be rewritten as

$$\tilde{\mathbf{r}}_{m_k} = \mathbf{S}_k \mathbf{x}_k + \boldsymbol{\rho}_k. \tag{3.38}$$

Solving equation (3.38) with the least squares (LS) algorithm yields

$$\hat{\mathbf{x}}_k = \left(\mathbf{S}_k^T \mathbf{S}_k\right)^{-1} \mathbf{S}_k^T \tilde{\mathbf{r}}_{m_k}. \tag{3.39}$$

Together with the measurement detection approaches proposed in the previous sections, the rEKF framework based tracker rEKF can be used to track a moving target in mixed LOS/NLOS environments.

3.6 Simulation Results

To verify the proposed tracking schemes, simulations are implemented as follows. Simulations are repeated over 100 Monte Carlo trials and each tracker is performed over $K = 1000$ time steps. The sampling time interval is set to be

$T_s = 0.2s$. The target is moving with random force in the cellular network with five stationary sensors located at

$\big(x_1^S = 2\text{km}, y_1^S = 7\text{km}\big)$, $\big(x_2^S = 12\text{km}, y_2^S = 7\text{km}\big)$, $\big(x_3^S = 7\text{km}, y_3^S = 12\text{km}\big)$,

$\big(x_4^S = 7\text{km}, y_4^S = 2\text{km}\big)$, $\big(x_5^S = 7\text{km}, y_5^S = 7\text{km}\big)$.

In the cellular network, one moving target is initially located at $\mathbf{x}_0 = \begin{bmatrix} 4300m & 4300m & 2m/s & 2m/s \end{bmatrix}^T$. The initial state estimate $\hat{\mathbf{x}}_0$ for each tracker is set as zero mean Gaussian random variable with a standard deviation of $50m$ for the the x and y coordinates and a standard deviation of $4m/s$ for the velocities along the x and y directions, around the initial true state $\mathbf{x}_0$ given above.

The LOS TOA measurement noise on each sensor is assumed to be i.i.d. zero mean Gaussian distributed with a standard deviation $\sigma = 150m$. The Markov chain exponential and mean-shifted Gaussian NLOS error occurrence is employed to simulate a practical NLOS conditions. The NLOS noise used in the simulations is either exponential with $\sigma_\eta = 400m$ or mean-shifted Gaussian characterized by $(\mu_\eta, \sigma_\eta) = (1400m, 400m)$.

Seven different mixed LOS/NLOS scenarios (C0, ..., C6) scenarios from mild to severe NLOS conditions used in the simulations for the cellular network are set as follows

C0: $\boldsymbol{\varepsilon} = \begin{bmatrix} 0 & 0 & 0 & 0 & 0 \end{bmatrix}$

C1: $\boldsymbol{\varepsilon} = \begin{bmatrix} 0 & 0.25 & 0 & 0.25 & 0 \end{bmatrix}$

C2: $\boldsymbol{\varepsilon} = \begin{bmatrix} 0 & 0.25 & 0.1 & 0.75 & 0 \end{bmatrix}$

C3: $\boldsymbol{\varepsilon} = \begin{bmatrix} 0.75 & 0.25 & 0.75 & 0.1 & 0.75 \end{bmatrix}$

C4: $\boldsymbol{\varepsilon} = \begin{bmatrix} 0.75 & 0.75 & 0.75 & 0.75 & 0.25 \end{bmatrix}$

C5: $\boldsymbol{\varepsilon} = \begin{bmatrix} 1 & 0.75 & 0.75 & 0.75 & 0.25 \end{bmatrix}$

C6: $\boldsymbol{\varepsilon} = \begin{bmatrix} 1 & 0.75 & 0.75 & 0.75 & 1 \end{bmatrix}$.

The mean error distance (MED) and the root mean square error (RMSE) are used to evaluate the performance of each tracker as mentioned in [8]. The MED is approximated by

$$\mathrm{MED}_k = \frac{1}{N}\sum_{n=1}^{N}\sqrt{(x_{k,n}-\hat{x}_{k,n})^2+(y_{k,n}-\hat{y}_{k,n})^2}. \tag{3.40}$$

where N is the number of Monte-Carlo trials.

The RMSE is approximated by

$$\mathrm{RMSE}_k = \sqrt{\frac{1}{N}\sum_{n=1}^{N}\left(\mathbf{x}_{k,n}^{p}-\hat{\mathbf{x}}_{k,n}^{p}\right)^T\left(\mathbf{x}_{k,n}^{p}-\hat{\mathbf{x}}_{k,n}^{p}\right)}. \tag{3.41}$$

The MED is used to evaluate the position tracking performance while the RMSE is used to evaluate the state tracking performance including all the four elements of the state vector. Note that the position (with two elements) of the moving target is only a part of the state vector. Hence, these two performance measurement indexes give related but somewhat different measures.

The MEDs of each tracker are summarized in Table 3.2. The RMSEs over time of each tracker under simulation scenario C2 with mean-shifted Gaussian NLOS noises are shown in Figure 3.4.

From Table 3.2, it is easy to see that the proposed tracking schemes including the EKF-SG, rEKF-SG, EKF-IMD and rEKF-IMD perform much better than the standard EKF and the rEKF in mixed LOS/NLOS environments. In LOS envi-

Table 3.2: Mean over time MEDs (m) of each tracker for random trajectory in the cellular network with Markov chain exponential and mean-shifted Gaussian NLOS errors occurrence

	C0	C1	C2	C3	C4	C5	C6
	exponential $\sigma_{\text{exp},\eta} = 400m$						
EKF	**20.32**	81.87	162.66	188.62	269.66	271.94	386.76
rEKF	21.59	59.72	114.07	152.09	229.43	233.14	348.06
EKF-SPMR	32.60	46.04	87.02	77.62	105.65	106.01	184.66
EKF-SG	21.69	30.87	57.53	67.62	103.13	108.13	195.98
rEKF-SG	23.20	30.72	**46.26**	69.22	**101.14**	**107.32**	**195.36**
EKF-IMD	21.27	30.76	59.54	69.85	106.61	118.66	197.46
rEKF-IMD	22.81	**30.67**	47.46	**68.43**	104.20	109.21	197.39
	shifted Gaussian $(\mu_{G,\eta}, \sigma_{G,\eta}) = (1400m, 400m)$						
EKF	**20.32**	276.76	556.88	741.83	1068.60	1088.90	1519.0
rEKF	21.59	172.47	381.57	698.22	1078.4	1105.3	1527.0
EKF-SPMR	32.60	72.07	179.22	147.70	389.36	452.81	1255.7
EKF-SG	21.69	23.26	24.00	60.85	161.37	328.12	688.37
rEKF-SG	23.20	25.30	26.16	65.56	203.82	358.69	704.72
EKF-IMD	21.27	**22.07**	**23.18**	**51.06**	**131.32**	**275.94**	**685.57**
rEKF-IMD	22.81	23.69	24.59	57.54	180.86	335.65	700.93

ronment, the tracking accuracy of the proposed schemes is not so good as the EKF with both mean-shifted Gaussian and exponential NLOS errors. The reason of this result is that the proposed tracking schemes miss detection some of the LOS measurements as NLOS ones.

With mean-shifter Gaussian NLOS errors, the EKF-IMD based tracking schemes works best in all mixed LOS/NLOS scenarios C1 to C6. The performance of the EKF-SG based tracking scheme is close to the EKF-IMD since the gating is fixed all the time. With exponential NLOS errors, the rEKF based tracking schemes work better than the EKF based tracking schemes. In some scenarios, the rEKF-SG works best and in other scenarios the rEKF-IMD works best.

The proposed tracking schemes perform better than the semi-parametric modified residual based EKF, which is labeled as EKF-SPMR, porposed in [8] in both LOS and mixed LOS/NLOS environments with both mean-shifted Gaussian and exponential NLOS errors.

The error cumulative distribution function (cdf) of each tracker is also used to evaluate the performance of each tracker, which is depicted in Figure 3.5. It can be observed that the 95% of the EKF, the rEKF and the EKF-SPMR are achieved at $458m$, $353m$ and $112m$, respectively. Meanwhile the 95% of the EKF-SG, the rEKF-SG, the EKF-IMD and the rEKF-IMD are around $50m$.

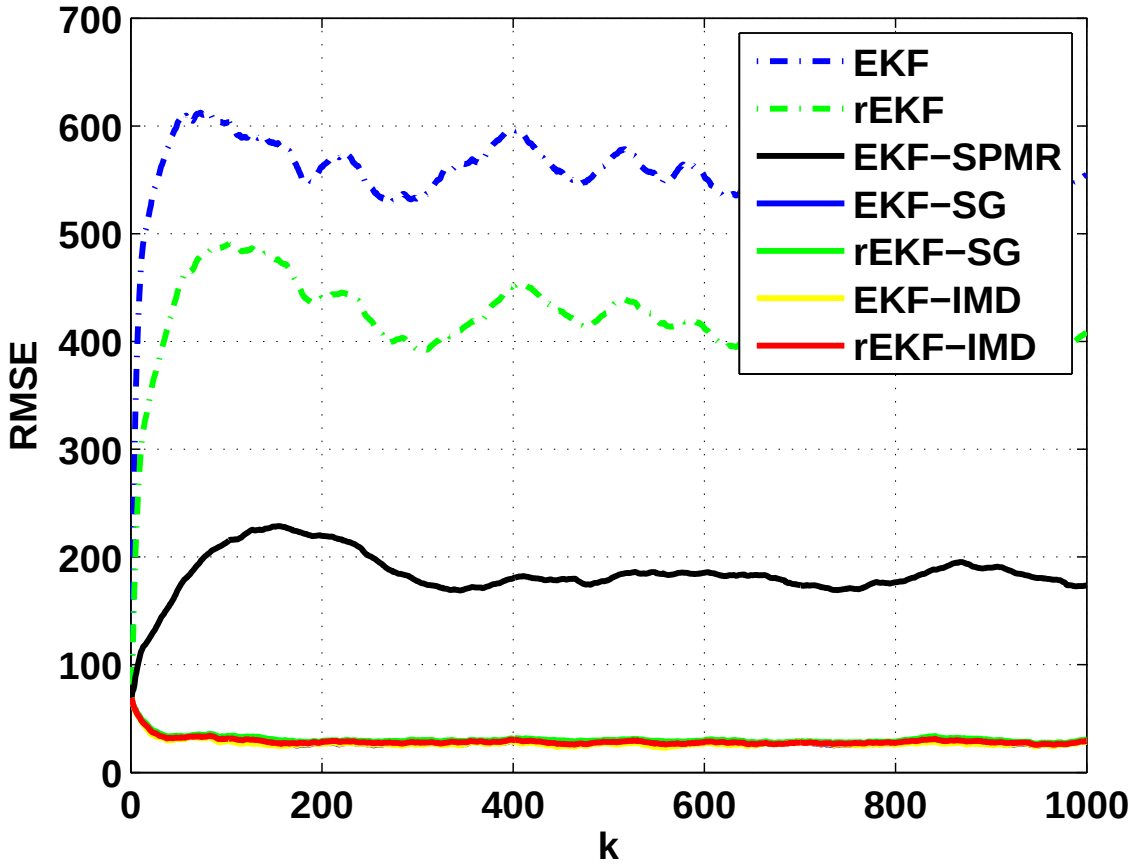

Figure 3.4: RMSEs of each tracker in mixed LOS/NLOS environment scenario C2 with mean-shifted Gaussian NLOS error

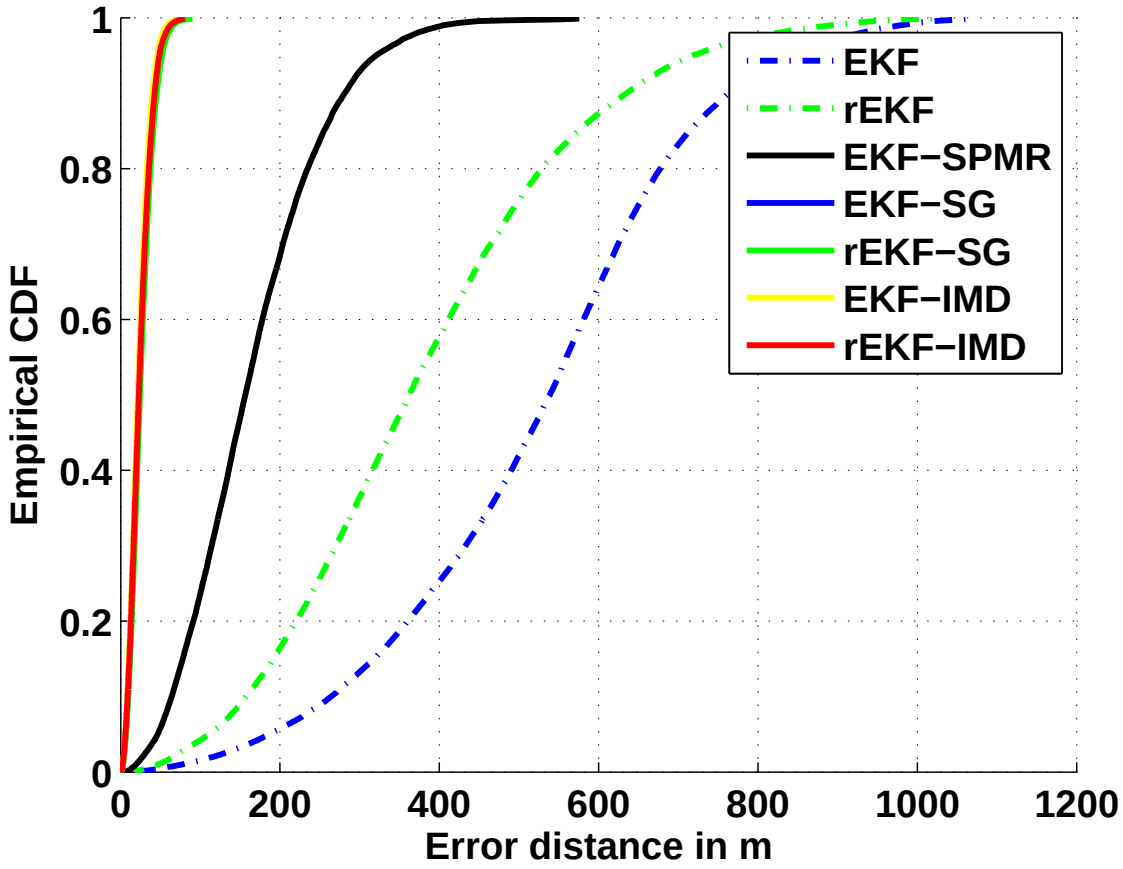

Figure 3.5: CDF of each tracker in mixed LOS/NLOS environment scenario C2 with mean-shifted Gaussian NLOS error

3.7 Conclusion

In this chapter, we discuss the detection algorithm for individual TOA measurement and the EKF and the rEKF based tracking schemes using selected LOS measurements by the gating based detection algorithm and the individual measurement detection algorithm. Simulations have shown the improved tracking accuracy with respect to the classical tracking algorithms and the recently proposed SPMR algorithms. However, all of these proposed tracking schemes require at least 3

LOS TOA measurements to achieve good performance. When this condition is not satisfied, the tracking accuracy decreases obviously especially in severe mixed LOS/NLOS environments. To overcome this weakness, we propose the individual measurement estimation and LOS detection based Kalman filter tracking scheme, which will be described in the Chapter 5 in detail.

Chapter 4

Road-constraint Assisted Dynamic Tracking Scheme using TDOA Measurements

In Chapter 3, the proposed measurement detection algorithm and the proposed tracking scheme are incorporated with the TOA measurements. In this chapter, we discuss the tracking algorithms using TDOA measurements.

In this chapter, we discuss the development of the proposed standard gating based measurement detection algorithm and the EKF and rEKF for TDOA measurements. In this tracking scheme, the prior knowledge of the road constraints are used as pseudo-measurements together with the selected TDOA measurements into the EKF and the rEKF to track a moving target in mixed LOS/NLOS environments. Performance of this tracking scheme is better than that without the road constraints.

4.1 Introduction

Time-difference-of-arrival is an important and popular technique in passive geolocation and target tracking. The TDOA technique is based on measuring the difference in the time of reception of signals at different sensors, without requiring a synchronization of all participating sensors and the moving target. It does not require knowledge of absolute time of the transmission. Therefore, only the synchronicity of the reference sensor and other sensors is necessary for TDOA-based positioning [55–57]. The major sources of error in TDOA measurements are measurement noises and non-line-of-sight (NLOS) signal propagations. The measurement noise is usually modeled as a zero mean Gaussian random variable, while NLOS errors usually have an unknown distribution with a positive mean, which is usually assumed to be a mean-shifted Gaussian distribution or an exponential distribution [8]. Compared with the measurement noise, the NLOS errors cause severe degradation of tracking accuracy.

In this chapter, the standard gating based measurement detection (IMD) approach proposed in Chapter 3 for TOA measurements is expanded into TDOA measurements. The detection approach can efficiently select LOS TDOA measurements from mixed LOS/NLOS measurements without greatly increasing the computational complexity. However, when the number of selected LOS TDOA measurements is less than 3, we cannot obtain the estimated state of the moving target. To handle this problem, the road constraint is introduced as a pseudo-measurement to assist the tracking in mixed LOS/NLOS environments. In LOS environment, the road constraints assisted method has been proved helpful to improve the performance of the traditional KF or EKF [58–70]. Together with the

measurement detection algorithm and the EKF or rEKF, the road constraints assisted tracking scheme does improve the tracking accuracy in mixed LOS/NLOS environments. Simulations have been given to demonstrate this improvement with respect to these without road constraints.

The rest of the chapter is organized as follows. Section 4.2 presents the standard gating based measurement detection algorithm. Section 4.3 describes the formation of the road constraints as pseudo-measurements in detail. Section 4.4 exhibits simulation results. Finally, conclusions are given in section 4.5.

4.2 Gating Based Detection Algorithm

In mixed LOS/NLOS environments, we treat the NLOS errors as statistical noise incorporated into the measurement noise of the measurement model. The measurement equation is rewritten as:

$$\mathbf{\Delta r}_k = \mathbf{\Delta d}_k + \mathbf{\Delta \eta}_k, \tag{4.1}$$

where $\mathbf{\Delta d}_k$ is the noise-free distance difference vector. The noise vector, $\mathbf{\Delta \eta}_k = \begin{bmatrix} \Delta\eta_{1,k} & \cdots & \Delta\eta_{M-1,k} \end{bmatrix}^{\mathrm{T}}$ is a mixture LOS/NLOS noise vector.

The noise model for an individual TDOA measurement is

$$\begin{aligned} \Delta r_{m,k} &= r_{1,k} - r_{m+1,k} \\ &= d_{1,k} - d_{m+1,k} + \eta_{1,k} - \eta_{m+1,k}, \end{aligned} \tag{4.2}$$

where $m = 1, \cdots, M-1$. The distance difference vector is obtained relative to the distance collected by sensor 1. The measurement function is give in Section 2.1.2.2

Table 2.1.

For each distance measurement, the measured vector can be described as:

$$r_{m,k} = d_{m,k} + \eta_{m,k}, \;\; m = 1, \cdots, M, \tag{4.3}$$

where $r_{m,k}$, $d_{m,k}$ and $\eta_{m,k}$ are the measured distance, the noise-free distance and the mixture LOS/NLOS noise at sensor m, the probability density function for $\eta_{m,k}$ is,

$$p(\eta_{m,k}) = (1 - \varepsilon_m) p_{\text{LOS}}(\eta_{m,k}) + \varepsilon_m p_{\text{NLOS}}(\eta_{m,k}) \tag{4.4}$$

where ε_m is the degree of contamination by NLOS errors at sensor m. The noise is effectively a mixture of LOS and NLOS noise where $p_{\text{LOS}}(\eta_{m,k})$ is zero mean Gaussian distributed and $p_{\text{NLOS}}(\eta_{m,k})$ is mean-shifted Gaussian distributed. The Markov chain modeled NLOS errors have been given in Chapter 2.

The states, LOS or NLOS, of the reference sensor and other sensors affect the state of the corresponding TDOA measurements. Since the received noise on each sensor is independent additive Gaussian noise, 4 different mixture LOS/NLOS noise conditions are summarized as follows.

1. When both the reference sensor and the sensor $m+1$ are LOS, the pdf of the noise is zero mean Gaussian distribution $\Delta\eta_{m,k} \sim \mathcal{N}\left(0, \sqrt{2}\sigma_{LOS}\right)$, where σ_{LOS} stands for the standard deviation of the LOS TOA measurements.

2. When the reference sensor is LOS and the sensor $m+1$ is NLOS, the pdf of the corresponding noise is mean-shifted Gaussian distribution $\Delta\eta_{m,k} \sim \mathcal{N}\left(-\mu_{NLOS}, \sqrt{\sigma_{LOS}^2 + \sigma_{NLOS}^2}\right)$. μ_{NLOS} and σ_{NLOS} are the mean and standard deviation of the NLOS noise, respectively.

3. When the reference sensor is NLOS and the sensor $m+1$ is LOS, the pdf of the corresponding noise is mean-shifted Gaussian distribution $\Delta\eta_{m,k} \sim \mathcal{N}\left(\mu_{NLOS}, \sqrt{\sigma_{LOS}^2 + \sigma_{NLOS}^2}\right)$.

4. When the reference sensor and the sensor $m+1$ are both NLOS, the pdf of the corresponding noise is zero mean Gaussian distribution $\Delta\eta_{m,k} \sim \mathcal{N}\left(0, \sqrt{2}\sigma_{NLOS}\right)$.

To detect the state of an individual measurement, 3 different GLRT scenarios are described as follows. The discussion of the GLRT algorithm has been given in Chapter 3.

1. For condition 1) and condition 2), the hypothesis are

$$\begin{aligned} H_0 &: \mu = 0 \\ H_1 &: \mu = -\mu_{NLOS}, \end{aligned} \tag{4.5}$$

where μ is the mean of $\Delta\eta_{m,k}$.

2. For condition 1) and condition 3), the hypothesis are

$$\begin{aligned} H_0 &: \mu = 0 \\ H_1 &: \mu = \mu_{NLOS}. \end{aligned} \tag{4.6}$$

3. For condition 1) and condition 4), the hypothesis are

$$\begin{aligned} H_0 &: \mu = 0, \sigma = \sqrt{2}\sigma_{LOS} \\ H_1 &: \mu = 0, \sigma = \sqrt{2}\sigma_{NLOS}, \end{aligned} \tag{4.7}$$

where σ stands for the standard deviation of $\Delta\eta_{m,k}$.

Note that H_0 is LOS hypothesis and H_1 is NLOS hypothesis. For all these different hypotheses, we can use the one hypothesis test proposed in Chapter 3 to detect all TDOA measurements with different false alarm probability.

In LOS environment, the TDOA measurements received by sensors are Gaussian distributions whose means are the true distance differences between two sensors and covariance matrix $\mathbf{R}'$. To detect LOS TDOA measurement, two hypotheses are proposed

$$H_0 \quad : \quad \triangle r_{m,k} \in CR_{m,k}, \tag{4.8}$$

$$H_1 \quad : \quad \triangle r_{m,k} \notin CR_{m,k}, \tag{4.9}$$

where $CR_{m,k}$ stands for the 3σ confidence region which is determined by true distance difference m and the covariance $\mathbf{R}'$ of the LOS distance difference noise. If hypothesis H_0 is correct, the measurement is considered as LOS, otherwise as NLOS. In real applications, it is impossible to obtain the noise-free distance different vector. So the prediction distance difference vector, calculated from the measurement equation, is used instead. The measurement detection criteria is simplified as

$$\triangle\hat{r}_{m,k} - R_{m,k} \leq \triangle r_{m,k} \leq \triangle\hat{r}_{m,k} + R_{m,k}, \tag{4.10}$$

where $\triangle\hat{r}_{m,k}$ is the predicted distance difference and $R_{m,k} = 3\sqrt{2}\sigma_{LOS} = 3\sqrt{2}\sigma_m$.

Under different mixture LOS/NLOS noises conditions, the false alarm rates calculated using the detection criteria are summarized in Table 4.1.

The weakness of this hypothesis test for TDOA measurements is the drop in the

Table 4.1: False alarm probability under different percentage of NLOS errors.

P_{FA}	1)	2)	3)	4)
$\varepsilon_m = 0.10$	0	0.0009	0.0009	0.0244
$\varepsilon_m = 0.25$	0	0.0023	0.0023	0.0610
$\varepsilon_m = 0.75$	0	0.0069	0.0069	0.1831

probability of detection or a higher probability of false alarm probability especially for mixture condition 4. To compensate for this weakness the lost of probability of detection or the high probability of false alarm probability especially for mixture condition 4, since the distribution of the $\Delta\eta_{m,k}$ is variational at different time steps. To compensate this weakness, we introduce the road constraint as a pseudo-measurement in the following section.

Except for condition 1), measurements collected in all the other conditions are considered as NLOS.

After detecting the LOS TDOA measurements, all of them are reserved into a dynamic data vector. Then they are used into an EKF or robust EKF to tracking the moving target. Since the dimension of the TDOA measurements is less than the TOA measurements in the same sensor network, the tracking accuracy is also decreased. To overcome this weakness, we make use of a knowledge of road constraint to improve the tracking accuracy. The road constraints assisted EKF is described as follows.

4.3 Road Constraints based EKF

As the moving target we are interested in is on the road, the road constraint can be used as a prior information to improve the tracking accuracy in mixed

LOS/NLOS environments. Here the road constraints are used as pseudo-measurements.

Assuming that the target is moving on a given road segment, the constraints are that the position of the moving target must lie on the road and the velocity of the moving target is also along with the direction of the road. The road direction can be denoted as follows

$$\tan\theta = \frac{y_k - y_{k-1}}{x_k - x_{k-1}}, \tag{4.11}$$

$$\tan\theta = \frac{\dot{y}_k}{\dot{x}_k}. \tag{4.12}$$

where θ is the direction of the straight road. Equations (4.11) and (4.12) can be re-written as

$$-x_{k-1}\tan\theta + y_{k-1} = x_k\tan\theta + y_k, \tag{4.13}$$

$$0 = \dot{y}_k - \dot{x}_k\tan\theta. \tag{4.14}$$

Equations (4.13) and (4.14) can be rewritten as

$$\begin{bmatrix} -x_{k-1}\tan\theta + y_{k-1} \\ 0 \end{bmatrix} = \begin{bmatrix} -\tan\theta & 1 & 0 & 0 \\ 0 & 0 & -\tan\theta & 1 \end{bmatrix} \begin{bmatrix} x_k \\ y_k \\ \dot{x}_k \\ \dot{y}_k \end{bmatrix}. \tag{4.15}$$

Base on equation (4.15), which is the ideal case without considering errors, the more realistic road constraint can be written into a measurement function as follows

$$\mathbf{r}_c = \mathbf{H}_c\mathbf{x}_k + \mathbf{u}_{c,k}, \tag{4.16}$$

where $\mathbf{u}_{c,k}$ is assumed to be zero mean Gaussian noise, which stands for the uncertainty of the constraints, such as road width and error of the road direction. $\mathbf{r}_c$ and the coefficient matrix $\mathbf{H}_c$ are defined as follows

$$\mathbf{r}_c = \begin{bmatrix} -x_{k-1}\tan\theta + y_{k-1} & 0 \end{bmatrix}^T, \tag{4.17}$$

$$\mathbf{H}_c = \begin{bmatrix} -\tan\theta & 1 & 0 & 0 \\ 0 & 0 & -\tan\theta & 1 \end{bmatrix}, \tag{4.18}$$

Using road constraint with a certain direction makes the target to move on the road with a certain direction. Here we use the road constraint as pseudo-measurement. The measurement function will be rewritten as

$$\begin{bmatrix} \mathbf{\Delta r}_k^d \\ \mathbf{r}_c \end{bmatrix} = \begin{bmatrix} \mathbf{h}_k^d(\mathbf{x}_k) \\ \mathbf{H}_c\mathbf{x}_k \end{bmatrix} + \begin{bmatrix} \mathbf{u}_k^d \\ \mathbf{u}_{c,k} \end{bmatrix}, \tag{4.19}$$

where $\mathbf{\Delta r}_k^d$ are dynamic LOS TDOA measurement vector. $\mathbf{h}_k^d(\cdot)$ and $\mathbf{u}_k^d$ are the dynamic mapping function and dynamic LOS noise vector, respectively.
Each element in $\mathbf{h}_k^d(\cdot)$ is defined as follows

$$\mathbf{h}_{k,m}^d(\mathbf{x}_k) = \sqrt{(x_k - x_1^S)^2 + (y_k - y_1^S)^2} - \sqrt{\left(x_k - x_{1+m}^S\right)^2 + \left(y_k - y_{1+m}^S\right)^2}. \tag{4.20}$$

where $m = 1, \cdots, M-1$.

The Jacobian matrix of $\mathbf{h}_k^d(\mathbf{x})$ with respect to $\mathbf{x}$ is defined as follows

$$\begin{aligned}
\mathbf{H}_k^d(\mathbf{x}) &:= \frac{\partial \mathbf{h}_k^d(\mathbf{x})}{\partial \mathbf{x}} \\
&= \begin{bmatrix} \frac{\partial \mathbf{h}_{k,1}^d(\mathbf{x}_k)}{\partial x_k} & \frac{\partial \mathbf{h}_{k,1}^d(\mathbf{x}_k)}{\partial y_k} & \frac{\partial \mathbf{h}_{k,1}^d(\mathbf{x}_k)}{\partial \dot{x}_k} & \frac{\partial \mathbf{h}_{k,1}^d(\mathbf{x}_k)}{\partial \dot{y}_k} \\ \cdots & \cdots & \cdots & \cdots \\ \frac{\partial \mathbf{h}_{k,M}^d(\mathbf{x}_k)}{\partial x_k} & \frac{\partial \mathbf{h}_{k,M}^d(\mathbf{x}_k)}{\partial y_k} & \frac{\partial \mathbf{h}_{k,M}^d(\mathbf{x}_k)}{\partial \dot{x}_k} & \frac{\partial \mathbf{h}_{k,M}^d(\mathbf{x}_k)}{\partial \dot{y}_k} \end{bmatrix} \\
&= \begin{bmatrix} \frac{\left(x_k - x_1^S\right)}{r_1} - \frac{\left(x_k - x_2^S\right)}{r_2} & \frac{\left(y_k - y_1^S\right)}{r_1} - \frac{\left(y_k - y_2^S\right)}{r_2} & 0 & 0 \\ \cdots & \cdots & \cdots & \cdots \\ \frac{\left(y_k - y_1^S\right)}{r_1} - \frac{\left(y_k - y_M^S\right)}{r_M} & \frac{\left(y_k - y_1^S\right)}{r_1} - \frac{\left(y_k - y_M^S\right)}{r_M} & 0 & 0 \end{bmatrix},
\end{aligned} \tag{4.21}$$

where

$$r_1 = \sqrt{\left(x_k - x_1^S\right)^2 + \left(y_k - y_1^S\right)^2}, \tag{4.22}$$

$$r_{1+m} = \sqrt{\left(x_k - x_{1+m}^S\right)^2 + \left(y_k - y_{1+m}^S\right)^2}, \tag{4.23}$$

where $m = 1, \cdots, M-1$.

At every time step, the individual measurement detection is implemented to detect whether a measurement is LOS or not. The selected LOS measurements are stored in a dynamic data array. Together with the road constraint, the EKF and rEKF are implemented based on the augmented measurement equation (4.19) to track the moving target. For detailed description of the IMD based EKF and the IMD rEKF, see Chapter 3.

4.4 Simulation Results

Simulations are repeated over 100 Monte Carlo trials and each tracker is performed over $K = 1000$ time steps. The sampling time interval is set at $T = 0.2s$. The initial state $\hat{\mathbf{x}}_0$ of the moving target is set randomly using a Gaussian random vector with a standard deviation of $50m$ for the positions and a standard deviation of $4m/s$ for the velocities, around the true initial state $\mathbf{x}_0 = \begin{bmatrix} 4300m & 4300m & 2m/s & 2m/s \end{bmatrix}^{\mathrm{T}}$. The initial error covariance matrix of the state is set as $\mathbf{P_0} = diag\left(\begin{bmatrix} 50^2 & 50^2 & 4^2 & 4^2 \end{bmatrix}\right)$. The cellular network described in Chapter 3 is employed.

The NLOS noise is assumed to be mean-shifted Gaussian or exponential distributed. NLOS Occurrence is Modeled as a two state Markov Chain.

Simulations are done under four NLOS occurrence scenarios:

Scenario D0: $\boldsymbol{\varepsilon} = \begin{bmatrix} 0 & 0 & 0 & 0 & 0 \end{bmatrix}$

Scenario D1: $\boldsymbol{\varepsilon} = \begin{bmatrix} 0 & 0.25 & 0 & 0.25 & 0 \end{bmatrix}$

Scenario D2: $\boldsymbol{\varepsilon} = \begin{bmatrix} 0 & 0.75 & 0 & 0.25 & 0 \end{bmatrix}$

Scenario D3: $\boldsymbol{\varepsilon} = \begin{bmatrix} 0 & 0.25 & 0.1 & 0.75 & 0 \end{bmatrix}$

For comparison, the classical EKF and rEKF, the EKF and rEKF with road constraint (EKF-c and rEKF-c), the EKF and rEKF combined with the IMD algorithm (EKF-IMD and rEKF-IMD), the EKF and rEKF combined both the IMD and road constraint (EKF-IMD-c and rEKF-IMD-c) are implemented. The LOS root mean square error bound (LOS RMSE-bound)(Appendix), deduced from the posterior Cramer-Rao bound (PCRB) [71, 72] is also implemented to evaluate performances of all trackers. The mean error distance (MED) of each tracker are

summarized in Table 4.2. The RMSEs of each tracker under simulation scenario D3 with mean-shifted Gaussian NLOS noises are shown in Figure 4.1.

Table 4.2: Mean over time MEDs (m) of each tracker for switch trajectory in ad-hoc network

	D0	D1	D2	D3
	exponential $\sigma_{\text{exp},\eta} = 400m$			
EKF	27.1	91.4	117.5	200.6
rEKF	26.1	71.1	97.3	182.2
EKF-c	**16.9**	43.7	120.1	57.3
rEKF-c	23.2	38.97	88.29	52.95
EKF-IMD	29.4	43.2	59.5	119.1
rEKF-IMD	25.1	47.1	59.8	113.0
EKF-IMD-c	20.5	**38.7**	**43.2**	**27.6**
rEKF-IMD-c	23.2	38.9	48.9	33.4
	shifted Gaussian $(\mu_{G,\eta}, \sigma_{G,\eta}) = (1400m, 400m)$			
EKF	27.1	311.1	391.3	672.4
rEKF	26.1	225.0	365.6	676.3
EKF-c	**16.9**	153.4	244.3	303.8
rEKF-c	23.2	85.4	159.6	284.3
EKF-IMD	29.4	30.3	35.4	121.3
rEKF-IMD	25.1	28.4	29.5	70.3
EKF-IMD-c	20.5	**21.2**	**26.0**	**29.2**
rEKF-IMD-c	23.2	22.8	26.3	36.3

From Table 4.2, it is easy to see that in all scenarios the proposed EKF-IMD-c approach (with road constraints) works better than all the other approaches. In mixed LOS/NLOS environments, both the EKF and the rEKF trackers perform poorly. The trackers with road constraint, i.e., the EKF-c and the rEKF-c trackers, work better than the EKF and the rEKF, but poorer than the EKF-IMD and rEKF-IMD trackers in all mixed LOS/NLOS scenarios with Gaussian NLOS errors, although they are doing better in some mixed LOS/NLOS scenarios than the EKF-IMD and rEKF-IMD trackers with exponential NLOS errors. However, with the assistance of the prior knowledge of road constraints, the performance of the EKF-IMD-c and the rEKF-IMD-c have been greatly improved and they perform better than other trackers in all mixed LOS/NLOS scenarios with Gaussian as well as exponential NLOS errors.

The LOS RMSE-bound bound performance comparisons of each tracker in scenario C3 with mean-shifted Gaussian NLOS errors is shown in Figure 4.1, respectively. It is obvious that the tracker EKF-IMD-c outperforms the tracker EKF-IMD.

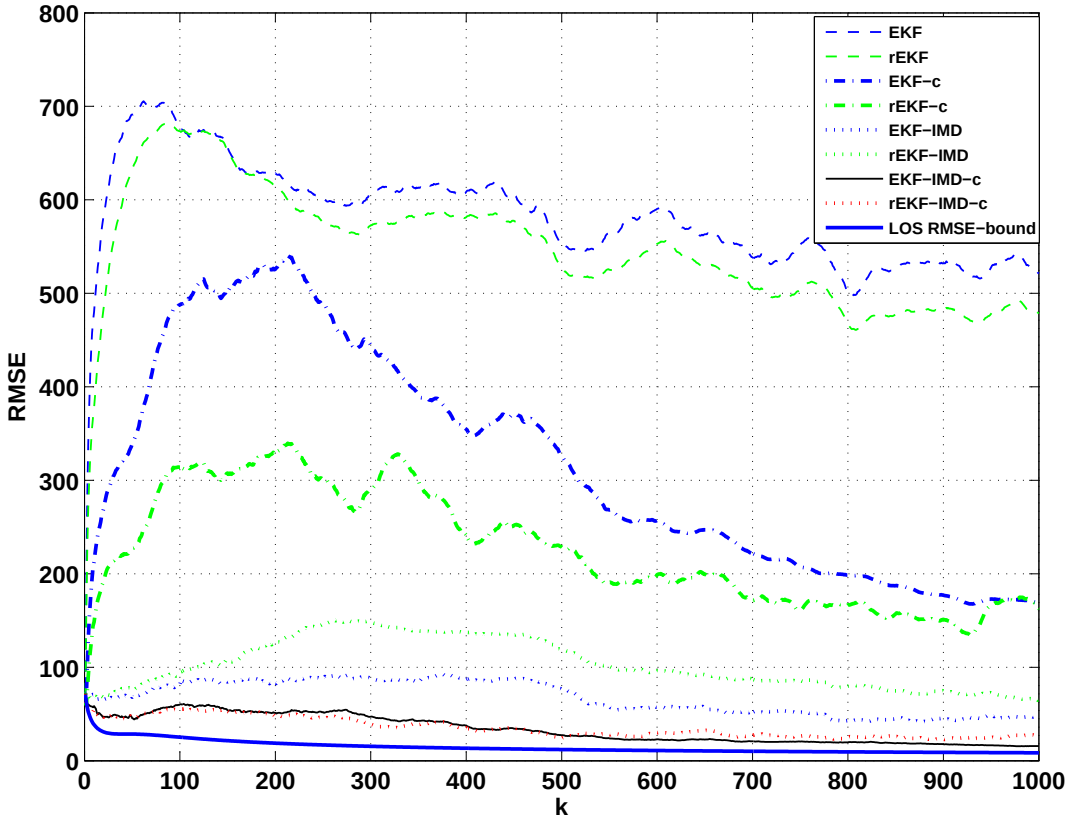

Figure 4.1: RMSEs in mixed LOS/NLOS environment scenario D3 with mean-shifted Gaussian NLOS error

4.5 Conclusion

In this chapter, we have proposed an approach to improving the tracking accuracy in mixed LOS/NLOS environments based on both individual measurement detection and road constraints. The IMD algorithm correctly selects most LOS TDOA measurements from mixed LOS/NLOS TDOA measurements while the prior knowledge of the road constraint is used as a pseudo-measurement. The augmented EKF is then implemented to track a moving target. Simulation results have demonstrated the improved performance of the proposed EKF-IMD-c tracker. This road constraint based tracking scheme can be easily used into the TOA based tracking scenarios, which will be considered in the future research work.

Appendix

Cramer-Rao bound (CRB) is often used as a benchmark for the comparison of various tracking algorithms. The error covariance matrix of $\hat{\mathbf{x}}_k$, denoted as $\mathbf{P}_k$, has a lower bound referred to as the CRB expressed as:

$$\mathbf{P}_k \triangleq \mathbb{E}\left\{\left(\hat{\mathbf{x}}_k - \mathbf{x}_k\right)\left(\hat{\mathbf{x}}_k - \mathbf{x}_k\right)^T\right\} \geq \mathbf{J}_k^{-1}, \tag{4.24}$$

where $\hat{\mathbf{x}}_k$ and $\mathbf{x}_k$ are the estimated state and true state of the moving target, respectively. Matrix $\mathbf{J}_k$ is the Fisher information matrix. In target tracking problems, the posterior CRB (PCRB) proposed in [71, 72] is often used to evaluate the performance of trackers. The elegant method of computing the Fisher information

matrix $\mathbf{J_k}$ recursively was presented in [71] as

$$\mathbf{J}_k = \mathbf{D}_{k-1}^{22} - \mathbf{D}_{k-1}^{21} \left(\mathbf{J}_{k-1} + \mathbf{D}_{k-1}^{11}\right)^{-1} \mathbf{D}_{k-1}^{12}, \tag{4.25}$$

where

$$\begin{aligned}
\mathbf{D}_{k-1}^{11} &= -\mathbb{E}\left\{\nabla_{\mathbf{x}_{k-1}} \left[\nabla_{\mathbf{x}_{k-1}} \log p\left(\mathbf{x}_k \left|\mathbf{x}_{k-1}\right.\right)\right]^T\right\}, && (4.26)\\
\mathbf{D}_{k-1}^{12} &= -\mathbb{E}\left\{\nabla_{\mathbf{x}_k} \left[\nabla_{\mathbf{x}_{k-1}} \log p\left(\mathbf{x}_k \left|\mathbf{x}_{k-1}\right.\right)\right]^T\right\}, && (4.27)\\
\mathbf{D}_{k-1}^{21} &= -\mathbb{E}\left\{\nabla_{\mathbf{x}_{k-1}} \left[\nabla_{\mathbf{x}_k} \log p\left(\mathbf{x}_k \left|\mathbf{x}_{k-1}\right.\right)\right]^T\right\}, && (4.28)\\
\mathbf{D}_{k-1}^{22} &= -\mathbb{E}\left\{\nabla_{\mathbf{x}_k} \left[\nabla_{\mathbf{x}_k} \log p\left(\mathbf{x}_k \left|\mathbf{x}_{k-1}\right.\right)\right]^T\right\} \\
&\quad -\mathbb{E}\left\{\nabla_{\mathbf{x}_k} \left[\nabla_{\mathbf{x}_k} \log p\left(\mathbf{r}_k \left|\mathbf{x}_k\right.\right)\right]^T\right\}, && (4.29)
\end{aligned}$$

with $\nabla_{\mathbf{x}_k}$ denoting the first partial derivation with respect to $\mathbf{x}_k$.

Due to the state evolution equation (2.9) and the measurement equation (4.20), the recursion of (4.25) can be written as [51]

$$\mathbf{J}_k = \left[\mathbf{F}^{-1}\right]^T \mathbf{J}_{k-1} \mathbf{F}^{-1} + \tilde{\mathbf{H}}_k^T \mathbf{R}_k^{-1} \tilde{\mathbf{H}}_k, \tag{4.30}$$

where $\tilde{\mathbf{H}}_k = \mathbf{H}_M\left(\mathbf{x}_k\right)$ is the Jacobian matrix given by equation (4.21) evaluating at the true value of the state vector of the moving target $\mathbf{x}_k$ (with $m_k = M$).

RMSE given in (3.41) is interpreted as the achieved position error in meters, is used to evaluate the performance of a tracking algorithm. From the PCRB, the RMSE-bound can be given as follows.

$$\mathrm{RMSE}_k = \sqrt{\frac{1}{N} \sum_{n=1}^{N} \left(\mathbf{x}_{k,n}^p - \hat{\mathbf{x}}_{k,n}^p\right)^T \left(\mathbf{x}_{k,n}^p - \hat{\mathbf{x}}_{k,n}^p\right)} \geq \sqrt{tr\left(\mathbf{J}_k{}^{-1}\right)} \tag{4.31}$$

where $tr(A)$ denotes taking the trace of matrix A.

Note that the RMSE-bound used in this chapter is under the condition of LOS without considering the road constraints and is therefore called the LOS RMSE-bound.

Chapter 5

Extension of Individual Measurement Estimation and LOS Detection using TOA Measurements

In this chapter a tracking scheme based on the Kalman filter frame work and the individual measurement estimation and detection algorithm for TOA measurements is discussed. This is a further development of the proposed IMD algorithm in Chapter 3. Details of the proposed individual measurement estimation and LOS detection based tracking scheme is given as follows.

5.1 Introduction

In this chapter, a new method based on estimation and line-of-sight (LOS) detection of individual time-of-arrival (TOA) measurement and Kalman filter (KF) is proposed to track a moving target in mixed line-of-sight and non-line-of-sight (LOS/NLOS) environments. In the proposed tracking algorithm, TOA measurements collected by multiple stationary sensors in a wireless sensor network are used. First, a pseudo-measured position is calculated by choosing the point along the circle defined by a given TOA measurement which has the shortest distance to the predicted position of a moving target. The pseudo-measured position is shown to be an approximately unbiased estimate of the true position of the target.

Second, each pseudo-measured position calculated is passed to a detector to be identified as either LOS or NLOS. The average of all the selected LOS pseudo-measured positions is then used as a new pseudo-measurement for the KF to track the moving target. Unlike all the existing target tracking algorithms in mixed LOS/NLOS environments, the proposed tracking algorithm is able to perform target tracking even with just one LOS TOA measurement at a given time instance without prior information of the NLOS noise which may be difficult to obtain in practice. Another advantage of the proposed tracking algorithm is its computational efficiency. Simulation results show that the proposed tracking algorithm performs better than some recent tracking algorithms, particularly in severe mixed LOS/NLOS environments.

Original contributions of this chapter are summarized as follows. We firstly propose the estimator for individual TOA measurement. The novel estimator is used to estimate a pseudo-measured position of a moving target from each one of

the TOA measurements. The pseudo-measured position estimated is proved to be unbiased. By detecting the pseudo-measured position is LOS or NLOS, we secondly make full use of all possible LOS measurements. In severe NLOS conditions, even one LOS TOA measurement can give a raw pseudo-measured position of the moving target to update the state vector of the Kalman filter.

The rest of this chapter is organized as follows. The individual measurement estimator for TOA measurement is presented in Section 5.2. The corresponding individual pseudo-measured detection algorithm is described in Section 5.3. The tracking strategy based on the IMED algorithm is given in Section 5.4. Simulation results are shown in Section 5.5. Conclusions are drawn in Section 5.6.

5.2 Individual Measurement Estimation

Traditional TOA measurement based target tracking algorithms, such as least squares or EKF, require at least three LOS TOA measurements at each time step to update the predicted state when no prior knowledge is available. However, in mixed LOS/NLOS environments, particularly when the NLOS error is severe, it is not always possible to obtain 3 or more LOS TOA measurements at each time step. Therefore, it is highly desirable to find an estimator that is able to provide an estimated position without requiring 3 or more LOS TOA measurements at each time step. To achieve this, we propose in this section a novel estimator to estimate a pseudo-measured position of the moving target from an individual LOS TOA measurement. We prove that under the LOS condition, the pseudo-measured position is approximately unbiased. In addition, the associated error covariance matrix of the pseudo-measured position is derived. To facilitate the derivation

and analysis of the pseudo-measured position, we assume throughout this section that the measurement noise in LOS is zero mean Gaussian noise. The details of detection of all the LOS measurements in mixed LOS/NLOS environments and the overall target tracking algorithm will be given in the next section.

5.2.1 Analysis

Under the LOS condition, the measurement function for a TOA or range measurement collected by sensor m at time step k is given by

$$r_{k,m} = \bar{r}_{k,m} + w_{k,m} = h_m(\mathbf{x}_k) + w_{k,m}, m = 1, \cdots, M \tag{5.1}$$

where $\bar{r}_{k,m}$ is the noise-free range and $w_{k,m}$ is the zero mean Gaussian noise with standard deviation σ_m.

With the assumption of zero mean Gaussian noise in both the state equation given in (2.9) and the measurement equation (5.1), the following results, which hold for the KF, will be used subsequently

$$\begin{aligned}
\mathbb{E}(\hat{\mathbf{x}}_k - \mathbf{x}_k) &= 0, & (5.2)\\
\mathbb{E}\left(\hat{\mathbf{x}}_k^- - \mathbf{x}_k\right) &= 0, & (5.3)\\
\mathbb{E}(\boldsymbol{r}_k - \mathbf{h}(\mathbf{x}_k)) &= 0, & (5.4)\\
\mathbb{E}\left(\left(\hat{\mathbf{x}}_k^- - \mathbf{x}_k\right)\left(\hat{\mathbf{x}}_k^- - \mathbf{x}_k\right)^T\right) &= \mathbf{P}_k^-, & (5.5)\\
\mathbb{E}\left(\left(\hat{\mathbf{x}}_k - \mathbf{x}_k\right)\left(\hat{\mathbf{x}}_k - \mathbf{x}_k\right)^T\right) &= \mathbf{P}_k, & (5.6)
\end{aligned}$$

where $\mathbb{E}(\cdot)$ is the expectation operator. $\mathbf{x}_k$ and $\hat{\mathbf{x}}_k$ are the true state of the moving target and its estimated state given by the KF, respectively. $\hat{\mathbf{x}}_k^- = \mathbf{F}\hat{\mathbf{x}}_{k-1}$ is the

predicted state. $\mathbf{P}_k$ is the error covariance matrix and $\mathbf{P}_k^-$ is the predicted error covariance matrix. Equations (5.2) and (5.3) show that the estimated state $\hat{\mathbf{x}}_k$ and the predicted state of the moving target $\hat{\mathbf{x}}_k^-$ are both unbiased estimates of the true state of the moving target $\mathbf{x}_k$.

From (5.1) and the definition of $h_m(\mathbf{x}_k)$, it is easy to see that the noise free measurement $\bar{r}_{k,m}$ determines a set of possible positions of the moving target on a circle centered at $\left(x_m^S, y_m^S\right)$ with radius $\bar{r}_{k,m}$. The true position of the moving target must be on the circle. However, because of the measurement noise, we can only obtain $r_{k,m}$ instead of $\bar{r}_{k,m}$. Hence, the best estimated position of the moving target from the measured range $r_{k,m}$ is the point on a circle centered at $\left(x_m^S, y_m^S\right)$ with radius $r_{k,m}$ that has minimum Euclidean distance to the true position, $\mathbf{x}_k^p = \begin{bmatrix} x_k & y_k \end{bmatrix}^T$, of the moving target. In practice, the true position of the moving target is unknown and is replaced with the predicted position, $\hat{\mathbf{x}}_k^{p,-} = \begin{bmatrix} \hat{x}_k^{p,-} & \hat{y}_k^{p,-} \end{bmatrix}^T$, which is calculated from the state equation. Such a replacement is reasonable since the predicted position is an unbiased estimate of the true position of the moving target (see (5.3)). In the following lemma, based on the predicted position and one TOA measurement, we present a method for finding a pseudo-measured position, a new and important concept introduced in this chapter.

Together with the measurement estimation method proposed in Chapter 3 section 3.3.1 and the assumptions given in equations (5.2) to (5.6), a Lemma is given as follows.

Lemma 5.1. *(Appendix A) Given the predicted position* $\hat{\mathbf{x}}_k^{p,-}$ *and a TOA measure-*

ment $r_{k,m}$, the solution to the following constrained optimization problem

$$\min_{\tilde{\mathbf{x}}_{k,m}^{p}} \left(\tilde{\mathbf{x}}_{k,m}^{p} - \hat{\mathbf{x}}_{\mathbf{k}}^{\mathbf{p},-}\right)\left(\tilde{\mathbf{x}}_{k,m}^{p} - \hat{\mathbf{x}}_{\mathbf{k}}^{\mathbf{p},-}\right)^{T}, s.t. \sqrt{\left(\tilde{\mathbf{x}}_{k,m}^{p} - \mathbf{x}_{m}^{S}\right)\left(\tilde{\mathbf{x}}_{k,m}^{p} - \mathbf{x}_{m}^{S}\right)^{T}} = r_{k,m}, \quad (5.7)$$

where "s.t." stands for "subject to", is given by

$$\tilde{\mathbf{x}}_{k,m}^{p} = \frac{r_{k,m}}{h_m\left(\hat{\mathbf{x}}_{k}^{p,-}\right)}\left(\hat{\mathbf{x}}_{k}^{p,-} - \mathbf{x}_{m}^{S}\right) + \mathbf{x}_{m}^{S}. \quad (5.8)$$

where $\tilde{\mathbf{x}}_{k,m}^{p} = \begin{bmatrix} \tilde{x}_{k,m}^{p} & \tilde{y}_{k,m}^{p} \end{bmatrix}^{T}$ is called a pseudo-measured position of the moving target.

The above lemma shows that a pseudo-measured position is calculated by choosing the point along the circle defined by a given TOA measurement which has a shortest distance to the predicted position of the moving target. In the following theorem, we prove that the pseudo-measured position is approximately unbiased. In addition, we also derive the associated error covariance matrix of the pseudo-measured position.

Theorem 5.1. *(Appendix B) Given a pseudo-measured position $\tilde{\mathbf{x}}_{k,m}^{p}$ associated with an individual LOS measurement $r_{k,m}$, $m = 1, \cdots, M$, and obtained in Lemma 5.1, we have that $\tilde{\mathbf{x}}_{k,m}^{p}$ is approximately unbiased, i.e., $\mathbb{E}\left(\tilde{\mathbf{x}}_{k,m}^{p}\right) \approx \mathbf{x}_{k}^{p}$. Moreover, the error covariance matrix of the pseudo-measured position $\mathbf{R}_{k,m}^{p} = \mathbb{E}\left(\left(\tilde{\mathbf{x}}_{k,m}^{p} - \mathbf{x}_{k}^{p}\right)\left(\tilde{\mathbf{x}}_{k,m}^{p} - \mathbf{x}_{k}^{p}\right)^{T}\right)$ is approximately given by*

$$\mathbf{R}_{k,m}^{p} \approx \sigma_{m}^{2}\frac{\left(\mathbf{x}_{k}^{p} - \mathbf{x}_{m}^{S}\right)\left(\mathbf{x}_{k}^{p} - \mathbf{x}_{m}^{S}\right)^{T}}{h_{m}^{2}\left(\mathbf{x}_{k}^{p}\right)} + \left(h_{m}^{2}\left(\mathbf{x}_{k}^{p}\right) + \sigma_{m}^{2}\right)\mathbf{G}\left(\mathbf{x}_{k}^{p}\right)\mathbf{P}_{k}^{p,-}\left(\mathbf{G}\left(\mathbf{x}_{k}^{p}\right)\right)^{T}, \quad (5.9)$$

where

$$\mathbf{P}_k^{p,-} = \mathbb{E}\left(\left(\hat{\mathbf{x}}_k^{p,-} - \mathbf{x}_k^p\right)\left(\hat{\mathbf{x}}_k^{p,-} - \mathbf{x}_k^p\right)^T\right) \tag{5.10}$$

$\mathbf{P}_k^{p,-}$ *being a* 2×2 *sub-matrix of* $\mathbf{P}_k^-$*, and*

$$\mathbf{G}\left(\mathbf{x}_k^p\right) = \begin{bmatrix} \frac{1}{h_m\left(\mathbf{x}_k^p\right)} - \frac{\left(x_k - x_m^S\right)^2}{h_m^3\left(\mathbf{x}_k^p\right)} & -\frac{\left(x_k - x_m^S\right)\left(y_k - y_m^S\right)}{h_m^3\left(\mathbf{x}_k^p\right)} \\ -\frac{\left(x_k - x_m^S\right)\left(y_k - y_m^S\right)}{h_m^3\left(\mathbf{x}_k^p\right)} & \frac{1}{h_m\left(\mathbf{x}_k^p\right)} - \frac{\left(y_k - y_m^S\right)^2}{h_m^3\left(\mathbf{x}_k^p\right)} \end{bmatrix}. \tag{5.11}$$

The significance of the above theorem is that it shows that the expected value of the pseudo-measured position is near the true position of the moving target if a TOA measurement is LOS. In practice, although we are unable to obtain the expected value of the pseudo-measured position, the pseudo-measured position will still give a reasonably good estimate of the moving target for an LOS TOA measurement. If the pseudo-measured position is calculated based on both the predicted position and an LOS TOA measurement, exploiting the pseudo-measured position will give a better estimate of the moving target than that by the KF or EKF which just relies on the predicted position of the target. We will elaborate more on this in the next Section.

Note that the value of $\mathbf{R}_{k,m}^p$ given in Theorem 1 depends on the true position of the target which is unavailable in practice. Hence, using the predicted position in place of the true position, the error covariance matrix of the pseudo-measured position is further approximated as $\tilde{\mathbf{R}}_{k,m}^p \approx \mathbf{R}_{k,m}^p \Big|_{\mathbf{x}_k^p = \hat{\mathbf{x}}_k^{p,-}}$.

5.2.2 Numerical Verification of Theorem 5.1

To verify the analytical results given in Theorem 5.1, numerical studies are presented in this subsection. We consider a target moving in a 2-D plane with

constant velocity. One stationary sensor is employed to collect the LOS TOA measurements.

The true initial position of the moving target is $\mathbf{x}_0 = \begin{bmatrix} 2000m & 2000m & 6m/s & 6m/s \end{bmatrix}^T$. The initial position used in the simulations is a random vector contaminated by zero mean Gaussian noise whose error covariance matrix $\mathbf{P_0} = \text{diag}\begin{Bmatrix} 50^2 & 50^2 & 1 & 1 \end{Bmatrix}$.

Measurement noise is assumed to be zero mean Gaussian with a certain standard deviation σ_w. 10^6 Monte-Carlo trials are implemented to obtain the mean and standard deviation of the pseudo-measured position under different measurement noise σ_w. Simulation results of the root mean square errors (RMSE) between the true position (in x and y coordinates) of the moving target and the experimental mean of the pseudo-measured position (in x and y coordinates) are shown in Table 5.1, for one time instance.

Table 5.1: True position of the moving target and the RMSEs between it and the experimental mean of the pseudo-measured position under different LOS TOA measurement noises, for one time instance.

	True position of the moving target $(x, y) = (2001.2, 2001.2)$		
	$\sigma_w = 50m$	$\sigma_w = 100m$	$\sigma_w = 150m$
RMSE $\tilde{x}$(m)	0.02	0.02	0.02
RMSE $\tilde{y}$(m)	0.01	0.03	0.01

From Table 5.1 it can be seen that the experimental mean of the pseudo-measured position under different LOS TOA measurement noises is very close to the true position of the moving target. The RMSE between the true position (in x and y coordinates) and the pseudo-measured position (in x and y coordinates) is not greater than $0.03m$ which is negligible.

Similarly, we also run 10^6 MC trials under different LOS measurement noise conditions to obtain the experimental standard deviation of the pseudo-measured position (in x and y coordinates). Theoretical standard deviations and the RMSEs

between them and the experimental standard deviations of the pseudo-measured position under different LOS TOA measurement noise are shown in the Table 5.2. Again, it can be seen that the difference between the the theoretical and experimental standard deviations is negligible.

Table 5.2: Theoretical standard deviations and RMSEs between them and experimental standard deviations of the pseudo-measured position under different LOS TOA measurement noise.

	$\sigma_w = 50m$	$\sigma_w = 100m$	$\sigma_w = 150m$
	Theoretical standard deviation		
Theoretical $(\sigma_{\tilde{x}}, \sigma_{\tilde{y}})$(m)	(36.05,36.05)	(71.06,71.06)	(106.30,106.30)
RMSE of $\sigma_{\tilde{x}}$(m)	0.19	0.23	0.26
RMSE of $\sigma_{\tilde{y}}$(m)	0.21	0.22	0.25

5.3 Individual Measurement LOS Detection

In the previous section, it has been shown that under the LOS condition, the pseudo-measured positions are approximately unbiased. However, in mixed LOS/NLOS environments, when the TOA measurement is contaminated by the NLOS error, the accuracy of the pseudo-measured position decreases. This effect can be used to test each pseudo-measured position against NLOS.

In this section, we show how to detect LOS pseudo-measured positions from all mixed LOS/NLOS pseudo-measured positions and then use the average of all detected LOS pseudo-measured positions as a new pseudo-measurement to update the KF to complete the target tracking task in mixed LOS/NLOS environments.

The individual measurement LOS detection algorithm to be discussed in this chapter is on the pseudo-measured position. The general idea is the same with the IMD discussed in Chapter 3. The details on determining the detection region are

different. The tracking scheme proposed in Chapter 3 on the IMD is EKF while here the KF is used.

As mentioned earlier, to obtain a pseudo-measured position $\tilde{\mathbf{x}}_{k,m}^{p}$ at time step k, we need the predicted position which is actually a sub-vector of the predicted state vector from the KF. Before we discuss the IMD method, it is convenient to briefly describe the KF first.

The IMED algorithm discussed in this chapter is an extension of the IMD algorithm discussed in Chapter 3. In the IMD algorithm, we focus on detecting the LOS TOA measurements from all mixed LOS/NLOS environments. When the selected LOS TOA measurements is ≥ 3, the EKF is used to track the moving target. When the selected LOS TOA measurements is < 3, the prediction state of the moving target is used as the estimated one. In this algorithm, we miss some of the LOS TOA measurements at some time steps. The accumulated error is big. To overcome this weakness, the IMED algorithm is proposed in this chapter. In this algorithm, each of the TOA measurement is transformed to be a pseudo-measured position. Then the pseudo-measured position is used as detection candidates. The LOS ones are used into a KF to track the moving target. At some time step, even only one TOA measurement is detected, the KF can be used. This is improved the performance of the IMD algorithm.

As the measurement equation given in Chapter 2 for TOA measurement is nonlinear and hence the KF cannot be applied directly, we replace it with the following linear pseudo-measurement equation

$$\bar{\mathbf{x}}_{k}^{p} = \mathbf{H}\mathbf{x}_{k} + \epsilon_{k}, \tag{5.12}$$

where $\bar{\mathbf{x}}_k^p = \frac{1}{n_k}\sum_{i=1}^{n_k} \tilde{\mathbf{x}}_{k,i}^p$ is the average LOS pseudo-measured position after the IMD. n_k is the total number of selected LOS measurements at time step k. ϵ_k stands for the measurement noise associated with $\bar{\mathbf{x}}_k^p$, and $\mathbf{H}$ is a constant matrix given by

$$\mathbf{H} = \begin{bmatrix} 1 & 0 & 0 & 0 \\ 0 & 1 & 0 & 0 \end{bmatrix}. \tag{5.13}$$

Based on the state equation given Chapter 2 and the new pseudo-measurement equation (5.12), we perform the KF as follows.

- **Prediction**

$$\hat{\mathbf{x}}_k^- = \mathbf{F}\hat{\mathbf{x}}_{k-1}, \tag{5.14}$$

$$\mathbf{P}_k^- = \mathbf{F}\mathbf{P}_{k-1}\mathbf{F}^T + \mathbf{Q}_u. \tag{5.15}$$

- **Update**

$$\mathbf{K}_k = \mathbf{P}_k^-\mathbf{H}^T\left(\mathbf{H}\mathbf{P}_k^-\mathbf{H}^T + \bar{\mathbf{R}}_k^p\right)^{-1}, \tag{5.16}$$

$$\hat{\mathbf{x}}_k = \hat{\mathbf{x}}_k^- + \mathbf{K}_k\bar{\mathbf{i}}_k^p, \tag{5.17}$$

$$\mathbf{P}_k = \left(\mathbf{I} - \mathbf{K}_k\mathbf{H}\right)\mathbf{P}_k^-, \tag{5.18}$$

where $\bar{\mathbf{i}}_k = \bar{\mathbf{x}}_k^p - \hat{\mathbf{x}}_k^{p,-}$ and $\hat{\mathbf{x}}_k^{p,-}$ is the predicted position obtained from the predicted state $\hat{\mathbf{x}}_k^-$ in (5.14). $\bar{\mathbf{R}}_k^p$ is the covariance matrix of $\bar{\mathbf{x}}_k^p$ given by $\mathbb{E}\left(\left(\bar{\mathbf{x}}_k^p - \mathbf{x}_k^p\right)\left(\bar{\mathbf{x}}_k^p - \mathbf{x}_k^p\right)^T\right)$. $\mathbf{K}_k$ is the Kalman gain.

While the average LOS pseudo-measured position is used for the above KF, to detect LOS pseudo-measured positions individually, it is necessary to obtain the

individual innovation $\mathbf{i}_{k,m}^{p} = \tilde{\mathbf{x}}_{k,m}^{p} - \hat{\mathbf{x}}_{k}^{p,-}, m = 1, \cdots, M$ based on each pseudo-measured position $\tilde{\mathbf{x}}_{k,m}^{p}$ calculated using the individual estimator proposed in the previous section.

Assume that it is under the LOS condition, then both $\tilde{\mathbf{x}}_{k,m}^{p}$ and $\hat{\mathbf{x}}_{k}^{p,-}$ are (approximately) unbiased estimations of the true position. It follows that

$$\mathbf{i}_{k,m}^{p} \sim \mathcal{N}\left(0, \mathbf{S}_{k,m}\right), \tag{5.19}$$

where the covariance matrix $\mathbf{S}_{k,m}$ for the pseudo-measured position $\tilde{\mathbf{x}}_{k,m}^{p}$ is

$$\begin{aligned}
\mathbf{S}_{k,m} &= \mathbb{E}\left(\left(\tilde{\mathbf{x}}_{k,m}^{p} - \hat{\mathbf{x}}_{k}^{p,-}\right)\left(\tilde{\mathbf{x}}_{k,m}^{p} - \hat{\mathbf{x}}_{k}^{p,-}\right)^{T}\right) \\
&= \mathbb{E}\left(\left(\left(\tilde{\mathbf{x}}_{k,m}^{p} - \mathbf{x}_{k}^{p}\right) - \left(\hat{\mathbf{x}}_{k}^{p,-} - \mathbf{x}_{k}^{p}\right)\right)\left(\left(\tilde{\mathbf{x}}_{k,m}^{p} - \mathbf{x}_{k}^{p}\right) - \left(\hat{\mathbf{x}}_{k}^{p,-} - \mathbf{x}_{k}^{p}\right)\right)^{T}\right) \\
&= \mathbb{E}\left(\left(\tilde{\mathbf{x}}_{k,m}^{p} - \mathbf{x}_{k}^{p}\right)\left(\tilde{\mathbf{x}}_{k,m}^{p} - \mathbf{x}_{k}^{p}\right)^{T}\right) + \mathbb{E}\left(\left(\hat{\mathbf{x}}_{k}^{p,-} - \mathbf{x}_{k}^{p}\right)\left(\hat{\mathbf{x}}_{k}^{p,-} - \mathbf{x}_{k}^{p}\right)^{T}\right) \\
&\quad -\mathbb{E}\left(\left(\tilde{\mathbf{x}}_{k,m}^{p} - \mathbf{x}_{k}^{p}\right)\left(\hat{\mathbf{x}}_{k}^{p,-} - \mathbf{x}_{k}^{p}\right)^{T}\right) - \mathbb{E}\left(\left(\hat{\mathbf{x}}_{k}^{p,-} - \mathbf{x}_{k}^{p}\right)\left(\tilde{\mathbf{x}}_{k,m}^{p} - \mathbf{x}_{k}^{p}\right)^{T}\right).
\end{aligned} \tag{5.20}$$

The first term in the right hand side of (5.20) has been given in (5.9), while the second term is $\mathbf{P}_{k}^{p,-}$ given in (5.10). Using a similar approach in deriving $\mathbf{R}_{k,m}^{p}$, the third and fourth terms in the right hand side of (5.20) can be derived as follows (the details omitted here to save space).

$$\mathbb{E}\left(\left(\tilde{\mathbf{x}}_{k,m}^{p} - \mathbf{x}_{k}^{p}\right)\left(\hat{\mathbf{x}}_{k}^{p,-} - \mathbf{x}_{k}^{p}\right)^{T}\right) = \mathbb{E}\left(\tilde{\mathbf{x}}_{k,m}^{p}\left(\hat{\mathbf{x}}_{k}^{p,-}\right)^{T}\right) - \mathbf{x}_{k}^{p}\left(\mathbf{x}_{k}^{p}\right)^{T} \approx h_{m}\left(\mathbf{x}_{k}^{p}\right)\mathbf{G}\left(\mathbf{x}_{k}^{p}\right)\mathbf{P}_{k}^{p,-}, \tag{5.21}$$

$$\mathbb{E}\left(\left(\hat{\mathbf{x}}_k^{p,-}-\mathbf{x}_k^p\right)\left(\tilde{\mathbf{x}}_{k,m}^p-\mathbf{x}_k^p\right)^T\right) = \mathbb{E}\left(\hat{\mathbf{x}}_k^{p,-}\left(\tilde{\mathbf{x}}_{k,m}^p\right)^T\right)-\mathbf{x}_k^p\left(\mathbf{x}_k^p\right)^T \approx h_m\left(\mathbf{x}_k^p\right)\mathbf{G}\left(\mathbf{x}_k^p\right)\mathbf{P}_k^{p,-}. \tag{5.22}$$

Substituting (5.9), (5.10), (5.21) and (5.22) into (5.20) and simplifying gives

$$\mathbf{S}_{k,m} \approx \mathbf{R}_{k,m}^p+\mathbf{P}_k^{p,-}-2h_m\left(\mathbf{x}_k^p\right)\mathbf{G}\left(\mathbf{x}_k^p\right)\mathbf{P}_k^{p,-} \approx \tilde{\mathbf{R}}_{k,m}^p+\mathbf{P}_k^{p,-}-2h_m\left(\hat{\mathbf{x}}_k^{p,-}\right)\mathbf{G}\left(\hat{\mathbf{x}}_k^{p,-}\right)\mathbf{P}_k^{p,-}. \tag{5.23}$$

Note that in practice the true position of the moving target $\mathbf{x}_k^p$ is unknown. Hence, we replace $\mathbf{x}_k^p$ with its predicted position $\hat{\mathbf{x}}_k^{p,-}$.

From the LOS and Gaussian assumptions the confidence region is an elliptical region defined as follows [73, 74]

$$v_{k,m}\left(\gamma_m\right)=\left\{\tilde{\mathbf{x}}_{k,m}^p:\left(\tilde{\mathbf{x}}_{k,m}^p-\hat{\mathbf{x}}_k^{p,-}\right)^T\mathbf{S}_{k,m}^{-1}\left(\tilde{\mathbf{x}}_{k,m}^p-\hat{\mathbf{x}}_k^{p,-}\right)<\gamma_m\right\}, \tag{5.24}$$

where γ_m is the threshold for determining the size of the confidence region for the pseudo-measured position obtained by sensor m.

The pseudo-measured position will satisfy the confidence criterion if it is calculated from a LOS measurement. Otherwise, the pseudo-measured position does not satisfy the confidence criterion as the zero-mean Gaussian assumption of the innovation is not fulfilled in NLOS environments.

To evaluate the confidence region, we introduce the test statistic

$$T_{k,m}=\left(\tilde{\mathbf{x}}_{k,m}^p-\hat{\mathbf{x}}_k^{p,-}\right)^T\mathbf{S}_{k,m}^{-1}\left(\tilde{\mathbf{x}}_{k,m}^p-\hat{\mathbf{x}}_k^{p,-}\right). \tag{5.25}$$

The distribution of $T_{k,m}$ is the chi-squared distribution with two degrees of free-

dom. The probability that a pseudo-measured position calculated from a LOS measurement falls in the confidence region is

$$\int_0^{\gamma_m} f_{\chi^2(2)}(x)dx = P_D, \tag{5.26}$$

where $f_{\chi^2(2)}(\cdot)$ is the chi-squared pdf with two degrees of freedom and P_D is the probability of detection (of LOS measurements). Given a P_D, the threshold γ_m can be calculated by (5.26). If $T_{k,m}$ is larger than the threshold γ_m, the pseudo-measured position is taken as an NLOS measurement and is discarded. Otherwise, it is considered as an LOS measurement and is retained. The rationale behind the proposed LOS detection (or NLOS rejection) criterion is based on the understanding that in the 2-D location plane, compared with positions corresponding to LOS measurements, positions corresponding to NLOS measurements are in general further away from the predicted position $\hat{\mathbf{x}}_k^{p,-}$. Hence, by choosing a proper threshold using (29) with a pre-set high P_D, we should be able to detect most of the LOS measurements while rejecting the majority of the NLOS measurements. Note that we are unable to choose the detection threshold based on the probability of false alarm P_{FA} directly since we do not assume prior knowledge of NLOS noise.

To show how to determine the threshold γ_m, assume that the known LOS noise for each sensor is independent and identically distributed (i.i.d.) Gaussian with $(\mu, \sigma) = (0m, 150m)$. We pre-set the theoretical P_D as $P_D = 0.99$. By (5.26), we calculate $\gamma_m = 9.21$. Note that γ_m is obtained independent of the NLOS noise. To illustrate the validity of (5.26), we assume, for simplicity, that for each sensor, the NLOS noise is i.i.d. mean-shifted Gaussian with $(\mu_\eta, \sigma_\eta) = (1400m, 400m)$ and the TOA measurements are subject to different percentages of NLOS error ε. Hence,

we consider only one stationary sensor and randomly generate 10,000 samples of TOA measurements for each ε. Using the threshold $\gamma_m = 9.21$, we then obtain the experimental P_D and the experimental probability of false alarm P_{FA} shown in Table 5.3.

Table 5.3: Experimental probabilities of detection and false alarm of one sensor with different fraction of NLOS errors.

ε	0.1	0.25	0.5	0.75
P_D	0.982	0.981	0.981	0.980
P_{FA}	0.014	0.022	0.037	0.051

As it can be seen from the above table, the experimental P_D for different ε is almost the same and near the theoretical $P_D = 0.99$, as expected from (5.26). On the other hand, the experimental P_{FA} increases with ε. Since positions corresponding to NLOS measurements are in general further away from the predicted position $\hat{\mathbf{x}}_k^{p,-}$, the experimental P_{FA} is still rather low even in the relatively severe mixed LOS/NLOS NLOS environments.

After the threshold γ_m is determined, the proposed LOS detection method is performed on each of the pseudo-measured positions $\tilde{\mathbf{x}}_{k,m}^p$ and the accepted ones are considered as LOS and stored in a dynamic data array denoted as $\left\{\tilde{\mathbf{x}}_{k,j}^p\right\}_{j=1}^{n_k}$, where n_k is the total number of selected LOS measurements at time step k. Note that in the LOS environment, n_k is a static value determined by the number of sensors M, but in the mixed LOS/NLOS environments, the value of n_k is dynamic and it is determined by the total number of LOS measurements detected at each time step k.

After performing the IMD, at the end of each time step k the average of all the

selected LOS pseudo-measured positions $\bar{\mathbf{x}}_k^p = \frac{1}{n_k}\sum_{i=1}^{n_k}\tilde{\mathbf{x}}_{k,i}^p$ is used to update the KF. To make good use of $\bar{\mathbf{x}}_k^p$, the error covariance of it should be calculated at every time step. Calculation of the error covariance of $\bar{\mathbf{x}}_k^p$ is detailed described in the following section.

5.4 Tracking Strategy

In this sub-section, we propose the new tracking algorithm based on the KF summarized in the previous section and the proposed IMED method.

Since each pseudo-measured position is an approximately unbiased estimate of the true target position, we have that

$$\mathbb{E}\left(\bar{\mathbf{x}}_k^p\right) = \mathbb{E}\left(\frac{1}{n_k}\sum_{i=1}^{n_k}\tilde{\mathbf{x}}_{k,i}^p\right) = \frac{1}{n_k}\sum_{i=1}^{n_k}\mathbb{E}\left(\tilde{\mathbf{x}}_{k,i}^p\right) \approx \mathbf{x}_k^p. \tag{5.27}$$

It means that $\bar{\mathbf{x}}_k^p$ is also an approximately unbiased estimate of the true target position.

The covariance matrix of the average pseudo-measured position $\bar{\mathbf{x}}_k^p$ is given by

$$\begin{aligned}\mathbb{E}\left(\left(\bar{\mathbf{x}}_k^p - \mathbf{x}_k^p\right)\left(\bar{\mathbf{x}}_k^p - \mathbf{x}_k^p\right)^T\right) &= \mathbb{E}\left(\left(\bar{\mathbf{x}}_k^p\right)\left(\bar{\mathbf{x}}_k^p\right)^T\right) - \mathbf{x}_k^p\left(\mathbf{x}_k^p\right)^T \\ &= \frac{1}{\left(n_k\right)^2}\sum_{i=1}^{n_k}\sum_{j=1}^{n_k}\mathbb{E}\left(\left(\tilde{\mathbf{x}}_{k,i}^p\right)\left(\tilde{\mathbf{x}}_{k,j}^p\right)^T\right) - \mathbf{x}_k^p\left(\mathbf{x}_k^p\right)^T.\end{aligned} \tag{5.28}$$

Using a similar approach to evaluating $\mathbb{E}\left(\tilde{\mathbf{x}}_{k,m}^p\left(\tilde{\mathbf{x}}_{k,m}^p\right)^T\right)$ as done in the previous

section, we can derive $\mathbb{E}\left(\left(\tilde{\mathbf{x}}_{k,i}^{p}\right)\left(\tilde{\mathbf{x}}_{k,j}^{p}\right)^{T}\right)$ as follows.

$$\mathbb{E}\left(\left(\tilde{\mathbf{x}}_{k,i}^{p}\right)\left(\tilde{\mathbf{x}}_{k,j}^{p}\right)^{T}\right) \approx \begin{cases} \mathbf{x}_{k}^{p}\left(\mathbf{x}_{k}^{p}\right)^{T} + h_{i}\left(\mathbf{x}_{k}^{p}\right)\mathbf{G}\left(\mathbf{x}_{k}^{p}\right)\mathbf{H}\mathbf{P}_{k}^{-}\mathbf{H}^{T}\left(h_{j}\left(\mathbf{x}_{k}^{p}\right)\mathbf{G}\left(\mathbf{x}_{k}^{p}\right)\right)^{T}, & i \neq j \\ \mathbf{R}_{k,i}^{p} + \mathbf{x}_{k}^{p}\left(\mathbf{x}_{k}^{p}\right)^{T}, & i = j \end{cases} \tag{5.29}$$

$$\begin{aligned} \bar{\mathbf{R}}_{k}^{p} &\approx \frac{1}{\left(n_{k}\right)^{2}}\left(\sum_{i=1}^{n_{k}}\sum_{j=1,j\neq i}^{n_{k}} h_{i}\left(\mathbf{x}_{k}^{p}\right)\mathbf{G}\left(\mathbf{x}_{k}^{p}\right)\mathbf{H}\mathbf{P}_{k}^{-}\mathbf{H}^{T}\left(h_{j}\left(\mathbf{x}_{k}^{p}\right)\mathbf{G}\left(\mathbf{x}_{k}^{p}\right)\right)^{T} + \sum_{i=1}^{n_{k}}\mathbf{R}_{k,i}^{p}\right) \\ &\approx \frac{1}{\left(n_{k}\right)^{2}}\left(\sum_{i=1}^{n_{k}}\sum_{j=1,j\neq i}^{n_{k}} h_{i}\left(\hat{\mathbf{x}}_{k}^{p,-}\right)\mathbf{G}\left(\hat{\mathbf{x}}_{k}^{p,-}\right)\mathbf{H}\mathbf{P}_{k}^{-}\mathbf{H}^{T}\left(h_{j}\left(\hat{\mathbf{x}}_{k}^{p,-}\right)\mathbf{G}\left(\hat{\mathbf{x}}_{k}^{p,-}\right)\right)^{T} + \sum_{i=1}^{n_{k}}\tilde{\mathbf{R}}_{k,i}^{p}\right). \end{aligned} \tag{5.30}$$

The tracking algorithm based on the proposed IMED method and the KF is summarized as follows.

Proposed Tracking Algorithm

Given:

1. An initial state of the moving target $\mathbf{x}_0$ and the corresponding initial error covariance matrix $\mathbf{P}_0$
2. Standard deviation $\sigma_m, m = 1, \cdots, M$ of the LOS measurement noise
3. The pre-set probability of detection and the corresponding threshold γ_m

IMED based Kalman Filter

- **For** $k = 1:1:K$
  - Do prediction to obtain $\hat{\mathbf{x}}_k^-$ and $\mathbf{P}_k^-$
  - set $n_k = 0$;
  - **For** $m = 1:1:M$
    - Calculate pseudo-measured position $\tilde{\mathbf{x}}_{k,m}^p$
    - Calculate corresponding covariance matrix $\tilde{\mathbf{R}}_{k,m}^p$ of each $\tilde{\mathbf{x}}_{k,m}^p$
    - Calculate $\mathbf{S}_{k,m}$
    - **If** $\left(\left(\tilde{\mathbf{x}}_{k,m}^p - \hat{\mathbf{x}}_k^{p,-}\right)^T \mathbf{S}_{k,m}^{-1} \left(\tilde{\mathbf{x}}_{k,m}^p - \hat{\mathbf{x}}_k^{p,-}\right) < \gamma_m\right)$
      - Reserve $\tilde{\mathbf{x}}_{k,m}^p$ as LOS pseudo-measured position
      - $n_k = n_k + 1$
    - **Else**
      - Drop $\tilde{\mathbf{x}}_{k,m}^p$
    - **End If**
  - **End For**
  - **If** $n_k \neq 0$
    - Calculate the average of all selected LOS pseudo-measured positions $\bar{\mathbf{x}}_k^p = \frac{1}{n_k} \sum_{i=1}^{n_k} \tilde{\mathbf{x}}_{k,i}^p$
    - Calculate the covariance matrix $\bar{\mathbf{R}}_k^p$
    - Calculate the Kalman gain $\mathbf{K}_k$
    - Update the predicted state using $\bar{\mathbf{x}}_k^p$
    - Update the error covariance matrix $\mathbf{P}_k$
  - **Else**
    - Use the predicted state as the estimated state for time step k
    - Update the error covariance matrix $\mathbf{P}_k$ using the prediction error covariance matrix
  - **End If**
- **End For**

5.5 Simulation results

Here, we consider the random force motion model as described in [8] and [22]. Simulations are repeated over 1000 Monte Carlo trials and each tracker is performed over $K = 1000$ time steps with a sampling time interval $0.2s$ in the ad-hoc network and the symmetric cellular network. The settings of the cellular network is given in Chapter 3. The settings of the ad-hoc network is as follows.

In the ad-hoc network, ten wireless stationary sensors are employed to collect TOA only or joint TOA/AOA measurements. They are located at $\left(x_1^S = 2.5\text{km}, y_1^S = 5\text{km}\right)$, $\left(x_2^S = 1\text{km}, y_2^S = 3.5\text{km}\right)$, $\left(x_3^S = 4.5\text{km}, y_3^S = 1.75\text{km}\right)$, $\left(x_4^S = 1.5\text{km}, y_4^S = 4\text{km}\right)$, $\left(x_5^S = 3\text{km}, y_5^S = 4.5\text{km}\right)$, $\left(x_6^S = 1.75\text{km}, y_6^S = 1\text{km}\right)$, $\left(x_7^S = 4\text{km}, y_7^S = 0.75\text{km}\right)$, $\left(x_8^S = 5\text{km}, y_8^S = 1.25\text{km}\right)$, $\left(x_9^S = 0.5\text{km}, y_9^S = 2\text{km}\right)$ and $\left(x_{10}^S = 3\text{km}, y_{10}^S = 0.25\text{km}\right)$. In the ad-hoc network the initial state $\hat{\mathbf{x}}_0$ of the moving target is set as a Gaussian random vector with a standard deviation of $50m$ for the x and y coordinates and a standard deviation of $4m/s$ for the velocities along the x and y directions, around the true initial state $\mathbf{x}_0 = \begin{bmatrix} 2200m & 2200m & 4m/s & 4m/s \end{bmatrix}^T$.

The LOS TOA measurement noise on each sensor is assumed to be i.i.d. zero mean Gaussian distributed with a standard deviation $\sigma = 150m$. The theoretical P_D is set to be 0.99 and the calculated threshold $\gamma_m = 9.21$, $m = 1, \cdots, M$.

Two different ways are adopted to simulate the NLOS occurrences over time. The first model assumes i.i.d. NLOS errors over time. The second one uses a two-state Markov chain for each sensor to model time dependence [8]. Discussions on the behaviors of the different trackers under these two models are given in the following subsections.

5.5.1 NLOS Occurrence Modeled as i.i.d.

In this simulation, we assume that the NLOS errors are i.i.d. over time and sensors meaning there is neither correlation between consecutive time steps for a fixed sensor nor correlation among different sensors for a fixed time step [22]. We compute the EKF, the semi-parametric modified residual based EKF [8], labeled as EKF-SPMR, the modified probability data association based KF [22], labeled as MPDA, the IMD based EKF proposed in Chapter 3, labeled as EKF-IMD and the proposed IMED based KF, labeled as KF-IMED. Different percentages of NLOS errors, including $30\%, 40\%, 50\%$ and 60%, are simulated to test the performance of each tracker. The NLOS noise is either exponential with $\sigma_\eta = 400m$ or mean-shifted Gaussian characterized by $(\mu_\eta, \sigma_\eta) = (1400m, 400m)$.

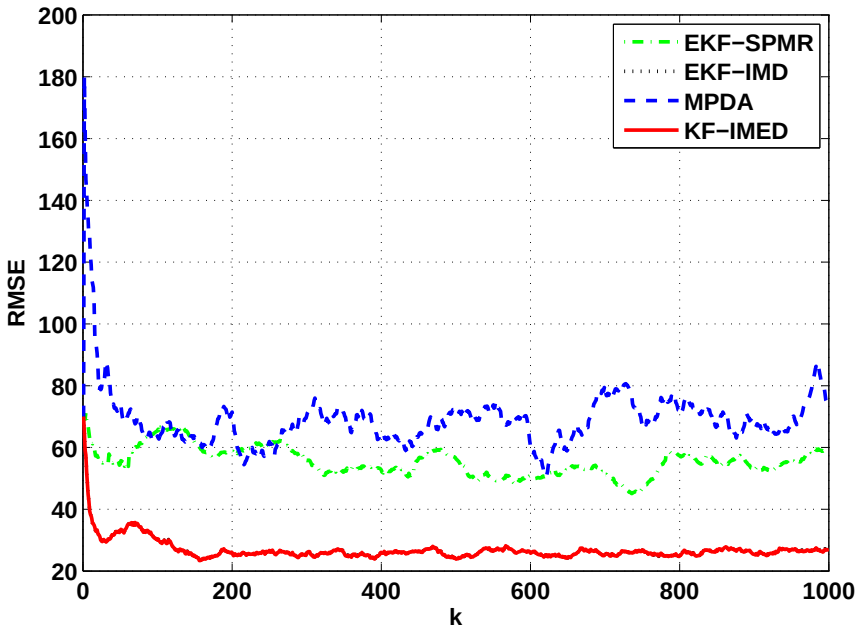

Figure 5.1: RMSEs of each tracker with random trajectory in the cellular network with 30% i.i.d. mean-shifted Gaussian NLOS errors.

Simulation results are summarized in Table 5.4 in terms of average MED over time. In the ideal LOS case (zero mean Gaussian measurement noise only) for which the EKF is expected to be the best tracker, the performance of the proposed KF-IMED is quite close to that of the EKF and is better than the that of the EKF-SPMR and MPDA by at least 40%. In all other scenarios (mixed LOS/NLOS), the KF-IMED outperforms all other trackers considerably, particularly in the highly contaminated scenarios. For example, in the case of 60% NLOS, the average MED by KF-IMED is only half of the average MED by MPDA and 1/3 of that by EKF-SPMR for the exponential NLOS noise. The performance improvement of the KF-IMED over the EKF-SPMR and MPDA is more obvious for the shifted Gaussian noise. Compared with the authors' preliminary EKF-IMD tracker, the performance improvement of the KF-IMED is also observed, particularly in the highly contaminated scenarios.

Figure 5.1 shows the RMSEs of each tracker over time for the case of 30% i.i.d. mean-shifted Gaussian NLOS errors. We exclude the EKF tracker since its RMSEs are much larger than those of other trackers. Although the EKF-SPMR and MPDA achieve relatively high precision in terms of RMSEs, the RMSEs are still around $50m$ to $80m$. On the other hand, both the EKF-IMD and the proposed KF-IMED have RMSEs less than $30m$ most of the time and have achieved better precision than the EKF-SPMR and MPDA. The EKF-IMD and the proposed KF-IMED produce almost identical tracking results because large outliers are discarded by using the same IMD method.

Table 5.4: Mean over time MEDs (m) of each tracker for random trajectory in the cellular network with i.i.d. exponential and mean-shifted Gaussian NLOS errors occurrence

	Random trajectory, cellular network				
	LOS	30% NLOS	40% NLOS	50% NLOS	60% NLOS
	exponential $\sigma_{\text{exp},\eta} = 400m$				
EKF	**20.33**	531.14	719.82	913.21	1101.90
EKF-SPMR	32.60	65.60	96.74	134.77	185.43
EKF-IMD	20.71	30.75	39.40	50.93	69.18
MPDA	37.20	58.86	73.85	92.46	121.74
KF-IMED	20.71	**30.25**	**38.08**	**48.59**	**64.52**
	shifted Gaussian $(\mu_\eta, \sigma_\eta) = (1400m, 400m)$				
EKF	**20.33**	292.60	667.01	844.02	1032.20
EKF-SPMR	32.60	47.22	85.66	122.73	171.83
EKF-IMD	20.71	23.09	30.06	36.09	47.62
MPDA	37.20	47.25	75.42	95.18	133.17
KF-IMED	20.71	**23.02**	**27.90**	**30.82**	**35.21**

5.5.2 NLOS Occurrence Modeled as Markov Chain

Dropping the i.i.d. assumption, a two-state Markov chain is adopted for each sensor to model the LOS and NLOS conditions. For a certain sensor m, it is in the state of LOS with probability $1 - \varepsilon_m$. In the state of NLOS, it occurs with probability ε_m. The definition of ε_m and the transition matrix used for the simulations are similar to those in Chapter 2 and [46]. By choosing different values for transition matrix in the simulations, we can simulate different mixed LOS/NLOS scenarios in the real world closely. The details of the transition matrix and the selection of its values are given in Chapter 2.

The NLOS noise used in the simulations is either exponential with $\sigma_\eta = 400m$ or mean-shifted Gaussian characterized by $(\mu_\eta, \sigma_\eta) = (800m, 300m)$ and $(\mu_\eta, \sigma_\eta) = (1400m, 400m)$ in the ad-hoc network and the cellular network, respectively. Simulations under NLOS scenarios A0 to A6 in the ad-hoc network and C0 to C6 in the cellular network are implemented, respectively. Scenarios C0 to C6 have shown in Chapter 3. Scenarios A0 to A6 are given as follows.

$$\text{A0: } \boldsymbol{\varepsilon} = \begin{bmatrix} 0 & 0 & 0 & 0 & 0 & 0 & 0 & 0 & 0 & 0 \end{bmatrix}$$

$$\text{A1: } \boldsymbol{\varepsilon} = \begin{bmatrix} .25 & .25 & .25 & .1 & .1 & .25 & .1 & .25 & .1 & .1 \end{bmatrix}$$

$$\text{A2: } \boldsymbol{\varepsilon} = \begin{bmatrix} .1 & .5 & .25 & .1 & .1 & .5 & .1 & .25 & .1 & .1 \end{bmatrix}$$

$$\text{A3: } \boldsymbol{\varepsilon} = \begin{bmatrix} .1 & .5 & .25 & .1 & .5 & .75 & .1 & .75 & .5 & .25 \end{bmatrix}$$

$$\text{A4: } \boldsymbol{\varepsilon} = \begin{bmatrix} .5 & .5 & .75 & .1 & .5 & .75 & .1 & .75 & .5 & .25 \end{bmatrix}$$

$$\text{A5: } \boldsymbol{\varepsilon} = \begin{bmatrix} .5 & .5 & .75 & .75 & .5 & .75 & .25 & .75 & .75 & .25 \end{bmatrix}$$

$$\text{A6: } \boldsymbol{\varepsilon} = \begin{bmatrix} 1 & .75 & .75 & .75 & .5 & .75 & 1 & .75 & .75 & .75 \end{bmatrix}.$$

Table 5.5: Mean over time MEDs (m) of each tracker for random trajectory in the ad-hoc network with Markov chain exponential and mean-shifted Gaussian NLOS errors occurrence

	Random trajectory, ad-hoc network						
	A0	A1	A2	A3	A4	A5	A6
	exponential $\sigma_{\text{exp},\eta} = 400m$						
EKF	**16.0**	70.31	97.83	136.48	142.16	155.98	186.89
EKF-SPMR	21.4	34.62	37.24	51.23	63.37	64.68	105.88
EKF-IMD	17.0	24.16	31.39	48.31	53.22	64.51	89.06
KF-IMED	17.0	**23.81**	**30.02**	**45.50**	**50.05**	**61.37**	**82.99**
	shifted Gaussian $(\mu_\eta, \sigma_\eta) = (800m, 300m)$						
EKF	**16.0**	70.31	219.0	313.18	843.76	1207.4	2204.5
EKF-SPMR	21.4	34.62	51.5	104.93	181.38	276.08	1038.9
EKF-IMD	17.0	26.22	**18.78**	22.18	24.72	31.78	60.81
KF-IMED	17.0	**19.36**	19.55	**22.18**	**24.02**	**27.23**	**26.64**

We compute the EKF, the EKF-SPMR, the EKF-IMD, and the proposed KF-IMED. Table 5.5 gives the average MEDs of each tracker calculated under different NLOS scenarios in the ad-hoc network with Gaussian and exponential NLOS errors. Table 5.6 gives the average MEDs of each tracker calculated under different NLOS scenarios in the cellular network with Gaussian and exponential NLOS errors.

Similar to the situation where NLOS occurrence is modeled as i.i.d., we observe from Tables 5.5 and 5.6 that in the ideal LOS case for which the EKF is expected

Table 5.6: Mean over time MEDs (m) of each tracker for random trajectory in the cellular network with Markov chain exponential and mean-shifted Gaussian NLOS errors occurrence

	Random trajectory, cellular network						
	C0	C1	C2	C3	C4	C5	C6
	exponential $\sigma_{\exp,\eta} = 400m$						
EKF	**20.33**	81.87	162.61	188.62	269.66	271.94	386.76
EKF-SPMR	32.60	46.04	87.02	77.62	105.65	106.01	184.66
EKF-IMD	20.71	33.10	59.29	69.85	106.61	111.91	196.23
KF-IMED	20.71	**33.10**	**56.04**	**62.69**	**94.04**	**99.05**	**181.75**
	shifted Gaussian $(\mu_\eta, \sigma_\eta) = (1400m, 400m)$						
EKF	**20.33**	276.76	556.87	741.83	1068.60	1088.90	1519.0
EKF-SPMR	32.60	72.07	179.22	147.70	389.36	452.81	1255.7
EKF-IMD	20.71	22.18	23.29	50.85	128.52	281.97	673.54
KF-IMED	20.71	**22.18**	**23.00**	**31.60**	**41.41**	**63.80**	**119.25**

to be the best tracker, the performance of the proposed KF-IMED is quite close to that of the EKF and is better than the that of the EKF-SPMR and MPDA by at least 20%. In most of the other scenarios (mixed LOS/NLOS), the KF-IMED outperforms other trackers, particularly in the highly contaminated scenarios with mean-shifted Gaussian NLOS error. For example, in the case of scenario $C6$ with mean-shifted Gaussian NLOS error, the average MED by KF-IMED is only about 20% of the average MED by EKF-SPMR for the ad-hoc network and less than 10% of the average MED by EKF-SPMR for the cellular network. On the other hand, we also notice that the performance improvement of KF-IMED over EKF-SPMR for exponential NLOS error is not as significant as that for mean-shifted Gaussian NLOS error, with the decrease of the average MED by KF-IMED compared with that by EKF-SPMR ranging from 2% to over 30%. Compared with the authors' preliminary EKF-IMD tracker, the performance improvement of KF-IMED in general is also observed.

The cumulative error distribution of the localization error for scenario $C4$ with mean-shifted Gaussian NLOS errors is shown in Figure 5.2. From this figure, it can

be seen that the 95% marks of the proposed tracker KF-IMED and the EKF-IMD are about $105m$ and $128m$, respectively. As for the EKF-SPMR and the EKF, the 95% marks increase to about $335m$ and $1160m$, respectively.

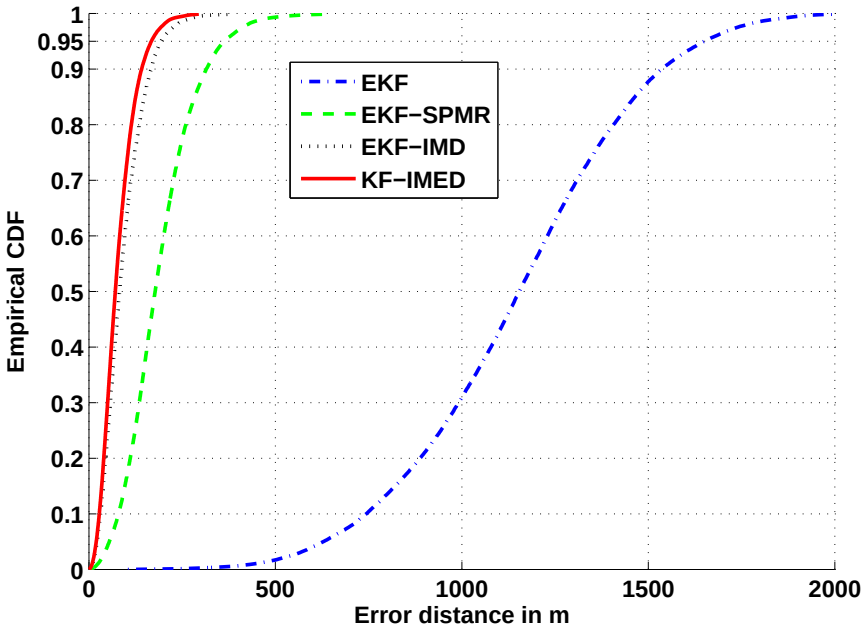

Figure 5.2: Cumulative distribution functions of different trackers in the cellular network for Scenario C4 with mean-shifted Gaussian NLOS errors.

5.5.3 Computational complexity

A rigorous analysis of the computational complexity of target tracking algorithms is in general quite difficult. Hence, we only carry out a simple comparison of the computational efficiency by recording the time consumed by all the trackers under discussion running with 1000 Monte Carlo trials under LOS scenario and the mixed LOS/NLOS scenario with 30% i.i.d. mean-shifted Gaussian NLOS errors, respectively. They are shown in Table 5.7. All simulations are implemented under

the same hardware and software conditions.

Table 5.7: Consumed time (s) of each tracker with 1000 Monte Carlo trials in LOS and mixed LOS/NLOS environments in the cellular network.

Algorithms	EKF	EKF-SPMR	EKF-IMD	MPDA	KF-IMED
LOS (s)	111.2	21663.1	190.5	3019.9	193.0
30% i.i.d. NLOS errors(s)	127.7	23276.8	190.1	3027.6	192.7

It is obvious that the EKF is the most efficient algorithm, as it consumes the minimum time under both the LOS condition and the mixed LOS/NLOS conditions. The time consumed by the EKF-IMD and the proposed KF-IMED trackers is close to that of the EKF tracker since the computational complexity does not increase substantially for the EKF-IMD and the proposed KF-IMED.

For the EKF-SPMR, both Cholesky decomposition and inverse for robust regression are introduced. In addition, it also takes some time to compute and estimate the pdf of mixture LOS/NLOS noise. From Table 5.7, it can be seen that the EKF-SPMR is the slowest algorithm. For the MPDA algorithm, additional matrix inversion operation is introduced into each group in the least squares algorithm, so the computational complexity of MPDA is greater than the EKF, the EKF-IMD and the proposed KF-IMED, but smaller than the EKF-SPMR.

5.6 Conclusion

In this chapter, we have proposed a new tracking algorithm based on an approximately unbiased estimator, a corresponding detector and the classical Kalman filter. We have proposed the new concept of a pseudo-measured position by choos-

ing the point, along the circle defined by a given TOA measurement, which has a shortest distance to the predicted position of a moving target, and also proved that the pseudo-measured position is an approximately unbiased estimate of the true position of the moving target. An efficient method has then been developed to detect LOS measurements among all mixed LOS/NLOS TOA measurements and discard NLOS ones, followed by the Kalman filter for target tracking. We do not require prior information of the NLOS noise and yet we are able to make good use of all the detected LOS TOA measurements even when there are fewer than 3 LOS TOA measurements available at a given time step. Simulations have shown that the proposed approach has out-performed (in terms of both the accuracy and the computational efficiency) the state-of-the-art methods [8, 22] in both LOS and mixed LOS/NLOS environments, particularly when the NLOS noise is strong. The proposed target tracking algorithm is for a single target and for big networks which have applications on tracking the movement of an outdoor emitter, e.g. a radio frequency (RF) communication device, within a small urban area. It may be applicable to smaller networks with some modification. The extension of the proposed tracking algorithm to the case of using joint TOA/AOA measurements is discussed in the following chapter.

Appendix A - Proof of Lemma 5.1

Proof. To solve the problem defined in (5.7), we rewrite it as an equivalent scalar equation

$$\min_{\tilde{x}^p_{k,m},\tilde{y}^p_{k,m}} \left(\tilde{x}^p_{k,m} - \hat{x}^{p,-}_k\right)^2 + \left(\tilde{y}^p_{k,m} - \hat{y}^{p,-}_k\right)^2, \text{s.t.} \left(\tilde{x}^p_{k,m} - x^S_m\right)^2 + \left(\tilde{y}^p_{k,m} - y^S_m\right)^2 = r^2_{k,m}. \tag{5.31}$$

The Lagrange multiplier method is used to solve the above constrained minimization problem by forming the following cost function

$$\xi = \left(\tilde{x}^p_{k,m} - \hat{x}^{p,-}_k\right)^2 + \left(\tilde{y}^p_{k,m} - \hat{y}^{p,-}_k\right)^2 + \lambda\left(\left(\tilde{x}^p_{k,m} - x^S_m\right)^2 + \left(\tilde{y}^p_{k,m} - y^S_m\right)^2 - r^2_{k,m}\right), \tag{5.32}$$

where λ is the Lagrange multiplier. Taking the first order derivative of ξ with respect to $\tilde{x}^p_{k,m}$, $\tilde{y}^p_{k,m}$ and λ, and setting them to zeros, we have

$$\frac{\partial \xi}{\partial \tilde{x}^p_{k,m}} = 2\left(\tilde{x}^p_{k,m} - \hat{x}^{p,-}_k\right) + 2\lambda\left(\tilde{x}^p_{k,m} - x^S_m\right) = 0, \tag{5.33}$$

$$\frac{\partial \xi}{\partial \tilde{y}^p_{k,m}} = 2\left(\tilde{y}^p_{k,m} - \hat{y}^{p,-}_k\right) + 2\lambda\left(\tilde{y}^p_{k,m} - y^S_m\right) = 0, \tag{5.34}$$

$$\frac{\partial \xi}{\partial \lambda} = \left(\tilde{x}^p_{k,m} - x^S_m\right)^2 + \left(\tilde{y}^p_{k,m} - y^S_m\right)^2 - r^2_{k,m} = 0. \tag{5.35}$$

From (5.33) and (5.34), we obtain

$$\tilde{x}^p_{k,m} = \frac{\lambda x^S_m + \hat{x}^{p,-}_k}{1+\lambda}, \tag{5.36}$$

$$\tilde{y}^p_{k,m} = \frac{\lambda y^S_m + \hat{y}^{p,-}_k}{1+\lambda},. \tag{5.37}$$

Plugging (5.36) and (5.37) into (5.35) and simplifying gives

$$\left(\frac{\lambda x_m^S + \hat{x}_k^{p,-}}{1+\lambda} - x_m^S\right)^2 + \left(\frac{\lambda y_m^S + \hat{y}_k^{p,-}}{1+\lambda} - y_m^S\right)^2 = r_{k,m}^2. \tag{5.38}$$

The solution of λ is given by

$$\lambda = \frac{\sqrt{\left(\hat{x}_k^{p,-} - x_m^S\right)^2 + \left(\hat{y}_k^{p,-} - y_m^S\right)^2}}{r_{k,m}} - 1 = \frac{h_m\left(\hat{\mathbf{x}}_k^{p,-}\right)}{r_{k,m}} - 1. \tag{5.39}$$

Substituting (5.39) into (5.36) and (5.37), we can solve $\tilde{x}_{k,m}^p$ and $\tilde{y}_{k,m}^p$ as follows

$$\tilde{x}_{k,m}^p = \frac{\left(h_m\left(\hat{\mathbf{x}}_k^{p,-}\right) - r_{k,m}\right) x_m^S + r_{k,m}\hat{x}_k^{p,-}}{h_{k,m}\left(\hat{\mathbf{x}}_k^{p,-}\right)}, \tag{5.40}$$

$$\tilde{y}_{k,m}^p = \frac{\left(h_m\left(\hat{\mathbf{x}}_k^{p,-}\right) - r_{k,m}\right) y_m^S + r_{k,m}\hat{y}_k^{p,-}}{h_{k,m}\left(\hat{\mathbf{x}}_k^{p,-}\right)}. \tag{5.41}$$

The solutions of $\tilde{x}_{k,m}^p$ and $\tilde{y}_{k,m}^p$ can also be rewritten as

$$\tilde{x}_{k,m}^p = \frac{r_{k,m}}{h_m\left(\hat{\mathbf{x}}_k^{p,-}\right)}\left(\hat{x}_k^{p,-} - x_m^S\right) + x_m^S, \tag{5.42}$$

$$\tilde{y}_{k,m}^p = \frac{r_{k,m}}{h_m\left(\hat{\mathbf{x}}_k^{p,-}\right)}\left(\hat{y}_k^{p,-} - y_m^S\right) + y_m^S, \tag{5.43}$$

or in vector form

$$\tilde{\mathbf{x}}_{k,m}^p = \frac{r_{k,m}}{h_m\left(\hat{\mathbf{x}}_k^{p,-}\right)}\left(\hat{\mathbf{x}}_k^{p,-} - \mathbf{x}_m^S\right) + \mathbf{x}_m^S. \tag{5.44}$$

□

Appendix B - Proof of Theorem 5.1

Proof. To prove $\mathbb{E}\left(\tilde{\mathbf{x}}_{k,m}^{p}\right) \approx \mathbf{x}_{k}^{p}$, we first calculate the conditional expectation of $\mathbb{E}\left(\tilde{\mathbf{x}}_{k,m}^{p} \middle| \hat{\mathbf{x}}_{k}^{p,-}\right)$. From (5.44), we know that

$$\mathbb{E}\left(\tilde{\mathbf{x}}_{k,m}^{p} \middle| \hat{\mathbf{x}}_{k}^{p,-}\right) = \left(\hat{\mathbf{x}}_{k}^{p,-} - \mathbf{x}_{m}^{S}\right) \frac{h_m\left(\mathbf{x}_{k}^{p}\right)}{h_m\left(\hat{\mathbf{x}}_{k}^{p,-}\right)} + \mathbf{x}_{m}^{S} = h_m\left(\mathbf{x}_{k}^{p}\right) \frac{\left(\hat{\mathbf{x}}_{k}^{p,-} - \mathbf{x}_{m}^{S}\right)}{h_m\left(\hat{\mathbf{x}}_{k}^{p,-}\right)} + \mathbf{x}_{m}^{S}. \tag{5.45}$$

Let $\mathbf{f}\left(\hat{\mathbf{x}}_{k}^{p,-}\right) = \frac{\left(\hat{\mathbf{x}}_{k}^{p,-} - \mathbf{x}_{m}^{S}\right)}{h_m\left(\hat{\mathbf{x}}_{k}^{p,-}\right)}$, and expand it around $\mathbf{x}_{k}^{p}$ by a first-order Taylor series expansion to obtain

$$\mathbf{f}\left(\hat{\mathbf{x}}_{k}^{p,-}\right) \approx \mathbf{f}\left(\mathbf{x}_{k}^{p}\right) + \mathbf{G}\left(\mathbf{x}_{k}^{p}\right)\left(\hat{\mathbf{x}}_{k}^{p,-} - \mathbf{x}_{k}^{p}\right), \tag{5.46}$$

where $\mathbf{G}\left(\mathbf{x}_{k}^{p}\right) = \frac{\partial \mathbf{f}\left(\mathbf{x}_{k}^{p}\right)}{\partial \mathbf{x}_{k}^{p}}$ and is given in (5.11). Note that the effect of the higher order terms of the Taylor expansions is negligible (details omitted here). Substituting (5.46) into (5.45), we have

$$\begin{aligned}
\mathbb{E}\left(\tilde{\mathbf{x}}_{k,m}^{p} \middle| \hat{\mathbf{x}}_{k}^{p,-}\right) &\approx h_m\left(\mathbf{x}_{k}^{p}\right)\left(\mathbf{f}\left(\mathbf{x}_{k}^{p}\right) + \mathbf{G}\left(\mathbf{x}_{k}^{p}\right)\left(\hat{\mathbf{x}}_{k}^{p,-} - \mathbf{x}_{k}^{p}\right)\right) + \mathbf{x}_{m}^{S} \\
&= h_m\left(\mathbf{x}_{k}^{p}\right)\left(\frac{\left(\mathbf{x}_{k}^{p} - \mathbf{x}_{m}^{S}\right)}{h_m\left(\mathbf{x}_{k}^{p}\right)} + \mathbf{G}\left(\mathbf{x}_{k}^{p}\right)\left(\hat{\mathbf{x}}_{k}^{p,-} - \mathbf{x}_{k}^{p}\right)\right) + \mathbf{x}_{m}^{S} \\
&= \mathbf{x}_{k}^{p} + h_m\left(\mathbf{x}_{k}^{p}\right)\mathbf{G}\left(\mathbf{x}_{k}^{p}\right)\left(\hat{\mathbf{x}}_{k}^{p,-} - \mathbf{x}_{k}^{p}\right).
\end{aligned} \tag{5.47}$$

Then we have the expectation of $\tilde{\mathbf{x}}_{k,m}^{p}$ as follows

$$\begin{aligned}
\mathbb{E}\left(\tilde{\mathbf{x}}_{k,m}^{p}\right) &= \mathbb{E}\left(\mathbb{E}\left(\tilde{\mathbf{x}}_{k,m}^{p} \middle| \hat{\mathbf{x}}_{k}^{p,-}\right)\right) \approx \mathbb{E}\left(\mathbf{x}_{k}^{p} + h_m\left(\mathbf{x}_{k}^{p}\right)\mathbf{G}\left(\mathbf{x}_{k}^{p}\right)\left(\hat{\mathbf{x}}_{k}^{p,-} - \mathbf{x}_{k}^{p}\right)\right) \\
&= \mathbf{x}_{k}^{p} + h_m\left(\mathbf{x}_{k}^{p}\right)\mathbf{G}\left(\mathbf{x}_{k}^{p}\right)\mathbb{E}\left(\left(\hat{\mathbf{x}}_{k}^{p,-} - \mathbf{x}_{k}^{p}\right)\right) = \mathbf{x}_{k}^{p}.
\end{aligned} \tag{5.48}$$

Next, we derive the error covariance matrix of the pseudo-measured position $\mathbf{R}_{k,m}^{p}$. By definition

$$\mathbf{R}_{k,m}^{p} = \mathbb{E}\left(\left(\tilde{\mathbf{x}}_{k,m}^{p} - \mathbf{x}_{k}^{p}\right)\left(\tilde{\mathbf{x}}_{k,m}^{p} - \mathbf{x}_{k}^{p}\right)^{T}\right) = \mathbb{E}\left(\tilde{\mathbf{x}}_{k,m}^{p}\left(\tilde{\mathbf{x}}_{k,m}^{p}\right)^{T}\right) - \mathbf{x}_{k}^{p}\left(\mathbf{x}_{k}^{p}\right)^{T}. \quad (5.49)$$

We exploit the following identity

$$\mathbb{E}\left(\tilde{\mathbf{x}}_{k,m}^{p}\left(\tilde{\mathbf{x}}_{k,m}^{p}\right)^{T}\right) = \mathbb{E}\left(\mathbb{E}\left(\tilde{\mathbf{x}}_{k,m}^{p}\left(\tilde{\mathbf{x}}_{k,m}^{p}\right)^{T}\left|\hat{\mathbf{x}}_{k}^{p,-}\right.\right)\right). \quad (5.50)$$

Now

$$\begin{aligned}
&\mathbb{E}\left(\tilde{\mathbf{x}}_{k,m}^{p}\left(\tilde{\mathbf{x}}_{k,m}^{p}\right)^{T}\left|\hat{\mathbf{x}}_{k}^{p,-}\right.\right) \\
&\quad= \mathbb{E}\left(\frac{\left(r_{k,m}\right)^{2}}{h_{m}^{2}(\hat{\mathbf{x}}_{k}^{p,-})}\left(\hat{\mathbf{x}}_{k}^{p,-} - \mathbf{x}_{m}^{S}\right)\left(\hat{\mathbf{x}}_{k}^{p,-} - \mathbf{x}_{m}^{S}\right)^{T}\left|\hat{\mathbf{x}}_{k}^{p,-}\right.\right) + \mathbf{x}_{m}^{S}\left(\mathbf{x}_{m}^{S}\right)^{T} \\
&\qquad+ \mathbb{E}\left(\frac{r_{k,m}}{h_{m}\left(\hat{\mathbf{x}}_{k}^{p,-}\right)}\left(\hat{\mathbf{x}}_{k}^{p,-} - \mathbf{x}_{m}^{S}\right)\left(\mathbf{x}_{m}^{S}\right)^{T}\left|\hat{\mathbf{x}}_{k}^{p,-}\right.\right) \\
&\qquad+ \mathbb{E}\left(\frac{r_{k,m}}{h_{m}\left(\hat{\mathbf{x}}_{k}^{p,-}\right)}\mathbf{x}_{m}^{S}\left(\hat{\mathbf{x}}_{k}^{p,-} - \mathbf{x}_{m}^{S}\right)^{T}\left|\hat{\mathbf{x}}_{k}^{p,-}\right.\right) \\
&\quad= \frac{\mathbb{E}\left(\left(r_{k,m}\right)^{2}\right)}{h_{m}^{2}(\hat{\mathbf{x}}_{k}^{p,-})}\left(\hat{\mathbf{x}}_{k}^{p,-} - \mathbf{x}_{m}^{S}\right)\left(\hat{\mathbf{x}}_{k}^{p,-} - \mathbf{x}_{m}^{S}\right)^{T} + \mathbf{x}_{m}^{S}\left(\mathbf{x}_{m}^{S}\right)^{T} \\
&\qquad+ \frac{\mathbb{E}\left(r_{k,m}\right)}{h_{m}\left(\hat{\mathbf{x}}_{k}^{p,-}\right)}\left(\hat{\mathbf{x}}_{k}^{p,-} - \mathbf{x}_{m}^{S}\right)\left(\mathbf{x}_{m}^{S}\right)^{T} + \frac{\mathbb{E}\left(r_{k,m}\right)}{h_{m}\left(\hat{\mathbf{x}}_{k}^{p,-}\right)}\mathbf{x}_{m}^{S}\left(\hat{\mathbf{x}}_{k}^{p,-} - \mathbf{x}_{m}^{S}\right)^{T} \\
&\quad= \frac{h_{m}^{2}\left(\mathbf{x}_{k}^{p}\right) + \sigma_{m}^{2}}{h_{m}^{2}(\hat{\mathbf{x}}_{k}^{p,-})}\left(\hat{\mathbf{x}}_{k}^{p,-} - \mathbf{x}_{m}^{S}\right)\left(\hat{\mathbf{x}}_{k}^{p,-} - \mathbf{x}_{m}^{S}\right)^{T} + \mathbf{x}_{m}^{S}\left(\mathbf{x}_{m}^{S}\right)^{T} \\
&\qquad+ \frac{h_{m}\left(\mathbf{x}_{k}^{p}\right)}{h_{m}\left(\hat{\mathbf{x}}_{k}^{p,-}\right)}\left(\hat{\mathbf{x}}_{k}^{p,-} - \mathbf{x}_{m}^{S}\right)\left(\mathbf{x}_{m}^{S}\right)^{T} + \frac{h_{m}\left(\mathbf{x}_{k}^{p}\right)}{h_{m}\left(\hat{\mathbf{x}}_{k}^{p,-}\right)}\mathbf{x}_{m}^{S}\left(\hat{\mathbf{x}}_{k}^{p,-} - \mathbf{x}_{m}^{S}\right)^{T}.
\end{aligned} \quad (5.51)$$

Since $\mathbb{E}\left(r_{k,m}\right) = h_{m}\left(\mathbf{x}_{k}^{p}\right)$ and $\mathbb{E}\left(\left(r_{k,m}\right)^{2}\right) = h_{m}^{2}(\mathbf{x}_{k}^{p}) + \sigma_{m}^{2}$. Taking the expectation

of (5.51), we have

$$\begin{aligned}
&\mathbb{E}\left(\mathbb{E}\left(\tilde{\mathbf{x}}_{k,m}^{p}\left(\tilde{\mathbf{x}}_{k,m}^{p}\right)^{T}\left|\hat{\mathbf{x}}_{k}^{p,-}\right.\right)\right) \\
&\quad=\mathbb{E}\left(\frac{\left(h_{m}\left(\mathbf{x}_{k}^{p}\right)\right)^{2}+\sigma_{m}^{2}}{h_{m}^{2}(\hat{\mathbf{x}}_{k}^{p,-})}\left(\hat{\mathbf{x}}_{k}^{p,-}-\mathbf{x}_{m}^{S}\right)\left(\hat{\mathbf{x}}_{k}^{p,-}-\mathbf{x}_{m}^{S}\right)^{T}\right)+\mathbf{x}_{m}^{S}\left(\mathbf{x}_{m}^{S}\right)^{T} \\
&\qquad+\mathbb{E}\left(\frac{h_{m}\left(\mathbf{x}_{k}^{p}\right)}{h_{m}\left(\hat{\mathbf{x}}_{k}^{p,-}\right)}\left(\hat{\mathbf{x}}_{k}^{p,-}-\mathbf{x}_{m}^{S}\right)\left(\mathbf{x}_{m}^{S}\right)^{T}\right) \\
&\qquad+\mathbb{E}\left(\frac{h_{m}\left(\mathbf{x}_{k}^{p}\right)}{h_{m}\left(\hat{\mathbf{x}}_{k}^{p,-}\right)}\mathbf{x}_{m}^{S}\left(\hat{\mathbf{x}}_{k}^{p,-}-\mathbf{x}_{m}^{S}\right)^{T}\right). \qquad (5.52)
\end{aligned}$$

We evaluate the first term in (5.52) as

$$\begin{aligned}
&\mathbb{E}\left(\frac{\left(h_{m}\left(\mathbf{x}_{k}^{p}\right)\right)^{2}+\sigma_{m}^{2}}{h_{m}^{2}(\hat{\mathbf{x}}_{k}^{p,-})}\left(\hat{\mathbf{x}}_{k}^{p,-}-\mathbf{x}_{m}^{S}\right)\left(\hat{\mathbf{x}}_{k}^{p,-}-\mathbf{x}_{m}^{S}\right)^{T}\right) \\
&\quad=\left(h_{m}^{2}(\mathbf{x}_{k}^{p})+\sigma_{m}^{2}\right)\mathbb{E}\left(\frac{\left(\hat{\mathbf{x}}_{k}^{p,-}-\mathbf{x}_{m}^{S}\right)}{h_{m}\left(\hat{\mathbf{x}}_{k}^{p,-}\right)}\left(\frac{\left(\hat{\mathbf{x}}_{k}^{p,-}-\mathbf{x}_{m}^{S}\right)}{h_{m}\left(\hat{\mathbf{x}}_{k}^{p,-}\right)}\right)^{T}\right) \\
&\quad\approx\left(h_{m}^{2}(\mathbf{x}_{k}^{p})+\sigma_{m}^{2}\right) \\
&\qquad\times\mathbb{E}\left(\left(\mathbf{f}\left(\mathbf{x}_{k}^{p}\right)+\mathbf{G}\left(\mathbf{x}_{k}^{p}\right)\left(\hat{\mathbf{x}}_{k}^{p,-}-\mathbf{x}_{k}^{p}\right)\right)\left(\mathbf{f}\left(\mathbf{x}_{k}^{p}\right)+\mathbf{G}\left(\mathbf{x}_{k}^{p}\right)\left(\hat{\mathbf{x}}_{k}^{p,-}-\mathbf{x}_{k}^{p}\right)\right)^{T}\right) \\
&\quad=\left(h_{m}^{2}(\mathbf{x}_{k}^{p})+\sigma_{m}^{2}\right)\left(\mathbf{f}\left(\mathbf{x}_{k}^{p}\right)\left(\mathbf{f}\left(\mathbf{x}_{k}^{p}\right)\right)^{T}+\mathbf{G}\left(\mathbf{x}_{k}^{p}\right)\mathbf{P}_{k}^{p,-}\left(\mathbf{G}\left(\mathbf{x}_{k}^{p}\right)\right)^{T}\right) \\
&\quad=\left(h_{m}^{2}(\mathbf{x}_{k}^{p})+\sigma_{m}^{2}\right)\left(\frac{\left(\mathbf{x}_{k}^{p}-\mathbf{x}_{m}^{S}\right)\left(\mathbf{x}_{k}^{p}-\mathbf{x}_{m}^{S}\right)^{T}}{h_{m}^{2}\left(\mathbf{x}_{k}^{p}\right)}+\mathbf{G}\left(\mathbf{x}_{k}^{p}\right)\mathbf{P}_{k}^{p,-}\left(\mathbf{G}\left(\mathbf{x}_{k}^{p}\right)\right)^{T}\right) \\
&\quad=\left(\mathbf{x}_{k}^{p}-\mathbf{x}_{m}^{S}\right)\left(\mathbf{x}_{k}^{p}-\mathbf{x}_{m}^{S}\right)^{T}+\sigma_{m}^{2}\frac{\left(\mathbf{x}_{k}^{p}-\mathbf{x}_{m}^{S}\right)\left(\mathbf{x}_{k}^{p}-\mathbf{x}_{m}^{S}\right)^{T}}{h_{m}^{2}(\mathbf{x}_{k}^{p})} \\
&\qquad+\left(h_{m}^{2}(\mathbf{x}_{k}^{p})+\sigma_{m}^{2}\right)\mathbf{G}(\mathbf{x}_{k}^{p})\mathbf{P}_{k}^{p,-}\mathbf{G}^{T}(\mathbf{x}_{k}^{p}). \qquad (5.53)
\end{aligned}$$

Next, we evaluate the third term in (5.52) as

$$\begin{aligned}
&\mathbb{E}\left(\frac{h_m\left(\mathbf{x}_k^p\right)}{h_m\left(\hat{\mathbf{x}}_k^{p,-}\right)}\left(\hat{\mathbf{x}}_k^{p,-}-\mathbf{x}_m^S\right)\left(\mathbf{x}_m^S\right)^T\right)\\
&\quad= h_m\left(\mathbf{x}_k^p\right)\mathbb{E}\left(\frac{\left(\hat{\mathbf{x}}_k^{p,-}-\mathbf{x}_m^S\right)}{h_m\left(\hat{\mathbf{x}}_k^{p,-}\right)}\right)\left(\mathbf{x}_m^S\right)^T\\
&\quad\approx h_m\left(\mathbf{x}_k^p\right)\mathbb{E}\left(\mathbf{f}\left(\mathbf{x}_k^p\right)+\mathbf{G}\left(\mathbf{x}_k^p\right)\left(\hat{\mathbf{x}}_k^{p,-}-\mathbf{x}_k^p\right)\right)\left(\mathbf{x}_m^S\right)^T\\
&\quad= \left(\mathbf{x}_k^p-\mathbf{x}_m^S\right)\left(\mathbf{x}_m^S\right)^T, \qquad (5.54)
\end{aligned}$$

and similarly the fourth term in (5.52) as

$$\begin{aligned}
\mathbb{E}\left(\frac{h_m\left(\mathbf{x}_k^p\right)}{h_m\left(\hat{\mathbf{x}}_k^{p,-}\right)}\mathbf{x}_m^S\left(\hat{\mathbf{x}}_k^{p,-}-\mathbf{x}_m^S\right)^T\right) &= h_m\left(\mathbf{x}_k^p\right)\mathbf{x}_m^S\mathbb{E}\left(\frac{\left(\hat{\mathbf{x}}_k^{p,-}-\mathbf{x}_m^S\right)^T}{h_m\left(\hat{\mathbf{x}}_k^{p,-}\right)}\right)\\
&\approx h_m\left(\mathbf{x}_k^p\right)\mathbf{x}_m^S\mathbb{E}\left(\mathbf{f}\left(\mathbf{x}_k^p\right)+\mathbf{G}\left(\mathbf{x}_k^p\right)\left(\hat{\mathbf{x}}_k^{p,-}-\mathbf{x}_k^p\right)\right)^T\\
&= \mathbf{x}_m^S\left(\mathbf{x}_k^p-\mathbf{x}_m^S\right)^T. \qquad (5.55)
\end{aligned}$$

Substituting (5.53) – (5.55) into (5.52) and then (5.52) into (5.49), taking into account of (5.50), we finally arrive at the error covariance matrix of the pseudo-measured position

$$\begin{aligned}
\mathbf{R}_{k,m}^p &\approx \left(\mathbf{x}_k^p-\mathbf{x}_m^S\right)\left(\mathbf{x}_k^p-\mathbf{x}_m^S\right)^T+\sigma_m^2\frac{\left(\mathbf{x}_k^p-\mathbf{x}_m^S\right)\left(\mathbf{x}_k^p-\mathbf{x}_m^S\right)^T}{h_m^2(\mathbf{x}_k^p)}\\
&\quad+\left(h_m^2(\mathbf{x}_k^p)+\sigma_m^2\right)\mathbf{G}\left(\mathbf{x}_k^p\right)\mathbf{P}_k^{p,-}\left(\mathbf{G}\left(\mathbf{x}_k^p\right)\right)^T\\
&\quad+\left(\mathbf{x}_k^p-\mathbf{x}_m^S\right)\left(\mathbf{x}_m^S\right)^T+\mathbf{x}_m^S\left(\mathbf{x}_k^p-\mathbf{x}_m^S\right)^T+\mathbf{x}_m^S\left(\mathbf{x}_m^S\right)^T-\mathbf{x}_k^p\left(\mathbf{x}_k^p\right)^T\\
&= \sigma_m^2\frac{\left(\mathbf{x}_k^p-\mathbf{x}_m^S\right)\left(\mathbf{x}_k^p-\mathbf{x}_m^S\right)^T}{h_m^2(\mathbf{x}_k^p)}+\left(h_m^2(\mathbf{x}_k^p)\right)\mathbf{G}\left(\mathbf{x}_k^p\right)\mathbf{P}_k^{p,-}\left(\mathbf{G}\left(\mathbf{x}_k^p\right)\right)^T. \qquad (5.56)
\end{aligned}$$

□

Chapter 6

Joint TOA/AOA Measurements and IMED Based Tracking Scheme

In this chapter a tracking scheme based on the Kalman filter framework and the individual measurement estimation and detection algorithm using joint TOA/AOA measurements is proposed. This is a further development of the proposed IMED algorithm in Chapter 5. Details of the proposed tracking scheme are given as follows.

6.1 Introduction

In target tracking, different kind of measurement techniques including time of arrival, time difference of arrival, received signal strength and angle-of-arrival are used [55]. Among target tracking algorithms using these measurements, TOA-

based and TDOA-based tracking algorithms are the most popular ones since the tracking accuracy is high and the computational complexity is low. Although the distances related TOA and TDOA measurements can achieve high accuracy, they generally requires at least 3 non-collinearly located LOS sensors to produce a two-dimensional (2-D) position of the moving target. Meanwhile, the AOA measurements based tracking schemes need only a minimum of two LOS sensors. But the AOA measurements based schemes are highly range dependent i.e. when the target is far away from the sensor, a small AOA measurement error will result in a large localization error. To handle this problem, many researchers are considering cooperative localization approaches [75–79].

With the above background, in this chapter we concentrate on joint TOA/AOA based measurements to improve the tracking accuracy in mixed LOS/NLOS environments. We develop the target tracking method based on individual measurement estimation and LOS detection in mixed LOS/NLOS environments into AOA measurements collected by multiple stationary sensors. A pseudo-measured position is first calculated by choosing the point along the circle defined by a given AOA measurement which has the shortest distance to the predicted position of a moving target. Then the pseudo-measured positions are passed to a detector to be identified either LOS or NLOS. The selected LOS TOA/AOA measurements are then combined into a KF to update the state of the moving target. Moreover, as no additional matrix inversion is required by the IMED method, the proposed tracking algorithm is also computationally efficient. Simulation results have been shown that the joint TOA/AOA based IMED tracking scheme performs better than the TOA only based IMED tracking scheme.

The rest of this chapter is organized as follows. Section 6.2 briefly describes the

system models required in the target tracking problem with AOA measurements. Section 6.3 presents the proposed IME method, with both theoretical analysis and numerical verification for AOA measurements. Simulations are presented in section 6.4 to illustrate the merits of the proposed tracking algorithm and finally conclusions are drawn in section 6.5. For convenience of presentation, proofs are given in the Appendix.

6.2 Problem Statement

The measurement equation for joint TOA/AOA measurements is defined as follows

$$\begin{bmatrix} \boldsymbol{r}_k \\ \boldsymbol{\beta}_k \end{bmatrix} = \begin{bmatrix} \mathbf{h}^{TOA}(\mathbf{x}_k) \\ \mathbf{h}^{AOA}(\mathbf{x}_k) \end{bmatrix} + \begin{bmatrix} \boldsymbol{\eta}_k^{TOA} \\ \boldsymbol{\eta}_k^{AOA} \end{bmatrix}, \tag{6.1}$$

where $\boldsymbol{\beta}_k$ is the measured angle vector at time step k.

The non-linear function vector $\mathbf{h}^{\mathbf{TOA}}(\cdot) = \begin{bmatrix} h_1^{TOA}(\mathbf{x}_k) & \cdots & h_M^{TOA}(\mathbf{x}_k) \end{bmatrix}^T$ and $\mathbf{h}^{\mathbf{AOA}}(\cdot) = \begin{bmatrix} h_1^{AOA}(\mathbf{x}_k) & \cdots & h_M^{AOA}(\mathbf{x}_k) \end{bmatrix}^T$ are the measurement function vectors for TOA and AOA measurements, respectively. The measurement functions AOA measurements is defined as follows

$$\mathbf{h}^{AOA}(\mathbf{x}_k) = \begin{bmatrix} \arctan\frac{y-y_1^S}{x-x_1^S} \\ \vdots \\ \arctan\frac{y-y_M^S}{x-x_M^S} \end{bmatrix}. \tag{6.2}$$

$\boldsymbol{\eta}_k^{TOA} = \begin{bmatrix} \eta_{k,1}^{TOA} & \ldots & \eta_{k,M}^{TOA} \end{bmatrix}^T$ and $\boldsymbol{\eta}_k^{AOA} = \begin{bmatrix} \eta_{k,1}^{AOA} & \ldots & \eta_{k,M}^{AOA} \end{bmatrix}^T$ are the mixture LOS/NLOS measurement noise vectors on TOA and AOA measurements, respec-

tively. The description of the mixture LOS/NLOS noise on TOA measurements is detailed described in Chapter 2. The definition of the mixture LOS/NLOS noise on AOA measurements is also assumed to be mean-shifted Gaussian or exponential distribution. The probability density function for $\eta_{k,m}^{AOA}$ is

$$p(\eta_m^{AOA}) = (1 - \varepsilon_m^{AOA}) p_{\text{LOS}}(w_{k,m}^{AOA}) + \varepsilon_m^{AOA} p_{\text{NLOS}}(\delta_{k,m}^{AOA}), m = 1, \cdots, M \tag{6.3}$$

where $\varepsilon_m^{AOA} \in [0, 1]$ is the degree of contamination by NLOS errors at sensor m on AOA measurement. The noise is effectively a mixture of LOS and NLOS noise where $p_{\text{LOS}}(w_{k,m}^{AOA})$ is a zero mean Gaussian noise and $p_{\text{NLOS}}(\delta_{k,m}^{AOA})$ is typically a mean-shifted Gaussian or exponentially distributed noise.

6.3 Individual Measurement Estimation for AOA Measurements

The individual measurement estimation for TOA measurements have been presented in Chapter 5. Here we just analyze the AOA measurements. Measuring AOA requires the system to be equipped with an antenna array. The AOA measurements can be obtained using algorithms such as the MUSIC and ESPRIT [80] [53]. In traditional tracking algorithms, such as EKF, the minimum number of AOA measurements is 2.

In the absence of noise, an accuracy estimation of the position of the target can be obtained using geometric equations. For AOA, each measurement points out a direction i.e. an angle to x axis or to y axis, so a line can be drawn starting from the stationary sensor with the given angle as gradient. The intersection point

of two or more lines indicates the estimate position of the target. This has been shown in Figure 2.1.

Under the LOS condition, the measurement function for a AOA or bearing-only measurement collected by sensor m at time step k is given by

$$\beta_{k,m} = \bar{\beta}_{k,m} + w_{k,m} = h_{AOA,m}\left(\mathbf{x}_k\right) + w_{k,m}, m = 1, \cdots, M \tag{6.4}$$

where $\bar{\beta}_{k,m}$ is the noise-free angle and $w_{k,m}$ is the zero mean Gaussian noise with standard deviation σ_m.

With the assumption of zero mean Gaussian noise in both the state equation (2.9) and the measurement equation (6.4), we can easily obtain the following results which will be useful subsequently

$$\begin{aligned}
\mathbb{E}\left(\hat{\mathbf{x}}_k - \mathbf{x}_k\right) &= 0, & (6.5)\\
\mathbb{E}\left(\hat{\mathbf{x}}_k^- - \mathbf{x}_k\right) &= 0, & (6.6)\\
\mathbb{E}\left(\boldsymbol{\beta}_k - \mathbf{h}^{AOA}\left(\mathbf{x}_k\right)\right) &= 0, & (6.7)\\
\mathbb{E}\left(\left(\hat{\mathbf{x}}_k^- - \mathbf{x}_k\right)\left(\hat{\mathbf{x}}_k^- - \mathbf{x}_k\right)^T\right) &= \mathbf{P}_k^-, & (6.8)\\
\mathbb{E}\left(\left(\hat{\mathbf{x}}_k - \mathbf{x}_k\right)\left(\hat{\mathbf{x}}_k - \mathbf{x}_k\right)^T\right) &= \mathbf{P}_k, & (6.9)
\end{aligned}$$

where $\mathbb{E}\left(\cdot\right)$ is the expectation operator. $\mathbf{x}_k$ and $\hat{\mathbf{x}}_k$ are the true state of the moving target and its estimated state given by the KF, respectively. $\hat{\mathbf{x}}_k^- = \mathbf{F}\hat{\mathbf{x}}_{k-1}$ is the predicted state. $\mathbf{P}_k$ is the error covariance matrix and $\mathbf{P}_k^-$ is the predicted error covariance matrix. Equations (6.5) and (6.6) show that the estimated state $\hat{\mathbf{x}}_k$ and the predicted state of the moving target $\hat{\mathbf{x}}_k^-$ are both unbiased estimates of the true state of the moving target $\mathbf{x}_k$. Equation (6.7) shows that the measured angle

vector $\boldsymbol{\beta}_k$ is an unbiased angle vector of the true angle vector.

From (6.4) and the definition of $h_m^{AOA}(\mathbf{x}_k)$, it is easy to see that the noise free measurement $\bar{\beta}_{k,m}$ determines a set of possible positions of the moving target on a direct line with a certain angle $\bar{\beta}_{k,m}$. The true position of the moving target must be on the line. However, because of the measurement noise, we can only obtain $\beta_{k,m}$ instead of $\bar{\beta}_{k,m}$. Hence, the best estimated position of the moving target from the measured angle $\beta_{k,m}$ is the point on a direct line with angle $\beta_{k,m}$ that has minimum Euclidean distance to the true position, $\mathbf{x}_k^p = \begin{bmatrix} x_k & y_k \end{bmatrix}^T$, of the moving target. This is shown in Figure 6.1.

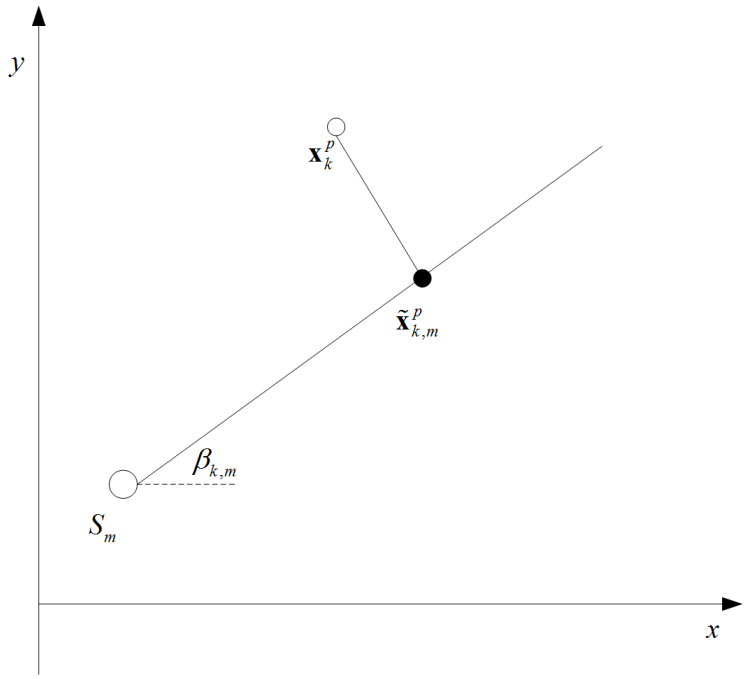

Figure 6.1: AOA-IMED.

In practice, the true position of the moving target is unknown and it is replaced by the predicted position, $\hat{\mathbf{x}}_k^{p,-} = \begin{bmatrix} \hat{x}_k^{p,-} & \hat{y}_k^{p,-} \end{bmatrix}^T$, which is calculated from the state equation. Such a replacement is reasonable since the predicted position is

an unbiased estimate of the true position of the moving target (see (6.6)). The weakness of the replacement is that it relays on the state model. In the following lemma, based on the predicted position and one AOA measurement, we present a method for finding a pseudo-measured position, a new and important concept introduced in this chapter.

Lemma 6.1. *(Appendix A) Given the predicted position* $\hat{\mathbf{x}}_k^{p,-}$ *and a AOA measurement* $\beta_{k,m}$*, the solution to the following constrained optimization problem*

$$\min \left(\tilde{\mathbf{x}}_k^p - \hat{\mathbf{x}}_k^{p,-}\right)^T \left(\tilde{\mathbf{x}}_k^p - \hat{\mathbf{x}}_k^{p,-}\right), \; s.t. \; \beta_{k,m} = \arg\tan \frac{\tilde{y}_{k,m}^p - y_{k,m}^S}{\tilde{x}_{k,m}^p - x_{k,m}^S}. \tag{6.10}$$

where "s.t." stands for "subject to", is given by equations (6.11) and (6.12).

$$\tilde{x}_{k,m}^p = \hat{x}_k^{p,-} + \tan\beta_{k,m} \frac{\left(\hat{y}_k^{p,-} - y_{k,m}^S\right) - \left(\hat{x}_k^{p,-} - x_{k,m}^S\right)\tan\beta_{k,m}}{1 + \tan^2\beta_{k,m}}, \tag{6.11}$$

$$\tilde{y}_{k,m}^p = \hat{y}_k^{p,-} - \frac{\left(\hat{y}_k^{p,-} - y_{k,m}^S\right) - \left(\hat{x}_k^{p,-} - x_{k,m}^S\right)\tan\beta_{k,m}}{1 + \tan^2\beta_{k,m}}, \tag{6.12}$$

where $\tilde{\mathbf{x}}_{k,m}^p = \begin{bmatrix} \tilde{x}_{k,m}^p & \tilde{y}_{k,m}^p \end{bmatrix}^T$ *is called a pseudo-measured position of the moving target.*

The above lemma shows that a pseudo-measured position is calculated by choosing the point along the direction line defined by a given AOA measurement which has a shortest distance to the predicted position of the moving target. In the following theorem, we prove that the pseudo-measured position is approximately unbiased.

Theorem 6.1. *(Appendix B) Suppose the measurement noise* $w_{k,m}$ *on sensor* m *is a small value,* $\cos w_{k,m} \approx 1$*,* $\sin w_{k,m} \approx w_{k,m}$ *and* $w_{k,m}^2 \approx 0$*. Given a pseudo-measured*

position $\tilde{\mathbf{x}}_{k,m}^{p}$ *associated with an individual LOS measurement* $\beta_{k,m}$, $m = 1, \cdots, M$, *we have that* $\tilde{\mathbf{x}}_{k,m}^{p}$ *is approximately unbiased, i.e.,* $\mathbb{E}\left(\tilde{\mathbf{x}}_{k,m}^{p}\right) \approx \mathbf{x}_{k}^{p}$.

The significance of the above theorem is that it shows that the expected value of the pseudo-measured position is near the true position of the moving target if a AOA measurement is LOS. In practice, although we are unable to obtain the expected value of the pseudo-measured position, the pseudo-measured position will still give a reasonably good estimate of the moving target for an LOS AOA measurement. If the pseudo-measured position is calculated based on both the predicted position and an LOS AOA measurement, exploiting the pseudo-measured position will give a better estimate of the moving target than that by the KF or EKF which just relies on the predicted position of the target. If the pseudo-measured position is calculated based on both the predicted position and a NLOS AOA measurement, huge error will occur and the calculated pseudo-measured will be far away from the predicted position of the moving target. This property is used to detect the pseudo-measured position is LOS or NLOS. The details have been given in Chapter 5.

After detection of each pseudo-measured position, the LOS ones are reserved while the NLOS ones are dropped. Then the corresponding LOS measurements are used into the KF to track the moving target. Simulations are shown in the following section to verify the proposed algorithm.

6.4 Simulation results

Here, we analyze the constant velocity moving model and the random force moving model in the cellular network described in Chapter 3.

Two different ways are adopted to simulate the NLOS occurrences over time. The first model assumes i.i.d. NLOS errors over time. The second one uses a two-state Markov chain for each sensor to model time dependence [8]. Discussions on the behaviors of the different trackers under these two models are given in the following subsections.

6.4.1 NLOS Occurrence Modeled as i.i.d.

In this simulation, we assume that the NLOS errors are i.i.d. over time and sensors meaning there is neither correlation between consecutive time steps for a fixed sensor nor correlation among different sensors for a fixed time step [22]. We compute the KF using joint TOA/AOA measurements, labeled as EKF-TA, the IMED based KF using TOA-only measurements, labeled as KF-IMED-T and the proposed IMED based KF using joint TOA/AOA measurements labeled as KF-IMED-TA. Different percentages of NLOS errors, including $30\%, 40\%, 50\%$ and 60%, are simulated to test the performance of each tracker. The NLOS noise is either exponential with $\sigma_\eta = 400m$ or mean-shifted Gaussian characterized by $(\mu_\eta, \sigma_\eta) = (1400m, 400m)$.

Simulation results are summarized in Tables 6.1 and 6.2 in terms of average MED over time. In the ideal LOS case (zero mean Gaussian measurement noise only) for which the EKF-TA is expected to be the best tracker, the performance of the proposed KF-IMED-TA is quite close to that of the EKF-TA and is better than that of the KF-IMED-T. In all other scenarios (mixed LOS/NLOS), the KF-IMED-TA outperforms all other trackers considerably, particularly in the highly contaminated scenarios. For example, in the case of 60% NLOS, the average MED

by KF-IMED-TA is only 2/3 of the average MED by KF-IMED-T for the Gaussian NLOS noise. Compared with the authors' preliminary KF-IMED-T tracker, the performance improvement of the KF-IMED-T is also observed, particularly in the highly contaminated scenarios.

Table 6.1: Mean over time MEDs (m) of each tracker for random force state model in the cellular network with i.i.d. exponential and mean-shifted Gaussian NLOS errors occurrence

	Random force, cellular network				
	LOS	30% NLOS	40% NLOS	50% NLOS	60% NLOS
	exponential $\sigma_{\text{exp},\eta} = 400m$,$\sigma_{\text{exp},\eta} = 5^0$				
EKF-TA	**17.67**	82.87	108.88	135.97	163.10
KF-IMED-T	20.42	49.81	68.02	89.14	113.15
KF-IMED-TA	17.83	**40.26**	**54.67**	**70.63**	**88.25**
	shifted Gaussian $(\mu_\eta, \sigma_\eta) = (1400m, 400m)$,$(\mu_\eta, \sigma_\eta) = (10^0, 5^0)$				
EKF-TA	**17.67**	219.48	293.73	370.71	449.58
KF-IMED-T	20.42	33.77	45.86	68.30	116.38
KF-IMED-TA	17.83	**27.99**	**36.69**	**51.97**	**79.29**

Table 6.2: Mean over time MEDs (m) of each tracker for constant velocity state model in the cellular network with i.i.d. exponential and mean-shifted Gaussian NLOS errors occurrence

	Constant velocity, cellular network				
	LOS	30% NLOS	40% NLOS	50% NLOS	60% NLOS
	exponential $\sigma_{\text{exp},\eta} = 400m$,$\sigma_{\text{exp},\eta} = 5^0$				
EKF-TA	**15.12**	82.97	109.39	136.80	164.25
KF-IMED-T	17.66	48.43	66.67	88.29	112.61
KF-IMED-TA	15.13	**39.17**	**53.08**	**69.57**	**88.02**
	shifted Gaussian $(\mu_\eta, \sigma_\eta) = (1400m, 400m)$,$(\mu_\eta, \sigma_\eta) = (10^0, 5^0)$				
EKF-TA	**15.12**	223.30	298.99	377.88	457.79
KF-IMED-T	17.66	32.14	44.85	67.40	112.07
KF-IMED-TA	15.13	**26.26**	**35.52**	**51.09**	**78.11**

Figure 6.2 shows the RMSEs of each tracker over time for the case of 40% i.i.d. mean-shifted Gaussian NLOS errors.

Although the KF-IMED-T achieves relatively high precision in terms of RMSEs, the RMSEs are still around $50m$ to $80m$. On the other hand, the proposed KF-IMED-TA has RMSEs less than $30m$ most of the time and have achieved better precision than the KF-IMED-T. With the assistance of the AOA measurements,

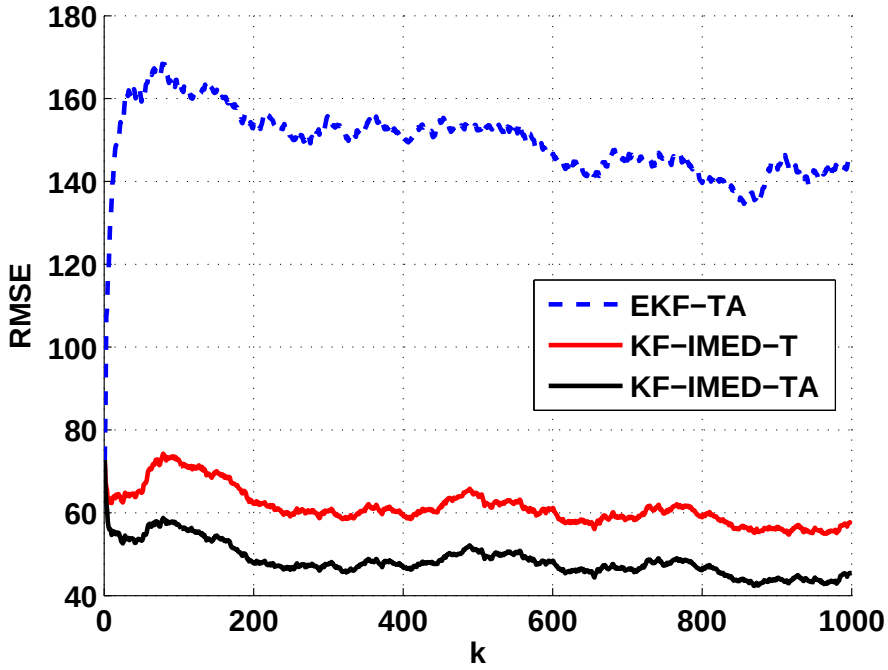

Figure 6.2: RMSEs of each tracker in the cellular network with 40% exponential NLOS errors.

the proposed KF-IMED-TA always performs better than the KF-IMED-T which uses only TOA measurements.

6.4.2 NLOS Occurrence Modeled as Markov Chain

Dropping the i.i.d. assumption, a two-state Markov chain is adopted for each sensor to model the LOS and NLOS conditions. For a certain sensor m, it is in the state of LOS with probability $1 - \varepsilon_m$. In the state of NLOS, it occurs with probability ε_m. The definition of ε_m and the transition matrix used for the simulations are the same as described in Chapter 2. By choosing different values for transition matrix in the simulations, we can simulate different mixed LOS/NLOS

scenarios in the real world closely. More details of the transition matrix and the selection of its values are given in Chapter 2. Simulations results under all NLOS scenarios C0 to C6 are summarized in Table 6.3.

Table 6.3: Mean over time MEDs (m) of each tracker for constant velocity state model in the cellular network with Markov chain exponential and mean-shifted Gaussian NLOS errors occurrence

	Constant velocity, cellular network						
	C0	C1	C2	C3	C4	C5	C6
	exponential $\sigma_{\text{exp},\eta} = 400m$						
EKF-TA	**15.43**	68.80	137.69	188.62	221.46	222.63	317.47
KF-IMED-T	18.30	28.36	50.55	62.69	103.63	108.73	194.95
KF-IMED-TA	15.55	**23.46**	**40.85**	**87.89**	**78.65**	**82.77**	**143.89**
	shifted Gaussian $(\mu_\eta, \sigma_\eta) = (1400m, 400m)$						
EKF	**15.43**	248.63	498.33	978.65	939.94	969.08	1362.5
KF-IMED-T	18.30	19.03	20.25	26.29	31.88	43.44	119.25
KF-IMED-TA	15.55	**16.01**	**17.16**	**21.20**	**23.58**	**26.18**	**46.71**

Table 6.4: Mean over time MEDs (m) of each tracker for random force state model in the cellular network with Markov chain exponential and mean-shifted Gaussian NLOS errors occurrence

	Random force, cellular network						
	C0	C1	C2	C3	C4	C5	C6
	exponential $\sigma_{\text{exp},\eta} = 400m$						
EKF-TA	**18.06**	73.69	145.57	233.90	235.62	237.04	337.59
KF-IMED-T	21.27	30.75	51.82	107.99	105.34	110.25	197.28
KF-IMED-TA	18.44	**25.79**	**42.08**	**79.78**	**79.99**	**84.30**	**143.81**
	shifted Gaussian $(\mu_\eta, \sigma_\eta) = (1400m, 400m)$						
EKF-TA	**18.06**	249.20	503.19	741.83	940.52	947.82	1346.5
KF-IMED-T	21.27	22.90	23.34	30.23	39.68	52.12	119.57
KF-IMED-TA	18.44	**19.76**	**20.06**	**24.99**	**30.05**	**32.01**	**64.54**

We compute the EKF-TA, the KF-IMED-T and the proposed KF-IMED-TA. Table 6.3 gives the average MEDs of each tracker using the constant velocity motion model calculated under different NLOS scenarios with Gaussian and exponential NLOS errors. Table 6.4 gives the average MEDs of each tracker moving with the random force motion model calculated under different NLOS scenarios in the cellular network with Gaussian and exponential NLOS errors.

Similar to the situation where NLOS occurrence is modeled as i.i.d., we observe from Tables 6.3 and 6.4 that in the ideal LOS case for which the EKF-TA is expected to be the best tracker, the performance of the proposed KF-IMED-TA is quite close to that of the EKF-TA and is better than the that of the KF-IMED-T. In most of the other scenarios (mixed LOS/NLOS), the KF-IMED-TA outperforms other trackers, particularly in the highly contaminated scenarios with mean-shifted Gaussian NLOS error. For example, in the case of scenario $C6$ with mean-shifted Gaussian NLOS error, the average MED by KF-IMED-TA is only about 50% of the average MED by KF-IMED-T in the cellular network. On the other hand, we also notice that the performance improvement of KF-IMED-TA over KF-IMED-T for exponential NLOS error is not as significant as that for mean-shifted Gaussian NLOS error.

The RMSEs of trackers KF-IMED-T and KF-IMED-TA for scenario $C4$ with mean-shifter Gaussian NLOS errors is shown in Figure 6.3. It is easy to see that the KF-IMED-TA does perform better than the KF-IMED-T. The cumulative error distribution of the localization error for scenario $C4$ with mean-shifted Gaussian NLOS errors is shown in Figure 6.4. From this figure, it can be seen that the 95% marks of the proposed tracker KF-IMED-TA and the KF-IMED-T are about $50m$ and $105m$, respectively.

6.5 Conclusion

In this chapter, we have proposed a new tracking scheme based the IMED algorithm and the classical Kalman filter using joint TOA/AOA measurements. We have expanded the concept of a pseudo-measured position, which is firstly proposed

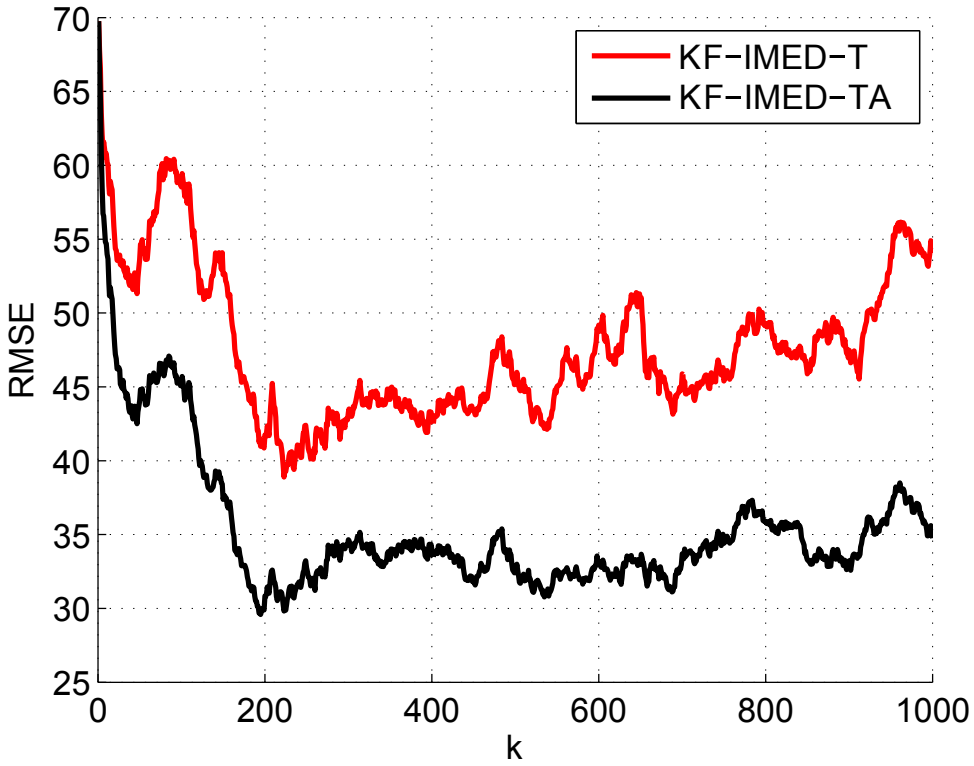

Figure 6.3: RMSEs of each tracker for scenarios C4 with Gaussian NLOS errors.

in Chapter 5, to AOA measurements. The pseudo-measured position estimated from individual AOA measurement has been proved to be an approximately unbiased estimate of the true position of the moving target. The efficient detection method has then been developed to detect LOS measurements among all mixed LOS/NLOS joint TOA/AOA measurements and discard NLOS ones, followed by the Kalman filter based on joint TOA/AOA measurements for target tracking. We do not require prior information of the NLOS noise and yet we are able to make good use of all the detected LOS TOA/AOA measurements even when there are only one LOS TOA/AOA measurements available at a given time step. Simulations have shown that the proposed approach has out-performed (in terms of

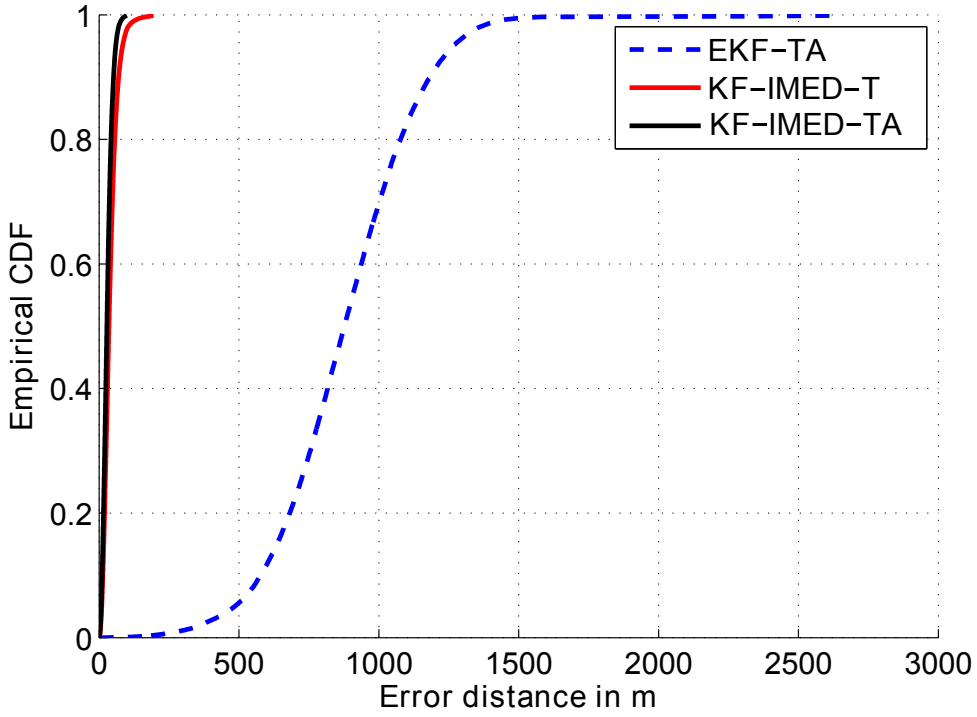

Figure 6.4: Cumulative distribution functions of different trackers for scenarios C4 with Gaussian NLOS errors.

the accuracy) the tracking scheme proposed in Chapter 5 in both LOS and mixed LOS/NLOS environments, particularly when the NLOS noise is strong.

Appendix A - Proof of Lemma 6.1

Proof. To solve the problem defined in (6.10), we rewrite it as an equivalent scalar equation

$$\min_{\tilde{x}^p_{k,m},\tilde{y}^p_{k,m}} \left(\tilde{x}^p_{k,m} - \hat{x}^{p,-}_k\right)^2 + \left(\tilde{y}^p_{k,m} - \hat{y}^{p,-}_k\right)^2, \text{s.t.} \beta_{k,m} = \arg\tan \frac{\tilde{y}^p_{k,m} - y^S_{k,m}}{\tilde{x}^p_{k,m} - x^S_{k,m}}. \quad (6.13)$$

The Lagrangian multiplier method can solve the constrained minimization prob-

lem by forming the auxiliary cost function

$$\xi = \left(\tilde{\mathbf{x}}_{k,m}^{p} - \hat{\mathbf{x}}_{k}^{p,-}\right)^{T} \left(\tilde{\mathbf{x}}_{k,m}^{p} - \hat{\mathbf{x}}_{k}^{p,-}\right) + \lambda \left(\beta_{k,m} - \arg\tan \frac{\tilde{y}_{k,m}^{p} - y_{k,m}^{S}}{\tilde{x}_{k,m}^{p} - x_{k,m}^{S}}\right), \tag{6.14}$$

where λ is the Lagrange multiplier.

The cost function (6.14) can be expanded as

$$\xi^{'} = \left(\tilde{x}_{k,m}^{p} - \hat{x}_{k}^{p,-}\right)^{2} + \left(\tilde{y}_{k,m}^{p} - \hat{y}_{k}^{p,-}\right)^{2} + 2\lambda^{'} \left(\left(\tilde{x}_{k,m}^{p} - x_{k,m}^{S}\right) \tan\beta_{k,m} - \left(\tilde{y}_{k,m}^{p} - y_{k,m}^{S}\right)\right). \tag{6.15}$$

Taking the partial derivations of $\xi^{'}$ with respect to $\tilde{x}_{k,m}$, $\tilde{y}_{k,m}$ and $\lambda^{'}$ gives

$$\begin{aligned}
\frac{\partial \xi^{'}}{\partial \tilde{x}_{k,m}^{p}} &= 2\left(\tilde{x}_{k,m}^{p} - \hat{x}_{k}^{p,-}\right) + 2\lambda^{'} \tan\beta_{k,m} = 0, && (6.16)\\
\frac{\partial \xi^{'}}{\partial \tilde{y}_{k,m}^{p}} &= 2\left(\tilde{y}_{k,m}^{p} - \hat{y}_{k}^{p,-}\right) - 2\lambda^{'} = 0, && (6.17)\\
\frac{\partial \xi^{'}}{\partial \lambda^{'}} &= \left(\tilde{x}_{k,m}^{p} - x_{k,m}^{S}\right) \tan\beta_{k,m} - \left(\tilde{y}_{k,m}^{p} - y_{k,m}^{S}\right) = 0. && (6.18)
\end{aligned}$$

Solutions of this constrained problem given in equations (6.19) and (6.20) as follows □

$$\begin{aligned}
\tilde{x}_{k,m}^{p} &= \hat{x}_{k}^{p,-} + \tan\beta_{k,m} \frac{\left(\hat{y}_{k}^{p,-} - y_{k,m}^{S}\right) - \left(\hat{x}_{k}^{p,-} - x_{k,m}^{S}\right) \tan\beta_{k,m}}{1 + \tan^{2}\beta_{k,m}}, && (6.19)\\
\tilde{y}_{k,m}^{p} &= \hat{y}_{k}^{p,-} - \frac{\left(\hat{y}_{k}^{p,-} - y_{k,m}^{S}\right) - \left(\hat{x}_{k}^{p,-} - x_{k,m}^{S}\right) \tan\beta_{k,m}}{1 + \tan^{2}\beta_{k,m}}, && (6.20)\\
\lambda^{'} &= \frac{\left(\hat{y}_{k}^{p,-} - y_{k,m}^{S}\right) - \left(\hat{x}_{k}^{p,-} - x_{k,m}^{S}\right) \tan\beta_{k,m}}{1 + \tan^{2}\beta_{k,m}}. && (6.21)
\end{aligned}$$

Appendix B - Proof of Theorem 6.1

Proof. Each element $\tilde{x}^p_{k,m}$ and $\tilde{y}^p_{k,m}$ of $\tilde{\mathbf{x}}^p_k$ are independent from each other. To prove $\mathbb{E}\left(\tilde{\mathbf{x}}^p_{k,m}\right) = \mathbf{x}^p_k$ is equivalent to prove $\mathbb{E}\left(\tilde{x}^p_{k,m}\right) = x^p_k$ and $\mathbb{E}\left(\tilde{y}^p_{k,m}\right) = y^p_k$.

According to the property of the conditional expectation, we know that the expectation of the estimated position $\tilde{x}$ and $\tilde{y}$ can be solved by

$$\begin{aligned}
\mathbb{E}\left(\tilde{x}^p_{k,m}\right) &= \mathbb{E}\left(\mathbb{E}\left(\tilde{x}^p_{k,m}\left|\hat{\mathbf{x}}^{p,-}_k\right.\right)\right) = \mathbb{E}\left(\mathbb{E}\left(\tilde{x}^p_{k,m}\left|\hat{x}^{p,-}_k, \hat{y}^{p,-}_k\right.\right)\right), \\
\mathbb{E}\left(\tilde{y}^p_{k,m}\right) &= \mathbb{E}\left(\mathbb{E}\left(\tilde{y}^p_{k,m}\left|\hat{\mathbf{x}}^{p,-}_k\right.\right)\right) = \mathbb{E}\left(\mathbb{E}\left(\tilde{y}^p_{k,m}\left|\hat{x}^{p,-}_k, \hat{y}^{p,-}_k\right.\right)\right). \qquad (6.22)
\end{aligned}$$

Firstly, we need to calculate the conditional expectations of $\mathbb{E}\left(\tilde{x}^p_{k,m}\left|\hat{x}^{p,-}_k, \hat{y}^{p,-}_k\right.\right)$ and $\mathbb{E}\left(\tilde{y}^p_{k,m}\left|\hat{x}^{p,-}_k, \hat{y}^{p,-}_k\right.\right)$.

To solve these problems, we make use of the trigonometric function $\tan\beta_{k,m} = \frac{\sin\beta_{k,m}}{\cos\beta_{k,m}}$ to simplify the expression of $\tilde{x}^p_{k,m}$ and $\tilde{y}^p_{k,m}$ given in equations (6.19) and (6.20) as follows

$$\begin{aligned}
\tilde{x}^p_{k,m} &= \hat{x}^{p,-}_k + \tan\beta_{k,m}\frac{\left(\hat{y}^{p,-}_k - y^S_{k,m}\right) - \left(\hat{x}^{p,-}_k - x^S_{k,m}\right)\tan\beta_{k,m}}{1+\tan^2\beta_{k,m}} \\
&= \hat{x}^{p,-}_k + \frac{\sin\beta_{k,m}}{\cos\beta_{k,m}}\frac{\left(\hat{y}^{p,-}_k - y^S_{k,m}\right) - \left(\hat{x}^{p,-}_k - x^S_{k,m}\right)\frac{\sin\beta_{k,m}}{\cos\beta_{k,m}}}{1+\frac{\sin^2\beta_{k,m}}{\cos^2\beta_{k,m}}} \\
&= \hat{x}^{p,-}_k + \sin\beta_{k,m}\cos\beta_{k,m}\left(\hat{y}^{p,-}_k - y^S_{k,m}\right) - \sin^2\beta_{k,m}\left(\hat{x}^{p,-}_k - x^S_{k,m}\right) \qquad (6.23) \\
\tilde{y}^p_{k,m} &= \hat{y}^{p,-}_k - \frac{\left(\hat{y}^{p,-}_k - y^S_{k,m}\right) - \left(\hat{x}^{p,-}_k - x^S_{k,m}\right)\tan\beta_{k,m}}{1+\tan^2\beta_{k,m}} \\
&= \hat{y}^{p,-}_k - \frac{\left(\hat{y}^{p,-}_k - y^S_{k,m}\right) - \left(\hat{x}^{p,-}_k - x^S_{k,m}\right)\frac{\sin\beta_{k,m}}{\cos\beta_{k,m}}}{1+\frac{\sin^2\beta_{k,m}}{\cos^2\beta_{k,m}}} \\
&= \hat{y}^{p,-}_k - \cos^2\beta_{k,m}\left(\hat{y}^{p,-}_k - y^S_{k,m}\right) + \sin\beta_{k,m}\cos\beta_{k,m}\left(\hat{x}^{p,-}_k - x^S_{k,m}\right) \qquad (6.24)
\end{aligned}$$

Using the measured angle equation $\beta_{k,m} = \bar{\beta}_{k,m} + w_{k,m}$ and the product to sum

formula, we have

$$\begin{aligned}
\sin\beta_{k,m} &= \sin\left(\bar{\beta}_{k,m} + w_{k,m}\right) \\
&= \sin\bar{\beta}_{k,m}\cos w_{k,m} + \sin w_{k,m}\cos\bar{\beta}_{k,m} \\
&\approx \sin\bar{\beta}_{k,m} + w_{k,m}\cos\bar{\beta}_{k,m}, \qquad (6.25) \\
\cos\beta_{k,m} &= \cos\left(\bar{\beta}_{k,m} + w_{k,m}\right) \\
&= \cos\bar{\beta}_{k,m}\cos w_{k,m} - \sin w_{k,m}\sin\bar{\beta}_{k,m} \\
&\approx \cos\bar{\beta}_{k,m} - w_{k,m}\sin\bar{\beta}_{k,m}. \qquad (6.26)
\end{aligned}$$

Substituting equations (6.25) and (6.26) into equations (6.23) and (6.24), we could get equations (6.27) and (6.28).

The estimation position $\tilde{x}^p_{k,m}$ and $\tilde{y}^p_{k,m}$ are functions of the random noise $w_{k,m}$. The conditional expectations of $\tilde{x}^p_{k,m}$ and $\tilde{y}^p_{k,m}$ given $\hat{x}^-_k$ and $\hat{y}^-_k$ are equations (6.29) and (6.31), respectively.

Since $x_k - x^S_{k,m} = r_{k,m}\cos\bar{\beta}_{k,m}$ and $y_k - y^S_{k,m} = r_{k,m}\sin\bar{\beta}_{k,m}$, where $r_{k,m}$ denotes the noise-free range between the sensor m and the moving target at time step k, the expectation of $\tilde{x}^p_{k,m}$ and $\tilde{y}^p_{k,m}$ given in equations (6.31) and (6.32) can be simplified as shown in equations (6.33) and (6.34).

$$
\begin{aligned}
\tilde{x}^p_{k,m} &= \hat{x}^-_k + \sin\beta_{k,m}\cos\beta_{k,m}\left(\hat{y}^-_k - y^S_{k,m}\right) - \sin^2\beta_{k,m}\left(\hat{x}^-_k - x^S_{k,m}\right) \\
&\approx \hat{x}^-_k + \left(\sin\bar{\beta}_{k,m} + w_{k,m}\cos\bar{\beta}_{k,m}\right)\left(\cos\bar{\beta}_{k,m} - w_{k,m}\sin\bar{\beta}_{k,m}\right)\left(\hat{y}^-_k - y^S_{k,m}\right) \\
&- \left(\sin\bar{\beta}_{k,m} + w_{k,m}\cos\bar{\beta}_{k,m}\right)^2\left(\hat{x}^-_k - x^S_{k,m}\right) \\
&= \hat{x}^-_k + \left(\sin\bar{\beta}_{k,m}\cos\bar{\beta}_{k,m} - w_{k,m}\sin\bar{\beta}_{k,m} - w^2_{k,m}\sin\bar{\beta}_{k,m}\cos\bar{\beta}_{k,m}\right)\left(\hat{y}^-_k - y^S_{k,m}\right) \\
&- \left(\sin^2\bar{\beta}_{k,m} + 2w_{k,m}\sin\bar{\beta}_{k,m}\cos\bar{\beta}_{k,m} + \left(w_{k,m}\cos\bar{\beta}_{k,m}\right)^2\right)\left(\hat{x}^-_k - x^S_{k,m}\right) \\
&\approx \hat{x}^-_k + \left(\sin\bar{\beta}_{k,m}\cos\bar{\beta}_{k,m} - w_{k,m}\sin\bar{\beta}_{k,m}\right)\left(\hat{y}^-_k - y^S_{k,m}\right) \\
&- \left(\sin^2\bar{\beta}_{k,m} + 2w_{k,m}\sin\bar{\beta}_{k,m}\cos\bar{\beta}_{k,m}\right)\left(\hat{x}^-_k - x^S_{k,m}\right),
\end{aligned}
\tag{6.27}
$$

$$
\begin{aligned}
\tilde{y}^p_{k,m} &= \hat{y}^-_k - \cos^2\beta_{k,m}\left(\hat{y}^-_k - y^S_{k,m}\right) + \sin\beta_{k,m}\cos\beta_{k,m}\left(\hat{x}^-_k - x^S_{k,m}\right) \\
&\approx \hat{y}^-_k - \left(\cos\bar{\beta}_{k,m} - w_{k,m}\sin\bar{\beta}_{k,m}\right)^2\left(\hat{y}^-_k - y^S_{k,m}\right) \\
&+ \left(\sin\bar{\beta}_{k,m} + w_{k,m}\cos\bar{\beta}_{k,m}\right)\left(\cos\bar{\beta}_{k,m} - w_{k,m}\sin\bar{\beta}_{k,m}\right)\left(\hat{x}^-_k - x^S_{k,m}\right) \\
&= \hat{y}^-_k + \left(\cos^2\bar{\beta}_{k,m} - 2w_{k,m}\cos\bar{\beta}_{k,m}\sin\bar{\beta}_{k,m} + \left(w_{k,m}\sin\bar{\beta}_{k,m}\right)^2\right)\left(\hat{y}^-_k - y^S_{k,m}\right) \\
&+ \left(\sin\bar{\beta}_{k,m}\cos\bar{\beta}_{k,m} + w_{k,m}\cos^2\bar{\beta}_{k,m} - w_{k,m}\sin^2\bar{\beta}_{k,m} - w^2_{k,m}\cos\bar{\beta}_{k,m}\sin\bar{\beta}_{k,m}\right) \\
&\times \left(\hat{x}^-_k - x^S_{k,m}\right) \\
&\approx \hat{y}^-_k + \left(\cos^2\bar{\beta}_{k,m} - 2w_{k,m}\cos\bar{\beta}_{k,m}\sin\bar{\beta}_{k,m}\right)\left(\hat{y}^-_k - y^S_{k,m}\right) \\
&+ \left(\sin\bar{\beta}_{k,m}\cos\bar{\beta}_{k,m} + w_{k,m}\cos^2\bar{\beta}_{k,m} - w_{k,m}\sin^2\bar{\beta}_{k,m}\right)\left(\hat{x}^-_k - x^S_{k,m}\right).
\end{aligned}
\tag{6.28}
$$

$$
\begin{aligned}
\mathbb{E}\left(\tilde{x}^p_{k,m}\left|\hat{x}^-_k,\hat{y}^-_k\right.\right) &\approx \hat{x}^-_k + \mathbb{E}\left(\sin\bar{\beta}_{k,m}\cos\bar{\beta}_{k,m} - w_{k,m}\sin\bar{\beta}_{k,m}\right)\left(\hat{y}^-_k - y^S_{k,m}\right)\\
&- \mathbb{E}\left(\sin^2\bar{\beta}_{k,m} + 2w_{k,m}\sin\bar{\beta}_{k,m}\cos\bar{\beta}_{k,m}\right)\left(\hat{x}^-_k - x^S_{k,m}\right)\\
&= \hat{x}^-_k + \sin\bar{\beta}_{k,m}\cos\bar{\beta}_{k,m}\left(\hat{y}^-_k - y^S_{k,m}\right)\\
&- \sin^2\bar{\beta}_{k,m}\left(\hat{x}^-_k - x^S_{k,m}\right) \qquad (6.29)\\
\mathbb{E}\left(\tilde{y}^p_{k,m}\left|\hat{x}^-_k,\hat{y}^-_k\right.\right) &\approx \hat{y}^-_k + \mathbb{E}\left(\cos^2\bar{\beta}_{k,m} - 2w_{k,m}\cos\bar{\beta}_{k,m}\sin\bar{\beta}_{k,m}\right)\left(\hat{y}^-_k - y^S_{k,m}\right)\\
&+ \mathbb{E}\left(\sin\bar{\beta}_{k,m}\cos\bar{\beta}_{k,m} + w_{k,m}\cos^2\bar{\beta}_{k,m} - w_{k,m}\sin^2\bar{\beta}_{k,m}\right)\left(\hat{x}^-_k - x^S_{k,m}\right)\\
&= \hat{y}^-_k - \cos^2\bar{\beta}_{k,m}\left(\hat{y}^-_k - y^S_{k,m}\right)\\
&+ \sin\bar{\beta}_{k,m}\cos\bar{\beta}_{k,m}\left(\hat{x}^-_k - x^S_{k,m}\right). \qquad (6.30)
\end{aligned}
$$

$$
\begin{aligned}
\mathbb{E}\left(\tilde{x}^p_{k,m}\right) &= \mathbb{E}\left(\mathbb{E}\left(\tilde{x}^p_{k,m}\left|\hat{x}^-_k,\hat{y}^-_k\right.\right)\right)\\
&\approx \mathbb{E}\left(\hat{x}^-_k + \sin\bar{\beta}_{k,m}\cos\bar{\beta}_{k,m}\left(\hat{y}^-_k - y^S_{k,m}\right) - \sin^2\bar{\beta}_{k,m}\left(\hat{x}^-_k - x^S_{k,m}\right)\right)\\
&= x_k + \sin\bar{\beta}_{k,m}\cos\bar{\beta}_{k,m}\left(y_k - y^S_{k,m}\right) - \sin^2\bar{\beta}_{k,m}\left(x_k - x^S_{k,m}\right), \qquad (6.31)\\
\mathbb{E}\left(\tilde{y}^p_{k,m}\right) &= \mathbb{E}\left(\mathbb{E}\left(\tilde{y}^p_{k,m}\left|\hat{x}^-_k,\hat{y}^-_k\right.\right)\right)\\
&\approx \mathbb{E}\left(\hat{y}^-_k - \cos^2\bar{\beta}_{k,m}\left(\hat{y}^-_k - y^S_{k,m}\right) + \sin\bar{\beta}_{k,m}\cos\bar{\beta}_{k,m}\left(\hat{x}^-_k - x^S_{k,m}\right)\right)\\
&= y_k - \cos^2\bar{\beta}_{k,m}\left(y_k - y^S_{k,m}\right) + \sin\bar{\beta}_{k,m}\cos\bar{\beta}_{k,m}\left(x_k - x^S_{k,m}\right). \qquad (6.32)
\end{aligned}
$$

$$\mathbb{E}\left(\tilde{x}^p_{k,m}\right) \approx x_k + \sin\bar{\beta}_{k,m}\cos\bar{\beta}_{k,m}r_{k,m}\sin\bar{\beta}_{k,m} - \sin^2\bar{\beta}_{k,m}\cos\bar{\beta}_{k,m}r_{k,m} = x_k, \tag{6.33}$$

$$\mathbb{E}\left(\tilde{y}^p_{k,m}\right) \approx y_k - \cos^2\bar{\beta}_{k,m}r_{k,m}\sin\bar{\beta}_{k,m} + \sin\bar{\beta}_{k,m}\cos\bar{\beta}_{k,m}\cos\bar{\beta}_{k,m}r_{k,m} = y_k. \tag{6.34}$$

□

Chapter 7

Conclusions and Future Work

The problem of target tracking in mixed line-of-sight and non-line-of-sight environments has been treated in this thesis. The NLOS propagation results in a decrease of tracking accuracy when using standard techniques such as the Kalman filter or the extended Kalman filter. In this thesis, we focus on mitigating the affection of NLOS errors. A summary of the work done is given in Section 7.1. An outlook to future work is given in Section 7.2.

7.1 Conclusions

In Chapter 3, standard gating and dynamic gating based individual measurement detection approaches using TOA measurements are presented. These approaches are simple but effective. In the standard gating based detection algorithm, the TOA measurements are detected individually using a hypothesis test. In the hypothesis test, the standard gating determined by a general likelihood ratio test (GLRT) is used to detect LOS measurements from all mixed ones. During the whole tracking processing, the gate is a fixed value given as a prior knowledge. In the dynamic gating based detection algorithm, the TOA measurements

are first mapped to be an estimated position of the moving target. Then the error covariance matrix of the moving target's state vector is used as gating to detect whether the estimated position is LOS or not. These selected LOS measurements are then used into an EKF or a rEKF to track the moving traget. The tracking accuracies in mild NLOS environments of the EKF and the rEKF are near to the tracking accuracies of the EKF and the rEKF in LOS only environments, which are evaluated by the MED and RMSE. The limitation of this algorithm is that it requires at least 3 LOS TOA or TDOA measurements to implement the EKF to achieve good tracking accuracy. When the number of LOS TOA measurements is less than 3, the prediction position of the moving target is used to instead. Thus, it introduces accumulated error into the tracking process especially in severe NLOS environments.

In Chapter 4, we discuss the road constraints assisted tracking scheme using TDOA measurements. The standard gating based detection approach is expanded into the TDOA measurements as well as the EKF and the rEKF. Together with road constraints, which are used as pseudo measurements, the tracking accuracy has been improved with respect to the ones without road constraints.

To overcome the weakness of the tracking scheme proposed in Chapter 3, the individual measurement estimation and LOS detection algorithms using TOA measurements are proposed in Chapter 5. The IME algorithm can calculate a pseudo-measured position from one individual TOA measurement. This pseudo-measured position has been proved to be approximately unbiased. It can be used into a KF to update the tracking result. The corresponding detection algorithm is also different from the standard gating based one. Here the detection threshold is dynamic. It is determined by the error covariance of the estimated position of the

moving target. All calculated pseudo-measured positions from TOA measurements are passed to the detector. Only some of them are selected as LOS ones while the other are treated as outlier which are contaminated by the NLOS errors. These selected LOS pseudo-measured position or the average of them is used into a KF. If only one pseudo-measured position is selected, the KF still has a pseudo-measured position to update the result. This overcomes the limitation of the standard gating based EKF or rEKF. When no selected LOS exists, the tracking algorithm using the prediction position calculated from the state evolution model is used to as the estimate position. Simulations have been given to demonstrate the performance of the IMED based KF. It works well even in severe mixed LOS/NLOS environments.

In Chapter 6, we develop the IMED algorithm using joint TOA/AOA measurements. The average of the selected LOS pseudo-measured positions of the hybrid TOA/AOA measurements is used into a KF to track the moving target. This tracking scheme improves the tracking accuracy in both LOS and mixed LOS/NLOS environments with respect to the TOA only tracking schemes.

7.2 Future Work

NLOS detection and mitigation play important roles in target tracking. The topics listed below are worthy for further research.

1. *Develop the IMED algorithm using joint TDOA/FDOA measurements*

   Recently, the tracking problem based on joint TDOA/FDOA measurements is becoming more and more popular. Several algorithms have been proposed to improve the tracking accuracy using TDOA/FDOA measurements [81–86, 86–95]. Most of these research on tracking with TDOA/FDOA problems

are discussed in LOS environment, which is an ideal context. In practice, the LOS assumptions are not always fulfilled. The discussion and research of target tracking with TDOA/FDOA in mixed LOS/NLOS environments will be an interesting and useful topic.

From the discussions shown in this thesis, it is clear to see that the proposed IMED algorithms for TOA and joint TOA/AOA measurements work well in mixed LOS/NLOS environments. Moreover, the computation complexity of the proposed algorithm is as low as the traditional EKF. Development of the IMED algorithm using the TDOA/FDOA measurements will be valuable research topic.

2. *Incorporate the IMED algorithm into UKF and PF*

   Recent year, the unscented Kalman filter (UKF), proposed in [96], and the particle filters have become very popular numerical methods for the solution of optimal estimation problems in non-linear scenarios [59, 60, 69, 97, 98]. The UKF addresses the non-linear state estimation problems by using a deterministic sampling approach. While the principal advantage of particle filter is that they do not rely on any local linearisation technique or any crude functional approximation. Incorporate the proposed IMED algorithm into the UKF to track a moving target in mixed LOS/NLOS environments will be a valuable research topic.

3. *Utilize the road map into the tracking problem in mixed LOS/NLOS environments*

   The weakness of the NLOS detection algorithms discussed in this thesis is that it cannot achieve good tracking accuracy when all of the measurements are

contaminated by NLOS error. So, additional context information is required to assist the target tracking in mixed LOS/NLOS environments. The popular additional information for target tracking is the road information which can be obtained easily. When the target is moving on a certain road, the road information can be combined into the tracking algorithm as a pseudo-measurement or a constraint. In Chapter 4, we have discussed the road constraints assisted tracking scheme using TDOA measurements. This road constraints assisted tracking scheme can also be used into TOA, AOA or other measurements. In the following research, field experiments will be implemented in a certain road network to verify the tracking accuracy.

4. *Real data applications*

   Currently, the proposed tracking schemes base on the individual measurement estimation and detection algorithm are verified by simulations. To further evaluate performances of the proposed tracking schemes and optimize the parameters used in these algorithms, real data application will be implemented in near future. Reasonably initializing the tracking problem will also be considered to improve the tracking accuracy in read data applications.

Author's Publication

Journal:

1. Lili Yi, Razul, S.G., Zhiping Lin and Chong-Meng See, "Target Tracking in Mixed LOS/NLOS Environments Based on Individual Measurement Estimation and LOS Detection" *IEEE Transactions on Wireless Communication*, volume 13, pp. 99-111, Jan. 2014.

Conferences:

1. Lili Yi, Razul, S.G., Zhiping Lin and Chong-Meng See, "Robust tracking in mixed LOS/NLOS environments", in *Proceedings of 2010 11th International Conference on Control Automation Robotics Vision (ICARCV)*, pp.497-500, Dec. 2010

2. Lili Yi, Razul, S.G., Zhiping Lin and Chong-Meng See, "Target tracking in mixed LOS/NLOS environments based on individual TOA measurement detection," in *Proceedings of 2010 IEEE Sensor Array and Multichannel Signal Processing Workshop (SAM)*, pp.153–156, Oct. 2010.

3. Lili Yi, Razul, S.G., Zhiping Lin and Chong-Meng See, "Road-constraint assisted target tracking in mixed LOS/NLOS environments based on TDOA

measurements," in *Proceedings of 2012 IEEE International Symposium on Circuits and Systems (ISCAS)*, pp.2581-2584, May 2012.

4. Lili Yi, Razul, S.G., Zhiping Lin and Chong-Meng See, "Gating and robust EKF based target tracking in mixed LOS/NLOS environments", in *Proceedings of 2012 IEEE International Symposium on Circuits and Systems (ISCAS)*, pp.1364-1367, May 2013.

5. Lili Yi, Razul, S.G., Zhiping Lin and Chong-Meng See, "Individual AOA measurement detection algorithm for target tracking in mixed LOS/NLOS environments", in *Proceedings of 2013 IEEE International Conference on Acoustics, Speech and Signal Processing (ICASSP)*, pp.3924-3928, May 2013.

Bibliography

[1] M. Vossiek, L. Wiebking, P. Gulden, J. Wieghardt, C. Hoffmann, and P. Heide, "Wireless local positioning," *IEEE Microwave Magazine*, vol. 4, no. 4, pp. 77–86, 2003.

[2] A. Sayed, A. Tarighat, and N. Khajehnouri, "Network-based wireless location: challenges faced in developing techniques for accurate wireless location information," *IEEE Signal Processing Magazine*, vol. 22, no. 4, pp. 24–40, 2005.

[3] F. Gustafsson and F. Gunnarsson, "Mobile positioning using wireless networks: possibilities and fundamental limitations based on available wireless network measurements," *IEEE Signal Processing Magazine*, vol. 22, no. 4, pp. 41–53, 2005.

[4] S. Gezici and H. Poor, "Position estimation via ultra-wide-band signals," *Proceedings of the IEEE*, vol. 97, no. 2, pp. 386–403, 2009.

[5] P. Misra and P. Enge., "Global positioning system signals, measurements and performance," *Ganga-Jamuna Press*, 2006.

[6] D. Torrieri, "Statistical theory of passive location systems," *IEEE Transac-*

tions on Aerospace and Electronic Systems, vol. AES-20, no. 2, pp. 183–198, 1984.

[7] Y. Chan and K. Ho, "A simple and efficient estimator for hyperbolic location," *IEEE Transactions on Signal Processing*, vol. 42, no. 8, pp. 1905–1915, 1994.

[8] U. Hammes, E. Wolsztynski, and A. Zoubir, "Robust tracking and geolocation for wireless networks in NLOS environments," *IEEE Journal of Selected Topics in Signal Processing*, vol. 3, no. 5, pp. 889–901, Oct. 2009.

[9] L. Yi, S. Gulam Razul, Z. Lin, and C.-M. See, "Target tracking in mixed LOS/NLOS environments based on individual toa measurement detection," in *Proceedings of 2010 IEEE Sensor Array and Multichannel Signal Processing Workshop (SAM)*, 2010, pp. 153–156.

[10] ——, "Road-constraint assisted target tracking in mixed LOS/NLOS environments based on TDOA measurements," in *Proceedings of 2012 IEEE International Symposium on Circuits and Systems (ISCAS)*, 2012, pp. 2581–2584.

[11] F. Quitin, C. Oestges, F. Horlin, and P. De Doncker, "Polarization measurements and modeling in indoor NLOS environments," *IEEE Transactions on Wireless Communications*, vol. 9, no. 1, pp. 21–25, Jan. 2010.

[12] H. Miao, K. Yu, and M. Juntti, "Positioning for NLOS propagation: Algorithm derivations and Cramer Rao Bounds," *IEEE Transactions on Vehicular Technology*, vol. 56, no. 5, pp. 2568–2580, Sep. 2007.

[13] S. Bartelmaos, K. Abed-Meraim, and E. Grosicki, "General selection crite-

ria for mobile location in NLOS situations," *IEEE Transactions on Wireless Communications*, vol. 7, no. 11, pp. 4393–4403, Nov. 2008.

[14] K. Yu and Y. Guo, "Statistical NLOS identification based on AOA, TOA, and signal strength," *IEEE Transactions on Vehicular Technology*, vol. 58, no. 1, pp. 274–286, Jan. 2009.

[15] S. Wang and M. Wylie-Green, "Geolocation propagation modeling for cellular-based mobile positioning," in *Proceedings of 2004 IEEE 60th Vehicular Technology Conference*, vol. 7, Sep. 2004, pp. 5155–5159.

[16] C. Ma, R. Klukas, and G. Lachapelle, "A nonline-of-sight error-mitigation method for TOA measurements," *IEEE Transactions on Vehicular Technology*, vol. 56, no. 2, pp. 641–651, March 2007.

[17] P.-C. Chen, "A non-line-of-sight error mitigation algorithm in location estimation," in *Proceedings of IEEE Wireless Communications and Networking Conference*, vol. 1, 1999, pp. 316–320.

[18] M. McGuire, K. Plataniotis, and A. Venetsanopoulos, "Robust estimation of mobile terminal position," *Electronics Letters*, vol. 36, no. 16, pp. 1426–1428, Aug. 2000.

[19] T. Perala and R. Piche, "Robust extended kalman filtering in hybrid positioning applications," in *Proceedings of 4th Workshop on Positioning, Navigation and Communication*, Mar. 2007, pp. 55–63.

[20] G.-L. Sun and W. Guo, "Bootstrapping m-estimators for reducing errors due to

non-line-of-sight (NLOS) propagation," *IEEE Communications Letters*, vol. 8, no. 8, pp. 509–510, Aug. 2004.

[21] J. Zhen and S. Zhang, "Adaptive AR model based robust mobile location estimation approach in NLOS environment," in *Proceedings of IEEE 59th Vehicular Technology Conference*, vol. 5, May 2004, pp. 2682–2685.

[22] U. Hammes and A. Zoubir, "Robust mobile terminal tracking in NLOS environments based on data association," *IEEE Transactions on Signal Processing*, vol. 58, no. 11, pp. 5872–5882, Nov. 2010.

[23] S. Bartelmaos, K. Abed-Meraim, and E. Grosicki, "General selection criteria for mobile location in NLoS situations," *IEEE Transactions on Wireless Communications*, vol. 7, no. 11, pp. 4393–4403, 2008.

[24] I. Guvenc and C.-C. Chong, "A survey on TOA based wireless localization and NLOS mitigation techniques," *IEEE Communications Surveys Tutorials*, vol. 11, no. 3, pp. 107–124, 2009.

[25] H. Jiyan and W. Qun, "Robust location algorithm for NLOS environments," *Journal of Systems Engineering and Electronics*, vol. 19, no. 4, pp. 812–818, 2008.

[26] S. Marano, W. Gifford, H. Wymeersch, and M. Win, "NLOS identification and mitigation for localization based on UWB experimental data," *IEEE Journal on Selected Areas in Communications*, vol. 28, no. 7, pp. 1026–1035, 2010.

[27] K. Yu and Y. Guo, "Statistical NLOS identification based on AOA, TOA, and

signal strength," *IEEE Transactions on Vehicular Technology*, vol. 58, no. 1, pp. 274–286, 2009.

[28] S. Al-Jazzar, J. Caffery, and H.-R. You, "Scattering-model-based methods for TOA location in NLOS environments," *IEEE Transactions on Vehicular Technology*, vol. 56, no. 2, pp. 583–593, 2007.

[29] S. Venkatraman, J. Caffery, and H.-R. You, "A novel ToA location algorithm using LoS range estimation for NLoS environments," *IEEE Transactions on Vehicular Technology*, vol. 53, no. 5, pp. 1515–1524, 2004.

[30] K. Yu and E. Dutkiewicz, "Geometry and motion-based positioning algorithms for mobile tracking in NLOS environments," *IEEE Transactions on Mobile Computing*, vol. 11, no. 2, pp. 254–263, 2012.

[31] S. Venkatesh and R. M. Buehrer, "NLOS mitigation using linear programming in ultrawideband location-aware networks," *IEEE Transactions on Vehicular Technology*, vol. 56, no. 5, pp. 3182–3198, 2007.

[32] H. Miao, K. Yu, and M. Juntti, "Positioning for NLOS propagation: Algorithm derivations and Cramer-Rao bounds," *IEEE Transactions on Vehicular Technology*, vol. 56, no. 5, pp. 2568–2580, 2007.

[33] S. Mazuelas, F. Lago, J. Blas, A. Bahillo, P. Fernandez, R. Lorenzo, and E. Abril, "Prior NLOS measurement correction for positioning in cellular wireless networks," *IEEE Transactions on Vehicular Technology*, vol. 58, no. 5, pp. 2585–2591, 2009.

[34] P.-C. Chen, "A non-line-of-sight error mitigation algorithm in location estimation," in *Processings of 1999 IEEE Wireless Communications and Networking Conference*, vol. 1, 1999, pp. 316–320.

[35] R. Ouyang and A.-S. Wong, "An enhanced TOA-based wireless location estimation algorithm for dense NLOS environments," in *IEEE Wireless Communications and Networking Conference*, Apr. 2009, pp. 1–6.

[36] C. Rohrig and M. Muller, "Indoor location tracking in non-line-of-sight environments using a ieee 802.15.4a wireless network," in *IEEE/RSJ International Conference on Intelligent Robots and Systems*, Oct. 2009, pp. 552–557.

[37] W. Wei, X. Jin-Yu, and Z. Zhong-Liang, "A new NLOS error mitigation algorithm in location estimation," *IEEE Transactions on Vehicular Technology,*, vol. 54, no. 6, pp. 2048–2053, Nov. 2005.

[38] B. L. Le, K. Ahmed, and H. Tsuji, "Mobile location estimator with NLOS mitigation using Kalman filtering," in *Proceedings of IEEE Wireless Communications and Networking*, vol. 3, Mar. 2003, pp. 1969–1973.

[39] N. Thomas, D. Cruickshank, and D. Laurenson, "A robust location estimator architecture with biased Kalman filtering of TOA data for wireless systems," in *Proceedings of IEEE Sixth International Symposium on Spread Spectrum Techniques and Applications,*, vol. 1, Sep. 2000, pp. 296–300.

[40] C.-D. Wann and C.-S. Hsueh, "NLOS mitigation with biased Kalman filters for range estimation in UWB systems," in *Proceedings of TENCON 2007 - 2007 IEEE Region 10 Conference*, Nov. 2007, pp. 1–4.

[41] S. Mazuelas, F. Lago, J. Blas, A. Bahillo, P. Fernandez, R. Lorenzo, and E. Abril, "Prior NLOS measurement correction for positioning in cellular wireless networks," *IEEE Transactions on Vehicular Technology,*, vol. 58, no. 5, pp. 2585–2591, Jun 2009.

[42] M. Najar, J. Huerta, J. Vidal, and J. Castro, "Mobile location with bias tracking in non-line-of-sight," in *Proceedings of IEEE International Conference on Acoustics, Speech, and Signal Processing (ICASSP)*, vol. 3, May 2004, pp. iii–956–9599.

[43] J. Huerta and J. Vidal, "LOS-NLOS situation tracking for positioning systems," in *Proceedings of IEEE 7th Workshop on Signal Processing Advances in Wireless Communications*, Jul. 2006, pp. 1–5.

[44] S. Al-Jazzar, J. Caffery, and H.-R. You, "Scattering-model-based methods for TOA location in NLOS environments," *IEEE Transactions on Vehicular Technology,*, vol. 56, no. 2, pp. 583–593, Mar. 2007.

[45] C. Fritsche, U. Hammes, A. Klein, and A. Zoubir, "Robust mobile terminal tracking in NLOS environments using interacting multiple model algorithm," in *Proceedings of IEEE International Conference on Acoustics, Speech and Signal Processing (ICASSP)*, 2009, pp. 3049–3052.

[46] J.-F. Liao and B.-S. Chen, "Robust mobile location estimator with NLOS mitigation using interacting multiple model algorithm," *IEEE Transactions on Wireless Communications*, vol. 5, no. 11, pp. 3002–3006, Nov. 2006.

[47] U. Hammes, E. Wolsztynski, and A. Zoubir, "Transformation-based robust

semiparametric estimation," *IEEE Signal Processing Letters*, vol. 15, pp. 845–848, 2008.

[48] Y. Bar-Shalom, X.-R. Li, and T. Kirubarajan, *Estimation with applications to tracking and navigation*. John Wiley & Sons, 2001.

[49] M. Arulampalam, S. Maskell, N. Gordon, and T. Clapp, "A tutorial on particle filters for online nonlinear/non-gaussian bayesian tracking," *IEEE Transactions on Signal Processing,*, vol. 50, no. 2, pp. 174–188, Feb. 2002.

[50] J. V. Candy, *Bayesian Signal Processing: classical, modern, and particle filtering methods*. John Wiley & Sons, Inc., 2008.

[51] B. Ristic, S. Arulampalm, and N. Gordon, *Beyond the Kalman filter: particle filters for tracking applications*. Artech House, Boston, 2004.

[52] R. Klukas and M. Fattouche, "Line-of-sight angle of arrival estimation in the outdoor multipath environment," *IEEE Transactions on Vehicular Technology*, vol. 47, no. 1, pp. 342–351, Feb. 1998.

[53] H. Miao, M. Juntti, and K. Yu, "2-D unitary esprit based joint AOA and AOD estimation for MIMO system," in *Proceedings IEEE 17th International Symposium on Personal, Indoor and Mobile Radio Communications*, Sep. 2006, pp. 1–5.

[54] Z. Durovic and B. Kovacevic, "Robust estimation with unknown noise statistics," *IEEE Transactions on Automatic Control*, vol. 44, no. 6, pp. 1292–1296, Jun. 1999.

[55] M. Porretta, P. Nepa, G. Manara, and F. Giannetti, "Location, location, location," *IEEE Vehicular Technology Magazine*, vol. 3, no. 2, pp. 20–29, Jun. 2008.

[56] J. Xu, M. Ma, and C. Law, "Position estimation using ultra-wideband time difference of arrival measurements," *IET Science, Measurement Technology*, vol. 2, no. 1, pp. 53–58, Jan. 2008.

[57] L. Kovavisaruch and K. Ho, "Modified Taylor-series method for source and receiver localization using TDOA measurements with erroneous receiver positions," in *Proceedings of IEEE International Symposium on Circuits and Systems, 2005*, may 2005, pp. 2295 – 2298 Vol. 3.

[58] M. Tahk and J. Speyer, "Target tracking problems subject to kinematic constraints," *IEEE Transactions on Automatic Control*, vol. 35, no. 3, pp. 324–326, Mar. 1990.

[59] W. Li and H. Leung, "Constrained unscented kalman filter based fusion of GPS/INS/digital map for vehicle localization," in *Proceedings of IEEE Intelligent Transportation Systems*, vol. 2, 2003, pp. 1362–1367 vol.2.

[60] L. Hong, N. Cui, M. Bakich, and J. Layne, "Multirate interacting multiple model particle filter for terrain-based ground target tracking," *IEE Proceedings -Control Theory and Applications*, vol. 153, no. 6, pp. 721–731, Nov. 2006.

[61] M. Tanelli, L. Piroddi, and S. Savaresi, "Real-time identification of tire-road friction conditions," *IET Control Theory Applications*, vol. 3, no. 7, pp. 891–906, Jul. 2009.

[62] M. Pawelczyk, "Analog active control of acoustic noise at a virtual location," *IEEE Transactions on Control Systems Technology*, vol. 17, no. 2, pp. 465–472, Mar. 2009.

[63] Y. Cheng and T. Singh, "Efficient particle filtering for road-constrained target tracking," *IEEE Transactions on Aerospace and Electronic Systems*, vol. 43, no. 4, pp. 1454–1469, Oct. 2007.

[64] H. Zhu, M. Li, Y. Zhu, and L. Ni, "HERO: online real-time vehicle tracking," *IEEE Transactions on Parallel and Distributed Systems*, vol. 20, no. 5, pp. 740–752, May 2009.

[65] S. Wu, S. Decker, P. Chang, T. Camus, and J. Eledath, "Collision sensing by stereo vision and radar sensor fusion," *IEEE Transactions on Intelligent Transportation Systems*, vol. 10, no. 4, pp. 606–614, Dec. 2009.

[66] D. Simon and D. Simon, "Kalman filtering with inequality constraints for turbofan engine health estimation," *IEE Proceedings Control Theory and Applications*, vol. 153, no. 3, pp. 371–378, 2006.

[67] M. Zhang, S. Knedlik, and O. Loffeld, "Road-constrained target tracking in GSM networks," in *Proceedings of 4th International Symposium on Wireless Communication Systems (ISWCS)*, 2007, pp. 138–142.

[68] ——, "An adaptive road-constrained IMM estimator for ground target tracking in GSM networks," in *Proceedings of International Conference on Information Fusion*, 2008, pp. 1–8.

[69] K. Li, H.-S. Tan, and J. Hedrick, "Map-aided GPS/INS localization using

a low-order constrained unscented kalman filter," in *Proceedings of the 48th IEEE Conference on Decision and Control*, 2009, pp. 4607–4612.

[70] D. Streller, "Road map assisted ground target tracking," in *Proceedings of International Conference on Information Fusion*, 2008, pp. 1–7.

[71] P. Tichavsky, C. Muravchik, and A. Nehorai, "Posterior Cramer-Rao bounds for discrete-time nonlinear filtering," *IEEE Transactions on Signal Processing*, vol. 46, no. 5, pp. 1386–1396, May 1998.

[72] O. Nickens, M. Fiona, F.and Darko, and R. Brandko, "Comparison of recursive algorithms for emitter localisation using TDOA measurements from a pair of UAVs," *IEEE Transactions on Aerospace and Electronic Systems*, vol. 47, pp. 1723–1732, Jul. 2011.

[73] Y. Bar-Shalom and F. T.E., *Tracking and Data Association*. Academic Press, 1988.

[74] T. Kirubarajan and Y. Bar-Shalom, "Probabilistic data association techniques for target tracking in clutter," *Proceedings of the IEEE*, vol. 92, no. 3, pp. 536–557, Mar. 2004.

[75] S. Venkatraman and J. Caffery, "Hybrid TOA/AOA techniques for mobile location in non-line-of-sight environments," in *Proceedings of 2004 IEEE Wireless Communications and Networking Conference (WCNC)*, vol. 1, 2004, pp. 274–278.

[76] N. Patwari, J. Ash, S. Kyperountas, A. Hero, R. Moses, and N. Correal,

"Locating the nodes: cooperative localization in wireless sensor networks," *IEEE Signal Processing Magazine*, vol. 22, no. 4, pp. 54–69, 2005.

[77] H. Wymeersch, J. Lien, and M. Win, "Cooperative localization in wireless networks," *Proceedings of the IEEE*, vol. 97, no. 2, pp. 427–450, 2009.

[78] G. Ding, Z. Tan, L. Zhang, Z. Zhang, and J. Zhang, "Hybrid TOA/AOA cooperative localization in non-line-of-sight environments," in *Proceedings of IEEE 75th Vehicular Technology Conference (VTC Spring)*, 2012, pp. 1–5.

[79] M. Horiba, E. Okamoto, T. Shinohara, and K. Matsumura, "An improved NLOS detection scheme for hybrid-TOA/AOA-based localization in indoor environments," in *Proceedings of IEEE International Conference on Ultra-Wideband (ICUWB)*, 2013, pp. 37–42.

[80] R. Klukas and M. Fattouche, "Line-of-sight angle of arrival estimation in the outdoor multipath environment," *IEEE Transactions on Vehicular Technology*, vol. 47, no. 1, pp. 342–351, Feb. 1998.

[81] K. Ho and W. Xu, "An accurate algebraic solution for moving source location using TDOA and FDOA measurements," *IEEE Transactions on Signal Processing*, vol. 52, no. 9, pp. 2453–2463, 2004.

[82] K. Ho, X. Lu, and L. Kovavisaruch, "Source localization using TDOA and FDOA measurements in the presence of receiver location errors: Analysis and solution," *IEEE Transactions on Signal Processing*, vol. 55, no. 2, pp. 684–696, 2007.

[83] M. Fowler and X. Hu, "Signal models for TDOA/FDOA estimation," *IEEE*

Transactions on Aerospace and Electronic Systems, vol. 44, no. 4, pp. 1543–1550, 2008.

[84] D. Musicki, R. Kaune, and W. Koch, "Mobile emitter geolocation and tracking using TDOA and FDOA measurements," *IEEE Transactions on Signal Processing*, vol. 58, no. 3, pp. 1863–1874, 2010.

[85] H.-W. Wei, R. Peng, Q. Wan, Z.-X. Chen, and S.-F. Ye, "Multidimensional scaling analysis for passive moving target localization with TDOA and FDOA measurements," *IEEE Transactions on Signal Processing*, vol. 58, no. 3, pp. 1677–1688, 2010.

[86] M. Sun and K. Ho, "An asymptotically efficient estimator for TDOA and FDOA positioning of multiple disjoint sources in the presence of sensor location uncertainties," *IEEE Transactions on Signal Processing*, vol. 59, no. 7, pp. 3434–3440, 2011.

[87] A. Yeredor and E. Angel, "Joint TDOA and FDOA estimation: A conditional bound and its use for optimally weighted localization," *IEEE Transactions on Signal Processing*, vol. 59, no. 4, pp. 1612–1623, 2011.

[88] K. Yang, L. Jiang, and Z.-Q. Luo, "Efficient semidefinite relaxation for robust geolocation of unknown emitter by a satellite cluster using TDOA and FDOA measurements," in *Proceedings 2011 IEEE International Conference on Acoustics, Speech and Signal Processing (ICASSP)*, 2011, pp. 2584–2587.

[89] F. Quo and K. Ho, "A quadratic constraint solution method for TDOA and FDOA localization," in *Proceedings of 2011 IEEE International Conference onAcoustics, Speech and Signal Processing (ICASSP)*, 2011, pp. 2588–2591.

[90] H. Li, Z. Deng, and Y. Yu, "Investigation on a NLOS error mitigation algorithm for TDOA mobile location," in *Proceedings of IET International Conference on Communication Technology and Application (ICCTA 2011)*, 2011, pp. 839–843.

[91] K. Ho, "Bias reduction for an explicit solution of source localization using TDOA," *IEEE Transactions on Signal Processing*, vol. 60, no. 5, pp. 2101–2114, 2012.

[92] H. Yu, G. Huang, J. Gao, and B. Liu, "An efficient constrained weighted least squares algorithm for moving source location using TDOA and FDOA measurements," *IEEE Transactions on Wireless Communications*, vol. 11, no. 1, pp. 44–47, 2012.

[93] Y.-C. Li, D. Oh, J.-H. Kim, J.-W. Chong, and J.-D. Kim, "A novel subspace-based joint TDOA and FDOA estimation using chirp signals for mobile multipath environment," in *Proceedings of 2012 IX International Symposium on Telecommunications (BIHTEL)*, 2012, pp. 1–5.

[94] H. Yu, G. Huang, J. Gao, and B. Yan, "Practical constrained least-square algorithm for moving source location using TDOA and FDOA measurements," *Journal of Systems Engineering and Electronics*, vol. 23, no. 4, pp. 488–494, 2012.

[95] G. Wang, Y. Li, and N. Ansari, "A semidefinite relaxation method for source localization using TDOA and FDOA measurements," *IEEE Transactions on Vehicular Technology*, vol. 62, no. 2, pp. 853–862, 2013.

[96] S. Julier and U. J.K., "A new extension of the kalman filter to nonlinear systems," in *Proceedings of Aerospace/Defence Sensing, Simulation and Controls*, 1997.

[97] S. Julier and J. Uhlmann, "Unscented filtering and nonlinear estimation," *Proceedings of the IEEE*, vol. 92, no. 3, pp. 401–422, Mar. 2004.

[98] J. M. Huerta, A. Giremus, J. Vidal, and J.-Y. Tourneret, "Joint particle filter and UKF position tracking under strong NLOS situation," in *Proceedings IEEE/SP 14th Workshop on Statistical Signal Processing*, Aug. 2007, pp. 537–541.